FLOW-LINE AND WET-AREAS CONFORMANCE TESTING OF WETLAND LOCATIONS USING LIDAR AND SRTM ELEVATION DATA

by

Jae J. Ogilvie

BSc. Forestry, University of New Brunswick, 2006

A Thesis Submitted in Partial Fulfillment
Of the Requirements for the Degree of

Masters of Science in Forestry

In the Graduate Academic Unit of
Forestry and Environmental Management

Supervisor: Paul Arp, PhD, ForEM

Examining Board: Fan-Rui Meng, PhD, ForEM
Emmanuel Stefanakis, PhD, GGE
Paul Arp, PhD, ForEM

This thesis is accepted by the
Dean of Graduate Studies

THE UNIVERSITY OF NEW BRUNSWICK

September 2017

ABSTRACT

This thesis reports on discerning flow networks and wetland borders across forested lands using digital elevation models (DEMs) and Light Detection and Ranging (LiDAR)-generated point cloud data for two contrasting forest zones. This selection refers to the boreal forest zone in northern Alberta's Ecosystem Management Emulating Natural Disturbance (EMEND) study area, north of Peace River, and to the temperate forest zone typical of the Acadian Forest in central New Brunswick, as represented by the University of New Brunswick forest in Fredericton (UNB Forest) study area. The DEMs refer to globally available Shuttle Radar Topography Mission (SRTM) elevation rasters with 30 and 90 m spatial resolution, and bare-earth DEMs generated from classified LiDAR point cloud data, interpolated at 1 metre (m) and resampled at 10 m and 30 m spatial resolutions. The methodology involves comparing how DEM-delineated flow-line and wetland-border predictions at 1, 10, 30 and 90 m spatial resolution relate with corresponding in-field GPS-tracks. It was found that wetland delineations were best when using a combination of DEM-generated wet area model thresholds pertaining to: DEM resolution at 1 m spatial resolution; cartographic depth-to-water index (DTW) < 1 m with flow lines formed at a 4 hectare (ha) minimum upstream contributing area threshold and presence of LiDAR-discerned hydrophytic vegetation patterns, as in raised bogs. The resulting best-fitted wetland borders conformed to the GPS-tracked borders within ±20 m nine times out of ten, while false positive and false negative wetland area determinations dropped below 20%. Flow-line locations were best derived from the 1m LiDAR DEMs once hydro-conditioned through general depression and road-specific breaching. Flow-line and wetland-border differences between the EMEND and UNB Forest delineations were

mainly due to sharper wetland-upland transitions and deeper incision of ephemeral, intermittent and permanent flow channels on rugged (UNB Forest) as opposed to flat terrain (EMEND).

TABLE OF CONTENTS

LIST OF TABLES

LIST OF FIGURES

ACKNOWLEDGEMENTS

I would like to thank Darren Tapp, Executive Director of Government of Alberta's Agriculture and Forestry, Forest Management Branch, for the opportunity to learn from, participate in and advance Alberta's wet areas mapping initiative as manifest in this thesis. Of key significance, I would like to sincerely thank Dr. Barry White, Director, Forest Program Management Section (and committee member) for his continued guidance, support and insight throughout my as-of-yet early career. I also wish to thank Chris Bater, Forest Management Specialist, for his technical assistance and project guidance. Thank you to Michael Currie and the late Heather Evans of Environment and Parks, Data Services, as well as Service New Brunswick, for their data support.

Thank you to my colleagues at the UNB Forest Watershed Research Centre, including Mark Castonguay, Shane Furze, Douglas Hiltz and Marie France Jones, for technical assistance. Thanks to Kyle Chisholm, David Campbell, Dustyn Martin-Ross and Connor Mooney for data collection, and to Duc Banh for keeping the computers up to task.

A special thanks to the chair of our centre, my employer and advisor, Dr. Paul Arp for your continued support throughout this and all other projects, and to my final committee member; Dr. Dirk Jaeger for his guidance and suggestions.

Finally, I wish to acknowledge and thank my wife and girls for their love, support and understanding while undertaking this MScF degree.

JO

CHAPTER 1

INTRODUCTION

The research reported in this thesis deals with analyzing and optimizing the pattern of topographically-derived flow networks (flow lines) and associated wet-areas and wetland patterns, as derived from digital elevation models (DEMs), with spatial resolutions varying from 1 to 90 m. This analysis was verified using field-tracked ephemeral to permanent flow lines and wetland borders, and was subsequently validated using already existing provincial flow-channel and wetland delineation data layers for temperate and boreal forest conditions. All of this was done within the digital wet-areas mapping (WAM) context, which uses DEMs for the delineation of overland flow directions, upstream watersheds and flow-contributing areas (also referred to as flow accumulation) and associated wet areas, as they range in application from small sub-catchments to entire trans-regional river watersheds (Murphy et al., 2007; White et al., 2012).

Prior to the availability of DEM data layers and the wet-areas mapping (WAM) process, catchment areas and associated stream networks were derived manually from locally available elevation contour maps (Jenson & Domingue, 1984; Band, 1986). The increased DEM availabilities and related developments of raster-based flow accumulation algorithms (O'Callaghan & Mark, 1984; Mark, 1988; Tarboton, 1997) have - for the most part - replaced the manual delineations by enabling nearly automatic determinations of upslope watershed and stream attributes for any points of water flow concerns, e.g., actual or potential road-stream or road-river crossings (Gautam, 2012; Dixon & Uddameri, 2016). Detailed examinations of the DEM-generated flow direction, flow accumulation

and watershed delineations, however, have shown that these are affected by DEM source, resolution, undetected natural and artificial flow blockages, and assumptions of upslope area requirements for flow-line initiation (Pryde et al., 2007; Remmel et al., 2008; Gillin et al., 2015).

To improve on ensuring continuous DEM-based ridge-to-outlet flow connectivity, topographic data need to be hydro-conditioned (Quin et. al., 1991; Zhang & Montgomery, 1994) such that their spatial resolutions as well as lateral and vertical accuracies are sufficient to realistically account for surface-water flow into and along all channels (rivers, streams, gullies, rills, ditches), and low-lying depressions (lakes, pools, ponds). In this regard, high-resolution DEMs - such as those derived from airborne laser scanning (ALS), also known as LiDAR (Light Detection and Ranging) - provide improved capabilities for a systematic and comprehensive mapping of flow-line networks and associated wet areas (Murphy et al., 2009). This strength in detail, however, can also be a detriment. For example, the majority of overland flow models require that DEM surfaces to be free of indeterminate natural or artificial flow direction points, referred to as pits, sinks or depressions. The underlying principle of topographically-driven overland flow demands that flow entering any DEM cell must be able to be routed further downslope, i.e., must be hydro-conditioned. As a result, DEM depressions are problematic for continuous overland flow-based modelling; including automated flow-network delineation (Heine et al., 2004; O'Callaghan & Mark, 1984), watershed mapping (Band, 1986; Liang & MacKay, 2000), and the indexing or thresholding of upslope flow contributing areas.

To achieve a continuous ridge-to-outlet overland flow network, all pits either need to be flooded ("filled") up to their hypothetical "pour points", where water resumes to flow downslope, or need to have the DEM elevations along modeled flow paths lowered ("breached") to allow for continuous flow through DEM-modeled obstructions. True flow interruptions occur at roads and dams without culvert installations (impoundments), beaver dams, or natural debris across true flow paths. DEM-based interruptions of true flow lines occur artificially due to faulty elevation point registration or classification, and the inability of a high-resolution elevation-collecting sensor (i.e. LiDAR) to detect flow connections underneath hard surface obstructions such as roadbeds, downed logs and vegetation debris straddling streams.

The question as to the identification of upland points to initialize ephemeral, intermittent, or permanent flows still remains unresolved across landscapes due to upland variations in topography, soil permeability, vegetation cover and type, and across regions due to variations in weather, seasons and climate. Technically, ephemeral, intermittent, or permanent channel initiation points can be defined by setting DEM-based flow accumulation thresholds, but these thresholds need to be identified, verified and validated within their location and region-specific contexts. The generally vegetation-obscured locations of ephemeral and intermittent flow channels and their flow-initiation points cannot be delineated from surface images alone, but require the availability of sufficiently detailed bare-earth digital elevation rasters to systematically generate the data layers for flow direction and flow accumulation.

While wet-areas mapping processes have been used to ascertain where landscapes vary in soil drainage from very poor to excessively well drained (Murphy et al., 2009), it is more difficult to determine which portions within the delineated wet areas can be classified as wetlands. Wetlands differ from wet areas based on the presence of hydrophytic vegetation as found in bogs, fens, marshes and swamps. Murphy et al. (2007) reported that most of the officially recognized wetland locations were nested inside the WAM-mapped wet-area zone across New Brunswick where the cartographic depth-to-water index (DTW) is < 0.5 m.

All of this leads to the following research question: can the topographically driven wet-areas mapping (WAM) process be used to help locate and ascertain the spatial extent of wetlands and their connectivity (as ascertained through predicted flow lines) across broad landscapes? Addressing this question requires resolving the following issues in qualitative and quantitative terms. **Issue 1:** To what extent does increased DEM spatial resolution lead to better flow channel and wetland border delineations. **Issue 2:** Flow initiation thresholds for predicted flow line delineation cannot be inferred from DEM data alone since these thresholds vary by season and soil type. **Issue 3:** Nominal terrain elevations, whether derived from LiDAR or other DEM technologies, do not necessarily represent true bare earth elevations due to unresolved vegetation structures or misclassification of elevation points.

To address these issues, this thesis includes a presentation of current GIS and remote sensing techniques pertaining to DEM generation and the delineation of flow channels and wetlands (**Chapter 2**). This includes addressing DEM hydro-conditioning challenges

by way of: (i) an illustrated literature review of currently available data layers and WAM processing, (ii) a timeline of wet areas mapping-related modeling issues and associated algorithm developments, (iii) techniques used for delineation verification and validation, and, (iv) a summary of traditional wetland delineation techniques and requirements. **Chapter 3** provides an overview of the study areas used for analyzing the flow-line and wetland-border delineation processes, namely the EMEND study area in Alberta north of Peace River, and the UNB Forest study area in Fredericton, New Brunswick. **Chapter 4** deals with determining the minimum distance between actual and DEM-derived predicted flow line locations, as modified by DEM spatial resolution and varying upslope contributing area for flow-line initiation. **Chapter 5** describes methods and results regarding DEM-derived wetland border derivation by varying DEM spatial resolution, upstream contributing area and wet areas model thresholds in qualitative terms. **Chapter 6** evaluates the results of Chapter 5 in quantitative terms, using the confusion matrix approach to classify overall accuracy of modeled wet areas, and overall distance conformance of modeled and GPS-tracked wetland borders. **Chapter 7** validates the optimal modeled output of chapter 6 through expanding wetland delineation process across the wider area surrounding the two case study areas in Alberta and New Brunswick. Finally, **Chapter 8 s**ummarizes the thesis results, claims of original research and makes recommendations regarding further work.

The aspect of the effect of DEM resolution on flow-channel and wetland-border delineation is addressed by resampling 1 m LiDAR DEMs at 10 and 30 m spatial resolution. The results so obtained are then compared with near-globally available Shuttle Radar Topography Mission (SRTM)-derived DEMs at 30 and 90 m spatial resolution.

The aspect of flow-line initiation for ephemeral to intermittent and permanent flow channels is addressed by changing upstream contributing area thresholds from 0.5 to 16 hectares in geometric factor-2 progression.

CHAPTER 2

PROCEDURES FOR DEM-LOCATING FLOW-CHANNELS AND WETLAND BORDERS: A REVIEW WITH EMPHASIS ON WET-AREAS MAPPING

2.1 Introduction

The influence of landscape topography on overland flow-derived hydrographic networks and associated wet areas has been well established in literature (Kirkby & Chorley, 1967; Dunne & Black, 1970; Anderson and Burt, 1978; Moore et al., 1993, Murphy et al., 2009). DEM-based flow network derivations were formulated by Mark, 1984, O'Callaghan & Mark, 1984, Band, 1986, Morris & Heerdegen, 1988, Goodrich & Woolhiser, 1991, Smith et al., 1990, Julien et al., 1995, and Tarboton, 1997. These derivations follow a generally accepted hydro-conditioning DEM protocol to ensure that the resulting flow network delineations are closely aligned with actual flow directions and cross-landscape flow connectivity shown in Figure 1 (red box). To ensure this connectivity, flow through sinks, pits, or depressions all need to be resolved. Otherwise, flow direction and hence flow connectivity remains indeterminate and flow accumulation ceases in each DEM pit, whether due to natural or DEM artificial causes. Building on the premise of DEM-based predicted flow line generation as shown in Figure 1 (red box), the wet-areas mapping (WAM) process as reported by Murphy (2009), was developed. With special emphasis on the development of the cartographic depth-to-water (DTW) concept which defines the theoretical depth to saturated soil as it relates to locating saturated to unsaturated soil conditions across landscapes within their surrounding topography, the

suite of WAM-resulting hydro-conditioned DEM surfaces, flow direction and accumulation rasters, predicted flow lines and cartographic depth-to-water rasters define the compliment of WAM-generated model outputs shown in Figure 1 (green box).

The objective of this chapter is to provide a literature overview of up-to-date DEM-based flow-network, wet-area and wetland border delineation processes as follows: **Objective 1:** To inform about two widely available DEM sources. **Objective 2:** To discuss the need for DEM surface preparation (hydro-conditioning) for overland flow and wet-areas modelling. **Objective 3:** To provide predicted flow line and wet areas mapping illustrations as generated by way of wet-areas mapping processes. **Objective 4:** To outline the timeline of wet areas mapping algorithm developments and model improvements as they pertain to the above points, and to this thesis in particular. This is done by reviewing currently available DEM sources, and outlining the WAM processes needed for step-by-step flow network and wetland border delineation, verification and validation. Finally, traditional to current methods pertaining to digital wetland delineation are summarized in the final section of this chapter.

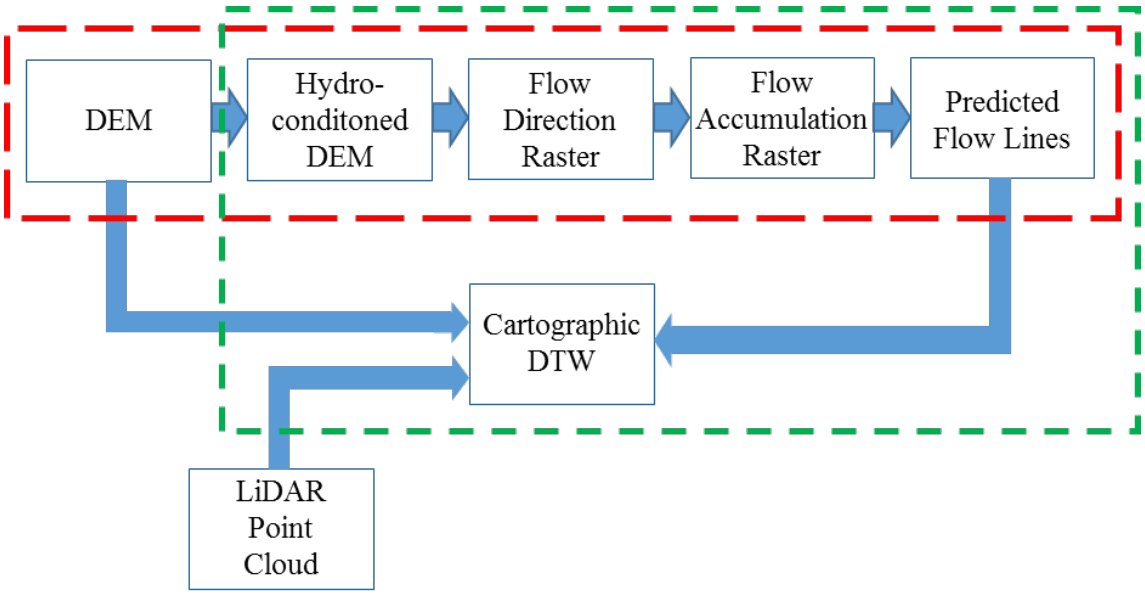

Figure 1. Protocol for DEM-based flow-network derivations and wet areas mapping (WAM). General workflow for predicted flow network derivation shown in red-dashed lines and WAM outputs shown in green-dashed line.

2.2 Elevation Sources

Shuttle Radar Topography Mission: 3 and 1 Arc-Second Global

Widely regarded as a major breakthrough in near-global digital mapping, the Shuttle Radar Topography Mission (SRTM) is a space-borne radar data acquisition captured in February, 2000 aboard space shuttle Endeavour. The international project carried out by the National Aeronautics and Space Administration (NASA) and the National Geospatial-Intelligence Agency (NGA), utilized C-band radar and X-SAR synthetic aperture radar (SAR) to capture elevation data at a resolution of 1 arc-second (approximately 30 m, depending on longitude) for 80% of the earth's surface. Due to the ready global availability of this dataset, it was used for comparative purposes in this thesis.

For the purposes of this paper, the efficacy of SRTM DEM at 3 and 1 arc second, transformed to a projected coordinate system at 90m and 30m respectively will be compared to LiDAR-derived bare earth DEMs at 1m resolution and down-sampled 10m and 30m resolutions.

LiDAR & Bare Earth DEMs

High resolution DEM datasets, such as those derived from airborne laser scanning (ALS) or (LiDAR), provide greatly improved capabilities for the capture of detailed surface topography and subsequent modelling of predicted flow networks, including previously unmapped ephemeral flows. Light Detection & Ranging (LiDAR), is an active remote sensing technology in which laser pulses are propagated from a sensor, reflect off a target object and are returned back to the sensor. This technology can be space-borne, as is the SRTM sensor, implemented on a tripod-based sensor platform, mobile systems like ground-based vehicles or, most commonly for wide scale data acquisition, aircraft. The integration of a laser sensor with high precision global positioning system (GPS) and an inertial measurement unit (IMU), when mounted in an aircraft, form an Airborne Laser Scanning (ALS) system. Although many different ALS systems exist, some for very specific purposes, with varying scan patterns, operating frequency ranges, energy wavelength, etc., the basic premise remains the same. As an ALS system scans an acquisition area, the energy reflected back to the LiDAR sensor is collected and XYZ points are discretized from a full energy-return waveform when there is sufficient energy reflection by a target object. This collection of observed target returns, referred to as a LiDAR point cloud, can be subsequently classified using semi or fully automated

procedures to extract features including buildings, forest canopy, and most important for overland flow modelling, ground points. Classified ground points, which are a subset of all points associated with the terminal target recorded for each LiDAR pulse (last returns), represent a "virtually deforested" landscape, which includes those LiDAR returns likely to be associated with ground, road surfaces, ditches, etc. which are then interpolated in to a "bare earth" raster surface.

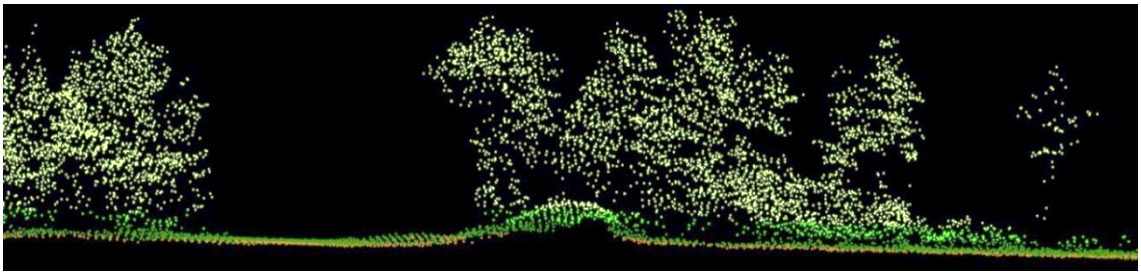

Figure 2. Example of ALS-derived classified LiDAR point cloud data. Ground-classified points are shown in brown, low vegetation (< 2.0 m) in green, and high vegetation (>= 2.0 m) in light yellow.

Bare earth DEM surfaces provide highly detailed topographic inputs to overland flow models, but the strength of the detail is also a detriment; the majority of overland flow models require that an elevation surface be free of zones of indeterminate flow direction, called depressions, pits or sinks. While natural landscapes often do consist of true natural depressions that may be influenced by subsidence, groundwater flow, etc., overland flow models generally assume depressions as artificial and require their removal or masking. Whether true depressions or DEM processing errors or anomalies, the underlying principle of topographically driven overland flow routing demands that flow entering any DEM cell must be able to be routed further downslope. As a result, DEM depressions are problematic for many overland flow-based modelling exercises including automated flow

network delineation (Heine et al., 2004; O'Callaghan & Mark, 1984), watershed mapping (Band, 1986; Liang & MacKay, 2000), and the estimation of a myriad of contributing area-based topographic indices.

2.3 DEM-based Flow-Channel Derivation

DEM Depression Removal (Hydro-conditioning)

Removal of spurious pits or depressions (a point or set of adjacent points surrounded by neighbors of higher elevations) in a DEM can be accomplished via either incremental (depression filling or flooding), decremental (landscape breaching or carving) or hybrid (combination) methods (Figure 3). Using 30 m spatial resolution raster datasets from United States Geological Survey (USGS), Tarboton et al. (1991) found that 0.9 to 4.7% of cells in a DEM can be labeled as a sink, while Lindsay (2016) found that using high resolution LiDAR-based DEMs from varying landscapes ranging from resolutions of 1 to 3 m, 6.3 to 10.9% of high resolution DEM cells can be labeled as a sink.

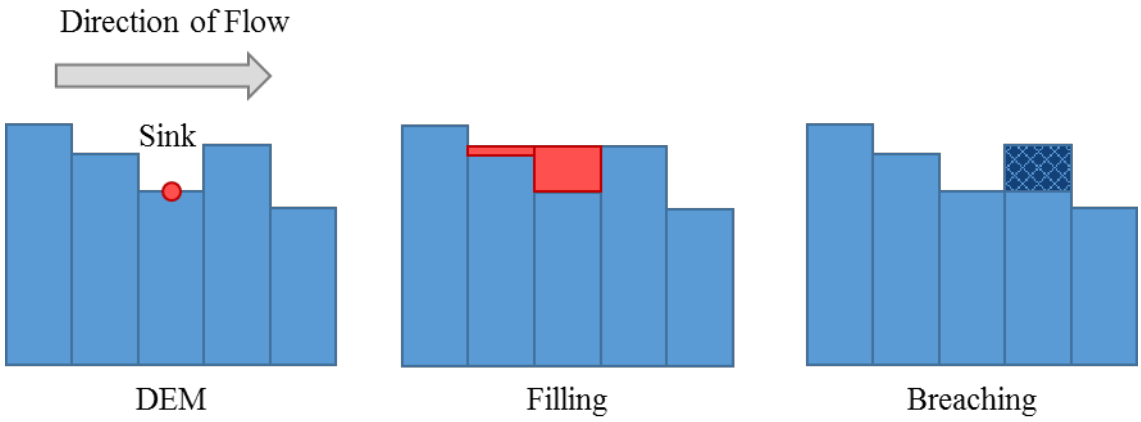

Figure 3. Conceptual elevation profile depicting filling and breaching techniques.

Incremental Approach (Depression Filling)

Depression filling involves artificially raising (incrementing) the DEM raster cell values of pits and any adjacent cells until an outward flow path can be determined for all cells in a DEM. The filling method of depression removal may be accomplished by many different algorithms (Jenson & Dominque, 1988; Tarboton et al., 1991; Planchon & Darboux, 2002; Wang & Liu, 2006; Yu et al., 2014), but regardless of the implementation, result in only one possible solution for a given DEM. While breaching and hybrid methods have been shown alter DEMs (z-change and n-count) significantly less than depression filling (Soille, 2004; Lindsay & Creed, 2005; Lindsay & Dhun, 2015), depression filling remains as the most common method of hydro-conditioning amongst GIS practitioners (Lindsay, 2016). Lindsay (2016) states that compared to breaching or hybrid approaches, despite its shortcomings, filling algorithms have had a longer history and much of the development effort has focused on improving algorithm efficiency. Shortcomings of depression filling are particularly evident in roaded landscapes where engineering and construction activities across river valleys are captured by the DEM. Digital elevation models generated from ALS data, unless otherwise corrected, cannot capture information about culverts or other watercourse crossings buried beneath a roadbed. As a consequence, roads built across natural valleys (Figure 4) are interpreted as dam-like impoundment features which will only allow overland flow across a road once the road-induced "dam" is flooded to the road crown (pour point). The resulting "filled" DEM no longer contains any of the original topographic information of the now-flooded cells, resulting in topographically inconsistent overland flow paths (Figure 5). Surface models resulting from depression filling algorithms do provide insight into potential flooding

situations that could arise from blocked culverts, e.g., as a result of beaver-damming activity or accumulation of debris at the mouth of culverts.

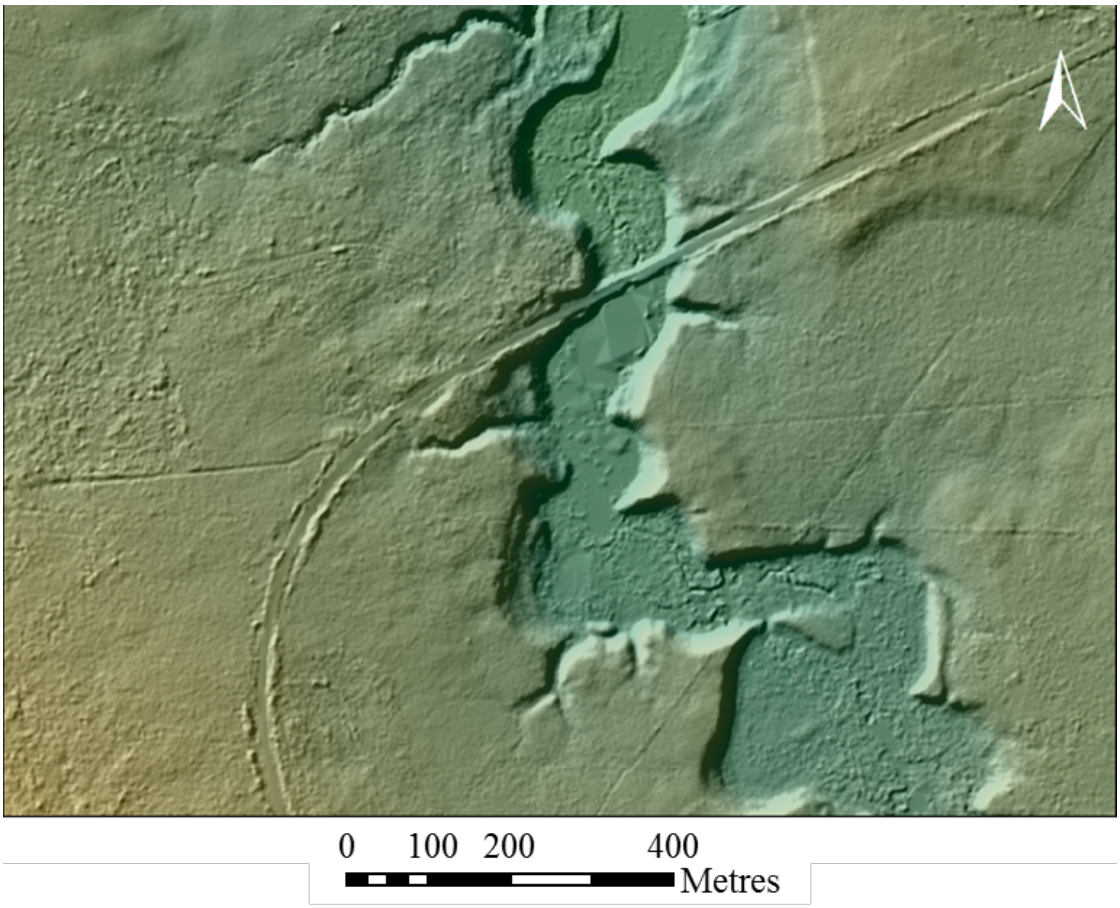

Figure 4. Shaded relief of 1 m LiDAR-derived bare earth elevation without hydro-conditioning techniques applied.

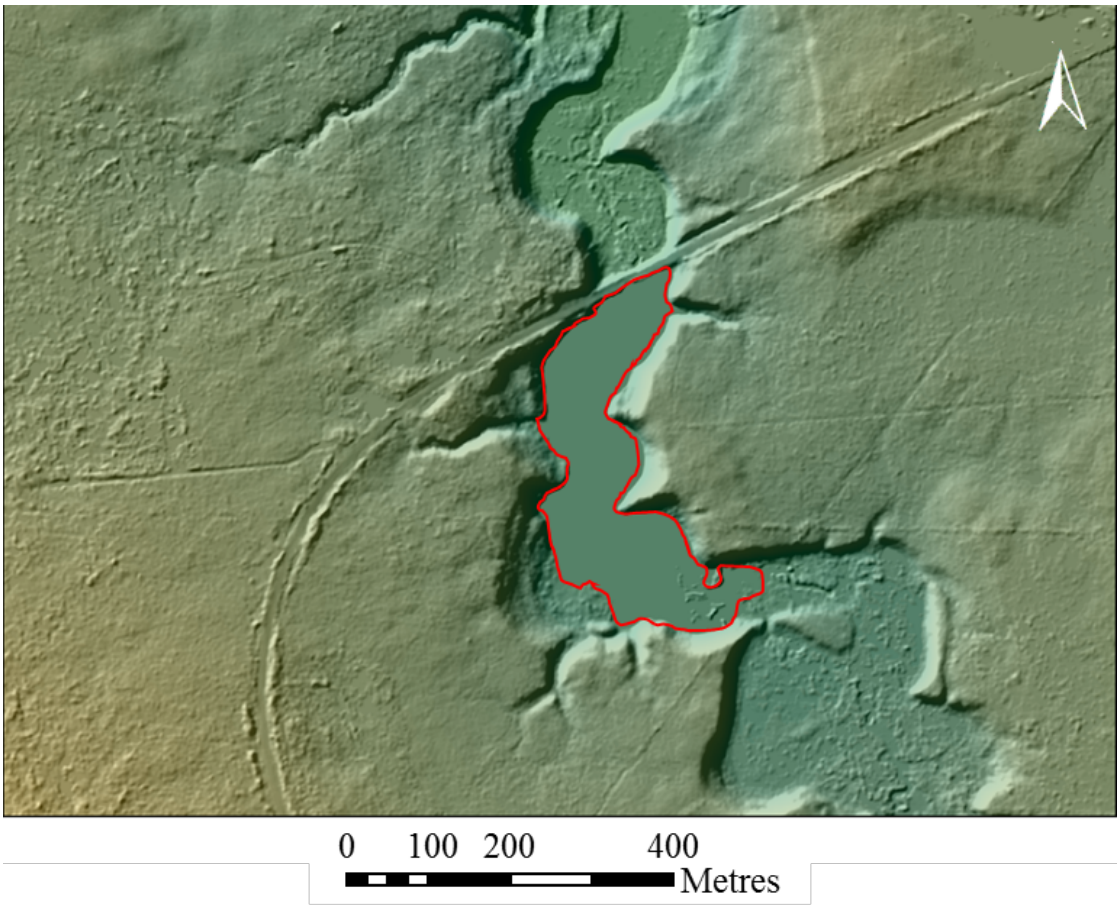

Figure 5. Shaded relief of 1 m LiDAR-derived bare earth elevation showing cells modified by depression filling. DEM area modified by depression filling highlighted with red outline.

Decremental Approach (Depression Breaching)

First proposed by Rieger (1993), depression breaching involves decrementing (lowering) cell values along a single path such that an outward flow path can be determined for all cells in a DEM. Unlike depression filling algorithms, the underlying algorithm chosen for the selection of the decrement path out of a sink can result in radically different solutions; particularly in areas of low relief. Depression breaching algorithms are computationally demanding and dependent on landscape topography, which has traditionally led to much

lower utilization relative to depression filling algorithms. Most depression breaching algorithms follow a least cumulative cost approach for breach path selection whereby paths may follow meandering or ditched DEM paths (of low relative elevation), for some distance before ultimately resolving a depression. This breaching mechanism works well in meandering streams or oxbows, but may incorrectly breach down a ditch path instead of crossing a raised road bed. As a consequence, a new road-specific breaching algorithm was developed for targeted depression removal along roads where breach paths are selected to minimize total number of cells modified, while all non-road adjacent depressions are breached using a "natural" breaching protocol which resolves depressions by minimizing total elevation change (Figure 5). The methods associated with the development of the road-specific are beyond the scope of this thesis.

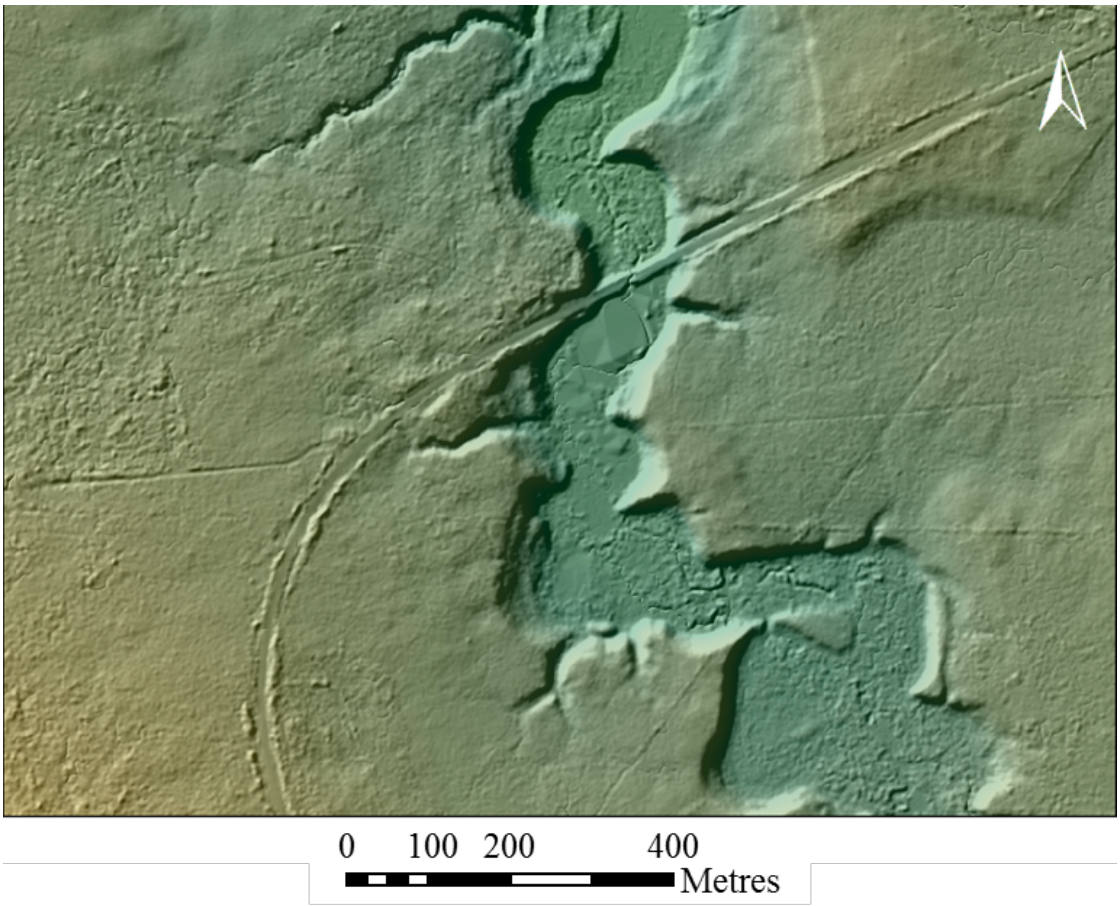

Figure 6. Shaded relief of 1 m LiDAR-derived bare earth elevation showing cells modified by depression breaching.

The selection of hydro-conditioning technique can have a significant influence on DEM elevation values and subsequent flow directions, which ultimately inform locations of synthetic stream channels, as shown in Figure 6 below.

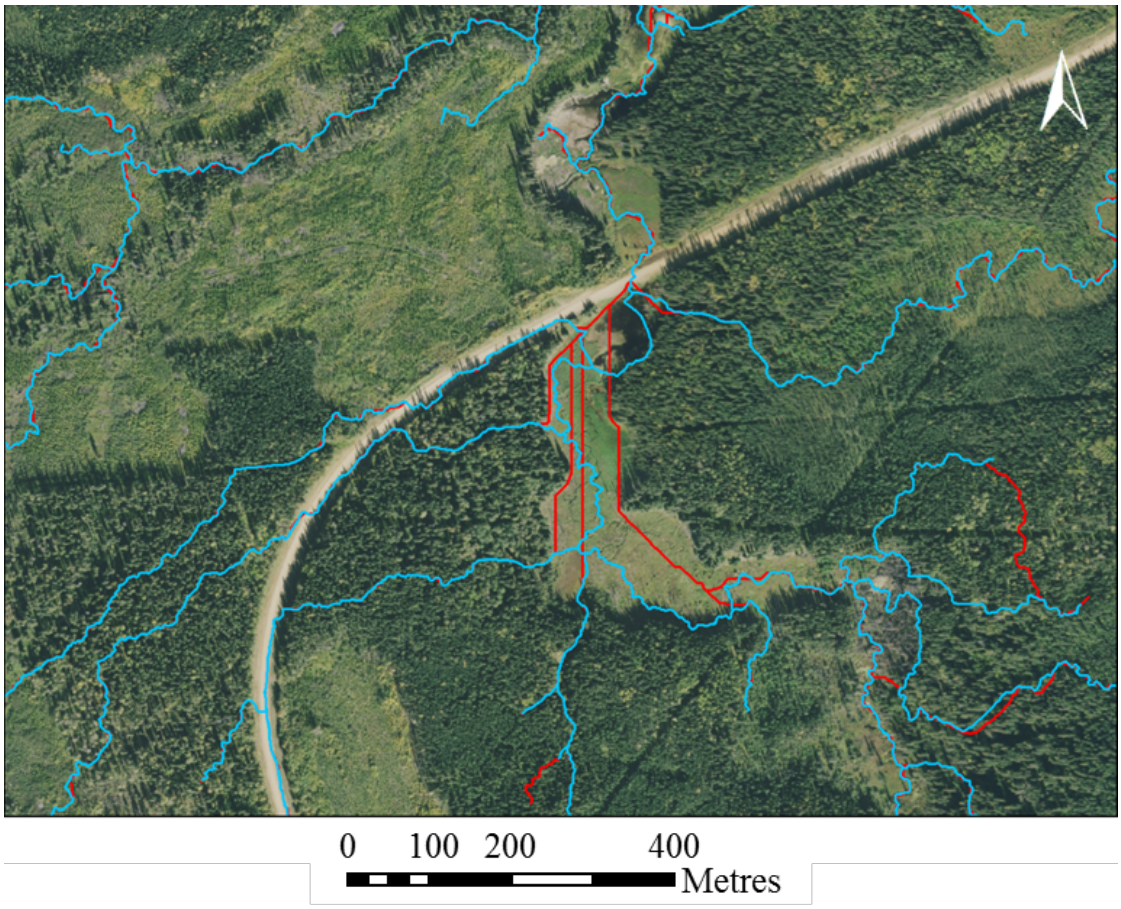

Figure 7. Influence of hydro-conditioning methods on stream channel derivation. Predicted flow lines generated using a 4 ha flow initiation threshold, using breaching (blue) and filling (red) hydro-conditioning methods.

Flow Direction

Modelling overland flow across a DEM surface requires a hydrologically conditioned DEM (Figure 5 & Figure 6) as input to a flow direction algorithm. For each cell in the input DEM raster, adjacent cell(s) of lower elevation are identified and coded in a flow direction raster to define downslope flow paths (O'Callaghan & Mark, 1984). Flow can either be allocated wholly to a single down-slope cell; a single flow direction (SFD), or partitioned across multiple adjacent cells of lower elevation; multiple flow directions,

(MFD). Using SFD algorithms, flow which originates over a two-dimensional pixel is treated as a point source (non-dimensional) and is projected downslope by a line (one dimensional) (Moore & Grayson, 1991), and the flow direction in each pixel is restricted to eight possible cardinal directions; referred to as the D8 flow direction algorithm (Costa-Cabral & Burges, 1994). The D-infinity MFD algorithm, as first proposed by Tarboton (1997), divides the 3 X 3 cell window of adjacent DEM cells into 8 triangular facets. The slope direction and magnitude of each facet are compared. The steepest downward direction is chosen and divided into two directions along the edges forming that facet. The proportion of flow along each edge is inversely proportional to the angle between the steepest downward directions and the edge; therefore at most two flow directions can be assigned to each cell. The contour length is defined as the grid cell size (DEM spatial resolution), and the slope is set to be the largest slope of 8 facets. (Tarboton, 1997; Pan et al., 2004). When processing high resolution DEMs (e.g., LiDAR-DEMs), single and multiple flow direction algorithms perform nearly identically since unit areas per cell are small and multi-cell partitioning generally still results in narrow downslope paths. An example of the algorithm result for the D8 flow direction is shown in Figure 8.

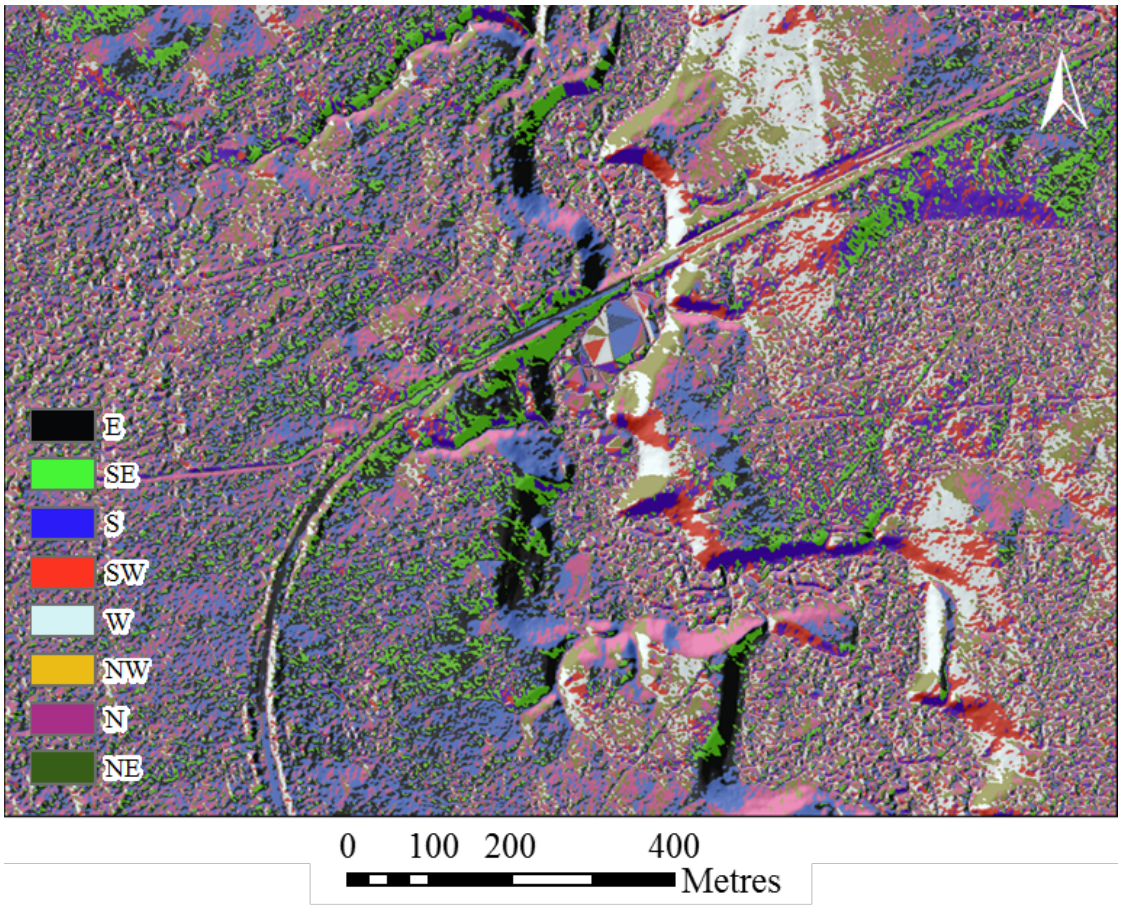

Figure 8. Example of D8 Flow Direction raster. For each DEM cell, color coded raster value denoting one of the D8 flow directions is assigned.

Flow Accumulation

Flow accumulation as informed from the flow direction raster, defines the total number of upstream cells that flow into any target raster cell. Depending on the class of flow direction algorithm used (SFD or MFD), flow accumulation may be constrained or non-constrained (Qin et al.; 2006). When flow accumulation raster thresholding is used to define predicted flow line locations, upstream contributing area values for non-constrained may fall below the minimum initiation threshold for flow line initiation, even down stream of an already initiated channel location, if there is sufficient divergence.

Modeled overland flow accumulation has been found to be a good indicator of moisture status, saturated areas and stream channels (Burt & Butcher, 1986; Moore et. al.; 1988; Wood et al.; 1990). An example of the D8-based constrained flow accumulation algorithm, is shown in Figure 9.

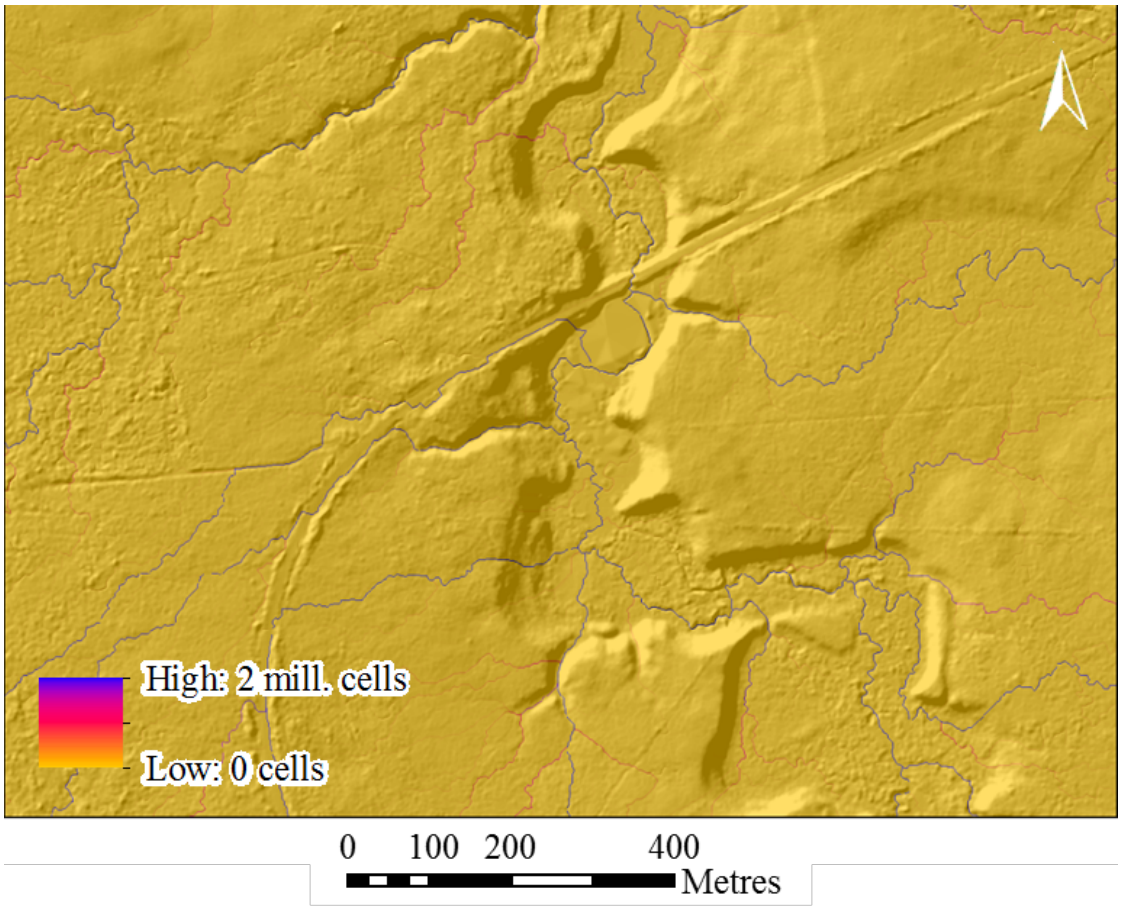

Figure 9. Example of D8 Flow Accumulation raster. For each DEM cell, areas of lower relative flow are shown in yellow, with increasing upstream contributing areas show in red and blue.

Flow-Line Initiation via Thresholding

Flow line delineations, predicted by overland flow accumulation models as defined by topographic detail of DEM data, requires the definition of flow initiation criteria.

McMaster (2002) states that specifying a constant critical support area, defined as the minimum accumulation area necessary to support channelized flow, is a generally accepted means of determining where channel headwaters begin and thus where flow networks initiate (Schumm, 1956; O'Callaghan & Mark, 1984; Band, 1986; Tarboton et al., 1991; Gardiner et al., 1991; Montgomery & Dietrich, 1992). Commonly defined by a static minimum upstream contributing area threshold or by a slope-area related threshold, the choice of stream initiation criteria not only influences drainage density, but also order and magnitude associated with all downstream flow lines in the hydrological network. Montgomery and Dietrich (1992) found that landscape segmentation into distinct hydrological units is limited by the scale at which stream channelization can be accurately modelled; setting a finite scale to any particular landscape. The threshold used is inversely proportional to the number of hydrological units (basins) that can be extracted from a landscape, with an ideal threshold equal to the hillslope length / accumulation that is minimally necessary to identify flow channel head initiation. Montgomery and Foufoula-Georgiou (1993) found that a threshold-based approach is most appropriate for modelling channel head over shorter geomorphic time scales (10^2-10^3 years) than modelling valley development (10^4-10^6 years). Murphy et al. (2008) found that using a 4 hectare upstream contributing area threshold for flow channel head initiation in the boreal region of Alberta, flow lines derived from LiDAR DEM have a more complex morphology and are in better agreement with field-mapped network than those derived from conventional DEM, but tended to extend upstream past permanent field-mapped channel heads (over estimate). An example of the influence of flow channel initiation threshold is shown in Figure 10 below.

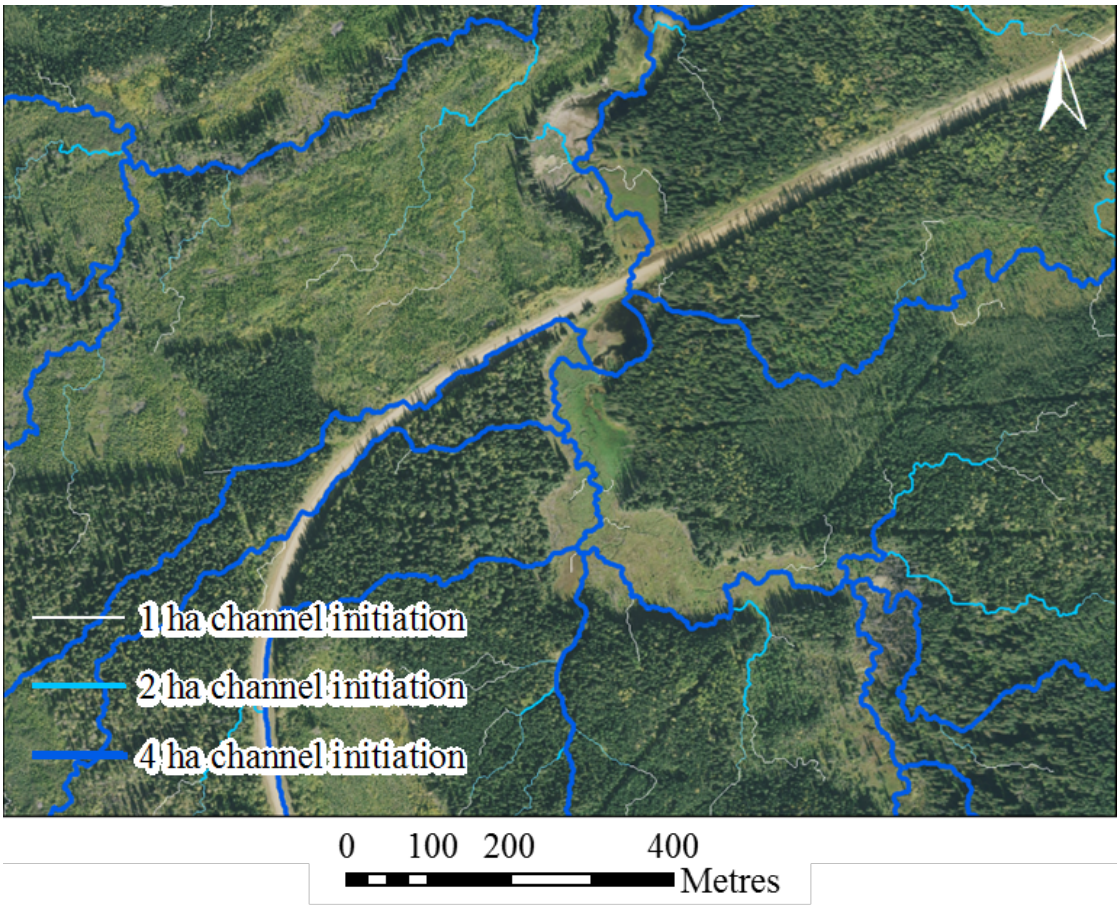

Figure 10. Example predicted flow lines generated by modifying the minimum upstream contributing area threshold. Networks generated at 8 hectares (bark blue lines), to 4 hectares (light blue lines) and 1 hectare (white lines).

2.4 Cartographic Depth-to-Water Modelling (DTW)

Overview

The cartographic depth-to-water (DTW) algorithm, which has been described in detail by Murphy et al. (2009), is formally derived as:

$$\mathrm{DTW}[\mathrm{m}] = \left[\sum \frac{dz_i}{dx_i} a\right] x_c,$$

where *dz/dx* is the slope of a cell, *i* represents a cell along the path, *a* is the unit length of the path along the flow path direction. The DTW model represents a hypothetical (modeled) cartographic depth to saturated soil; not the subsurface groundwater table, measured in cm or m from the DEM surface. One common method of developing predictive models of topographically controlled soil moisture from digital elevation data utilizes the Topographic Wetness Index (TWI), also known as the Compound Topographic Index (CTI) is defined as ln(a/tan B), where *a* is the upstream contributing area and tan *B* represents local slope in radians (Beven & Kirkby, 1979). This steady state wetness index has been shown to be highly scale dependent, with model performance decreasing as DEM spatial resolution increases (Murphy et al., 2009). Alternatively, the cartographic depth-to-water (DTW) index, developed at the University of New Brunswick (Meng, et al., 2006), has been shown to more closely model field-mapped patterns of soil moisture conditions (Murphy et al., 2009). Unlike the deterministic TWI algorithm, Murphy et al. (2009) states that the cartographic depth-to-water index is based on a more empirical approach, and soils that are very close in elevation to their assigned surface water feature are more likely to be saturated at the surface and the likelihood of this saturation decreases in a manner dependent on the slope away from defined channel locations.

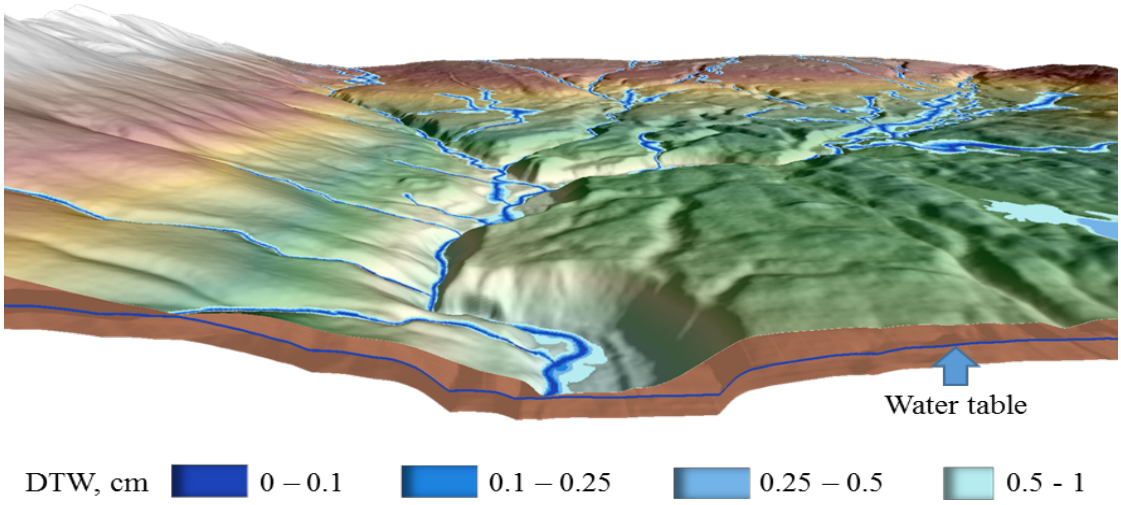

Figure 11. Conceptual Cartographic Depth-to-Water (DTW) profile. DEM-interpreted flow-channel network and associated wet areas with cartographic depth-to-water < 1m across the landscape.

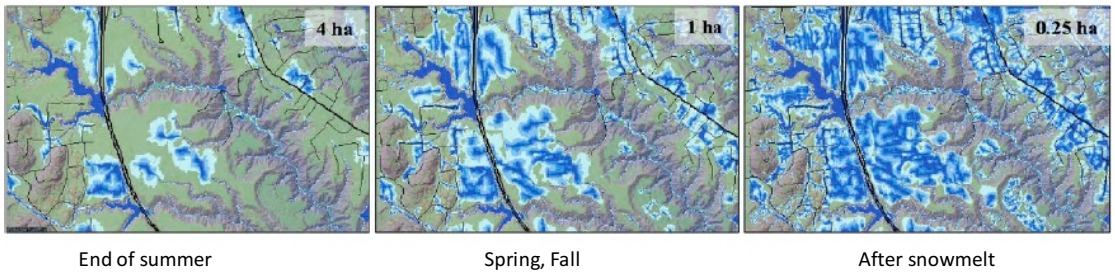

Figure 12. DEM-interpreted flow line network and associated wet areas, by season. Cartographic depth-to-water < 1m across the landscape, by season, as emulated using 4, 1 and 0.25 ha for upslope channel flow initiation.

DTW Correction: DEM-based Discernment of Hydrophytic Vegetation Patterns

Since the "bare-earth" elevation features in wetlands stem from a subset of the elevations of terminal (last) LiDAR pulse returns, it has become important to discern how vegetation type affects the elevation and DTW pattern within wetlands. Typically, layered black spruce vegetation and dense peat mats produce a highly convoluted digital elevation

pattern at 1 m resolution. In contrast, fens, swamp and marshes produce a fairly elevation flat pattern. As a result, within- and across-wetland topographies can vary from rough to smooth (Figure 13).

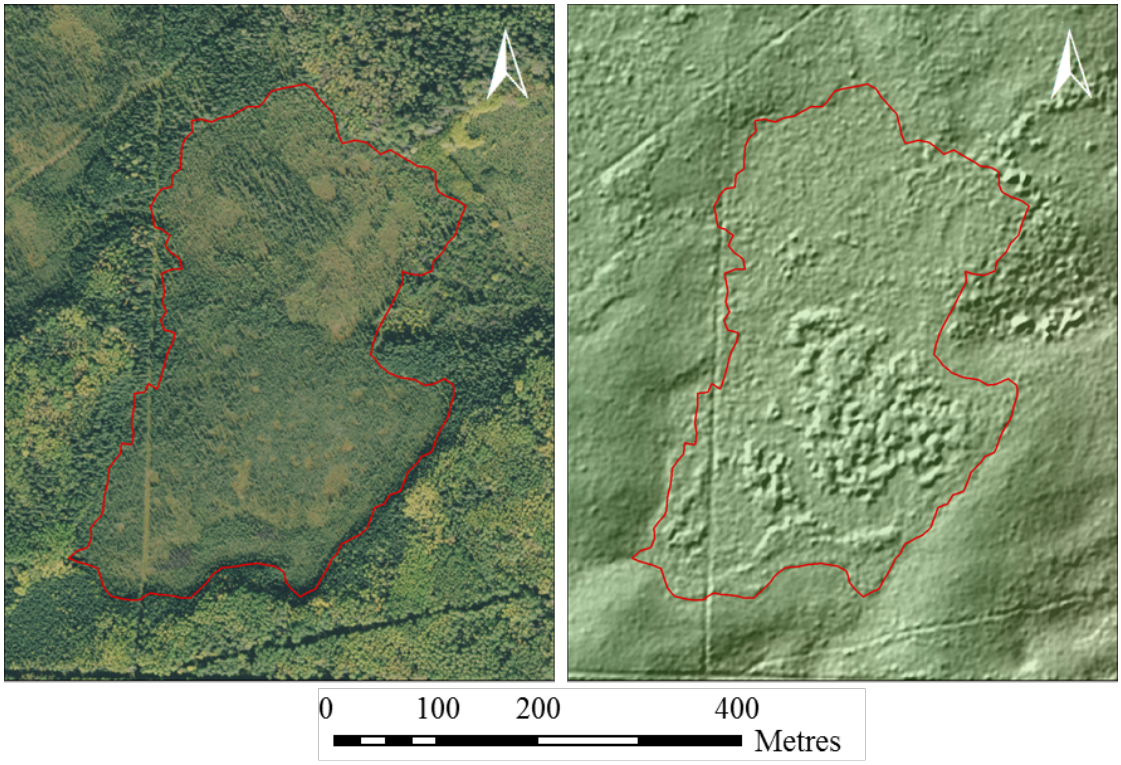

Figure 13. LiDAR-derived bare earth representation of raised bog features and surrounding fens. Orthoimage provided by Valtus Imagery Services for the EMEND study area and field-mapped wetland border in red (left). Bare earth DEM representation showing DEM-texture differences within the same field-mapped wetland border (red) on right.

The procedure used for locating the rough versus smooth textural patterns within and across wetlands is outlined by way of the flow chart by way of the LiDAR bare earth DEM- and full feature (first LiDAR return) Digital Surface Model (DSM)-based Hydrophytic DTW=0 seeding (HDS) in Figure 14, but parameterization of the HDS algorithm is beyond the scope of this thesis.

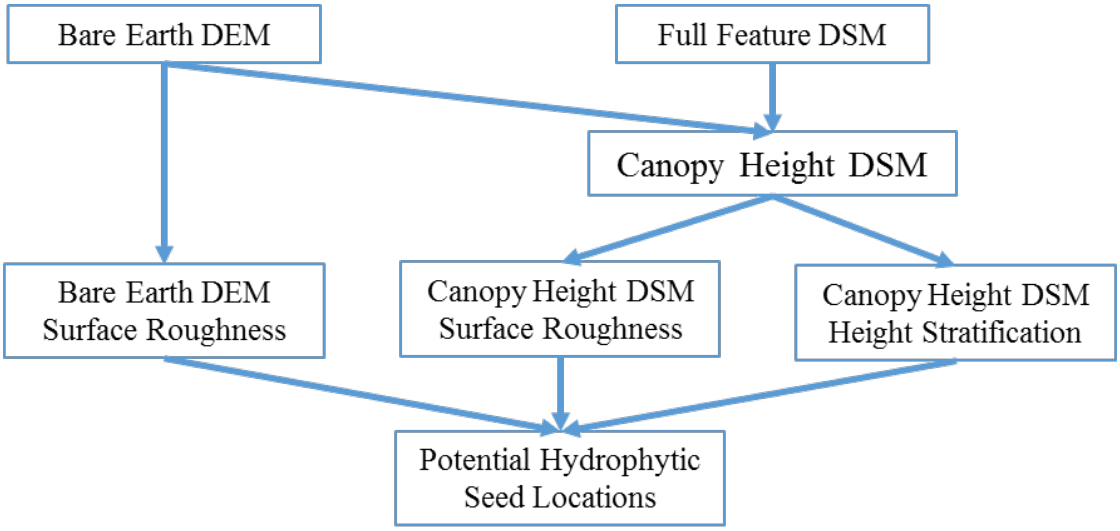

Figure 14. Generalized flow chart for the Hydrophytic DTW=0 Locator (HDS) using LiDAR-derived bare-earth DEMs and full-feature DSMs.

To separate actual wetland locations from upland locations with similar DEM-textural patterns, it is necessary further classify potential HDS zones, whether by manual or automated means, to remove false positive predictions. In this way, DEM-texture-similar areas (i.e. regenerating clearcut forest stands, aged 10-15 years) can be eliminated from the HDS model output.

As part of HDS algorithm development, the LiDAR derivatives the uncalibrated first return LiDAR pulse intensity (Figure 15, right) was also used for hydrophytic vegetation type differentiation. The uncalibrated LiDAR intensity images, however, vary in consistency by scan angle, sensor type, flying height, and wavelength of laser energy (Yan et al., 2012), and were therefore found to be unsuitable for reliable hydrophytic vegetation type discernment (Figure 16) across large scales.

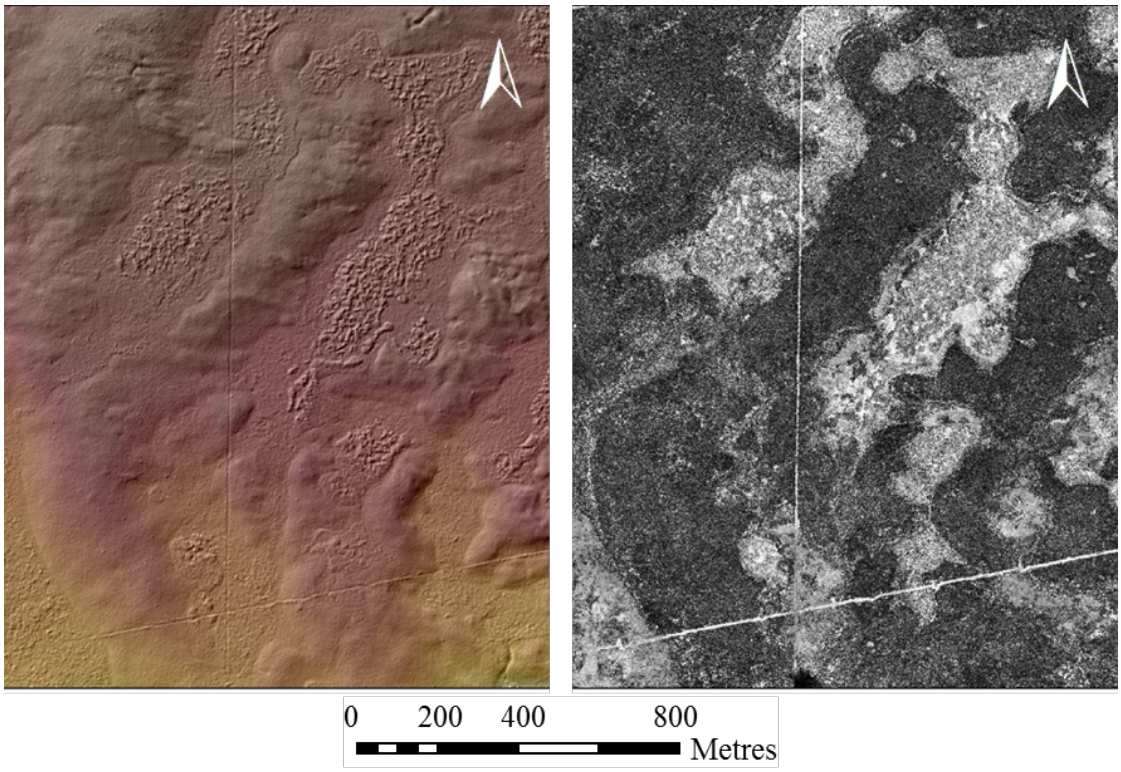

Figure 15. Comparison of LiDAR-derived bare earth and intensity surfaces. Bare earth LiDAR DEM (left) and full feature LiDAR uncalibrated full feature LiDAR pulse intensity image (right), for a subsection of the EMEND study area.

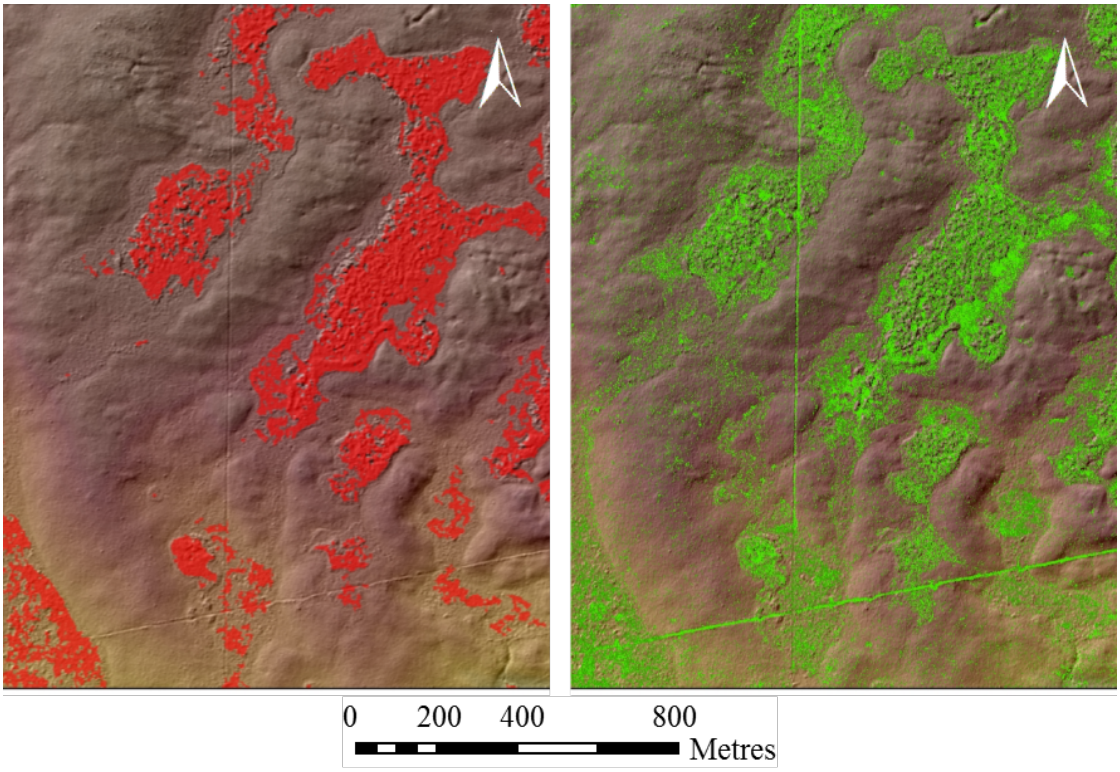

Figure 16. Comparison of LiDAR-derived hydrophytic vegetation layers. DEM texture-based HDL layer prediction, shown in red (left), and the first-return LiDAR pulse intensity-based hydrophytic vegetation prediction later, shown in green (right).

An example of correct and false HDS-based model prediction is shown in Figure 17. Without manual or automated intervention, some of the regenerating post-harvest forest areas become identified as “wetlands” since their locations are identified within the DTW algorithm as containing water at the DEM surface. These areas can be removed in several ways: (i) manual removal, using HDS areas as overlays on surface images, as well as the LiDAR-based bare-earth DEMs and full-feature DSMs; (ii) automated removal, using (a) forest inventory data layers that identify previously cut areas of certain age, or (b) using DTW and DEM morphologic thresholds.

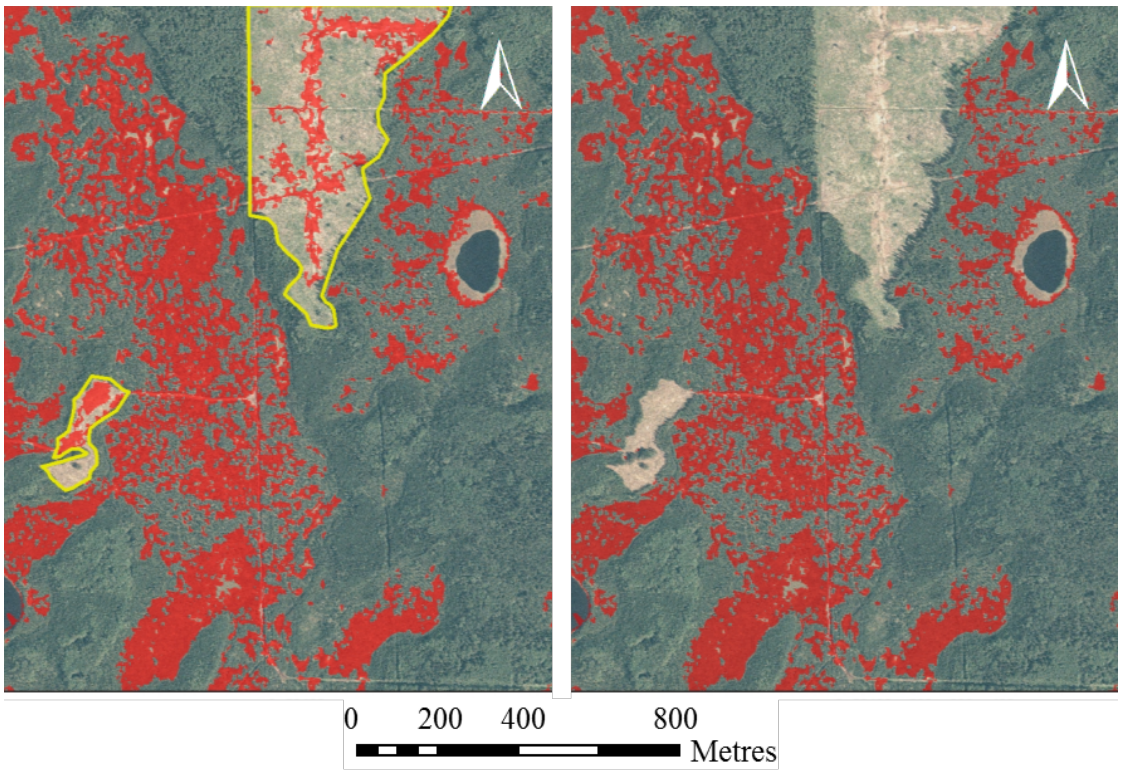

Figure 17. LiDAR-based HDS false positives. Hydrophytic DTW=0 layer (red) showing clearcut-related false positives (left pane, yellow outline), and with errors removed (right pane).

Thresholding, Verifying and Validating Wetland Borders

Once DEM-determined flow-channel networks and hydro-seeded DTW raster layers are obtained, the overall wetland-border delineation becomes a matter of determining the optimal DTW-defining wetland-border threshold. This can be accomplished in various ways. The simplest qualitative method refers overlaying the DEM-derived DTW contours on high-quality surface images and visually deciding which DTW contours fits most of the image-recognized wetlands the best. For direct in-field verification, GPS-tracking serves to capture to actual course of flow channels and wetland borders, although ill-defined flow paths and diffuse wetland borders and lead difficulties in consistent tracking.

Overlaying these tracks on the DEM-derived flow channels and DTW contours facilitates quantitative model-to-GPS-track conformance testing and related optimizing in terms of e.g., (i) plotting the distances frequencies between modeled and tracked flow channels and wetland borders, and (ii) the extent of false positive and false negative wetland-area occurrences per DTW contour (see Chapters 4, 5 and 6) .

The best flow-channel and wetland derivations can then be validated against recent or historical images, and/or existing data layers informing about officially mapped wetlands and flow-channel networks. From a visual perspective, flow channel and wetland border delineations can also be validated by scanning elevation profiles for bare-earth, full feature (e.g. forest canopy height) the cartographically determined water table. The profiles so generated and overlaid in direct reference to the profile scan line within the DEM-shaded relief and surface images allow for direct inspection of the DEM and DTW generated flow-channel and wetland border results, as illustrated in Figure 18. This figure shows how bare-earth, depth to saturated soil (wet areas) and canopy height elevations vary in profile across an upland-through-wetland scan line. Note the general agreement with the forest (cut and uncut), road, flow channels, wetland and water table features. As to be expected, the water table reaches towards or near to bare-earth elevations at the flow-channel and wetland locations.

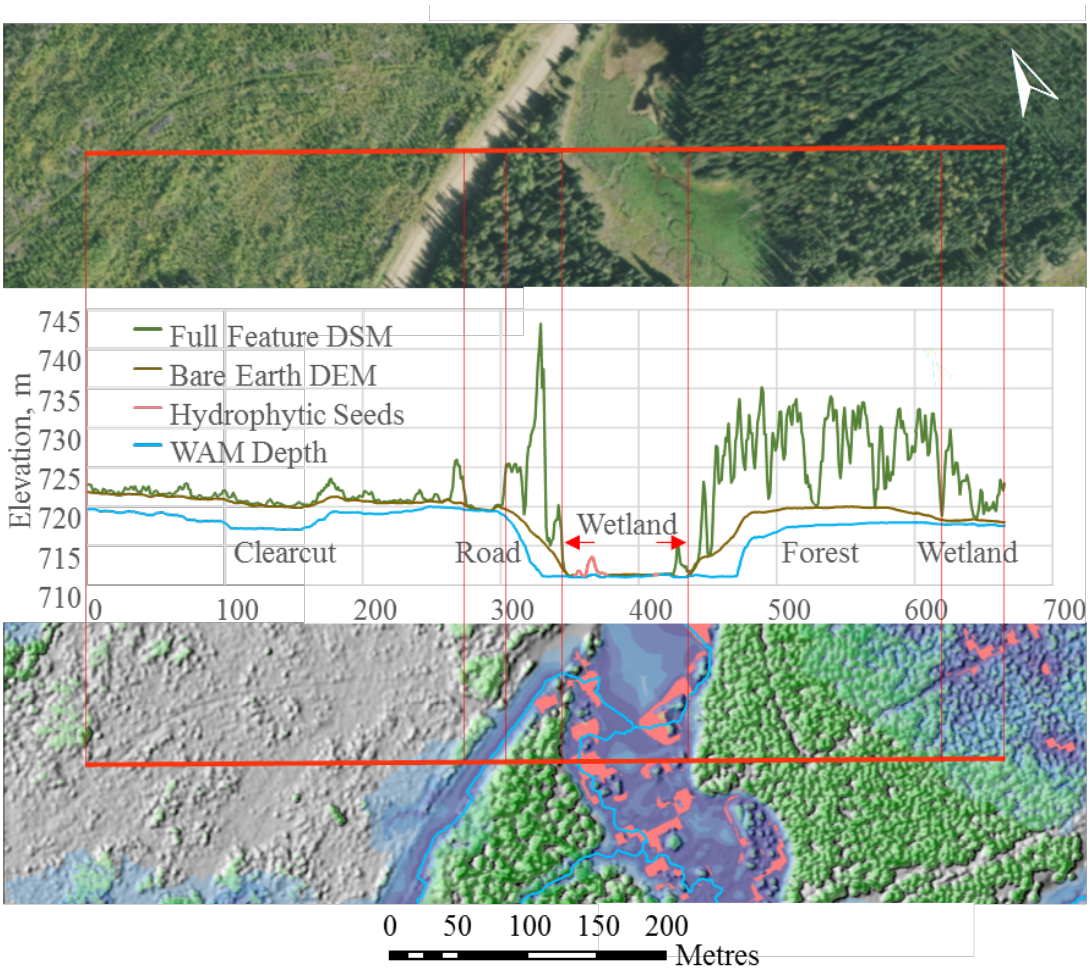

Figure 18. Profile view of modeled WAM and LiDAR-derived surfaces. DEM-interpreted flow-line network and associated wet areas with cartographic depth-to-water < 1 m acoss the wetland complex, also showing (i) local vegeation distribubition pattern by topographic location, and (ii) the relation between DEM elevation, depth-to-water elevation, and canopy height along the scan line across the wetland. Top pane shows top-down orthoimage, provided by Valtus Imagery Service and profile line (red). Bottom pane shows top-down view of shaded-relief full feature DSM raster wth associated wet areas (blue), and HDS zones (red).

Thesis –generated WAM Advances

Initially developed for use on relatively low resolution provincial DEM datasets, early WAM model output relied entirely on coarse spatial resolution DEM datasets with only basic hydro-conditioning via depresison breaching. As a consequence, model results not

only inherited any inacuracies of early DEM products, but also lacked the ability to maintain much of the character of original topographic data due to the influence of the depression filling algorithms in use (Linday, 2016). Advancements to the early WAM model included hydro-enforcement or "stream buning" of provincially mapped water features by lowering DEM cell values to encourage overland flow through mapped feature locations, which reduced the overall impact of depression filling, but caused new issues with occasional parallel modeled stream channel locations where DEM local lowland topography and mapped hydrological features were not concident, and hydro-enforcement lead some modeled channels to run adjacent to DEM-defined lowlands.

Availability of LiDAR-derived bare earth DEM datasets led to much redevelopment of the WAM model relating to efficient processing of high resolution DEM data for seamless model output across large areas. Initial modeling work in New Brunswick and Alberta identified the need to advancements to hydro-conditioning techniques; specifically at stream-road intersections where DEM depression filling yielded inaccurate results not representative of the high resolution DEM topography (Figure 7). In 2010, basic road-specific breaching was developed targeted on mapped watercourse crossing locations. Due to inconcistent coverage of these watercourse crossing datasets, automated procedures for road-specific breaching were developed; forcing overland flow across crowned road features at "ideal" locations.

Model development for the province of Alberta began in the foothills region where topographic relief was sufficient for proper definition of predicted flow lines and associated wet areas, but when implementing the WAM model in the borel region

(including the EMEND study area), it became apparent that further model improvements would be necessary. A landscape largely characterized by raised bogs; discreet, raised dome-shaped masses of peat occupying former lakes or shallow depression in the landscape (Glaser & Janssens, 1986), the purely topographically-driven WAM model was unable to appropriately model wet locations in these areas. Hydrophytic DTW seeding (HDS) based on LiDAR derivatives (as described above) was developed in an attempt to overcome this limitation by forcing the WAM process to specifically set DTW = 0 across raised bogs, thereby allowing for the model to predict surrounding moisture gradients as described by local topography.

Additional work was undertaken to improve overland flow routing as it pertains to the proper meandering of streams and flow towards and through very flat areas. Additional DEM depression breaching algorithms were integrated at the landscape level that allow for an increased proportion of original topographic information to be used in the WAM model without the destructive use of flood-fill hydro-conditioning techniques. All of this led to more realistic representations of modeled channel locations (and associated wet areas and wetland features (Chapertes 4 to 7) .

2.4 Review of Geomatic Wetland Delineation Procedures

For more than half a century, natural resource managers and scientists have exploited remotely sensed data to increase efficiencies in data collection through quantification and characterization of landcape patterns (Cowardin & Myers, 1974; Knight et al., 2013). Falling in to distinct categories, there are three general pathways for remote delineation of wetlands; (i) visible and near infrared orthophoto interpretation, (ii) Radio Detection

and Ranging (RADAR)-based classification (Knight et al., 2013; Millard & Richardson, 2013), and (iii) topographically-driven models (Agren et al., 2014; Murphy et al., 2009).

Whether implementing manual or automated techniques, wetland delineations through photo-interpretations the classification of visible and/or near infrared spectral image bands for the delineation of landscape features meeting certain spectral signature criteria (Li & Zhu, 2005). Disadvantages of this technique arise due to the inability of the classifier to differentiate wet and dry areas accurately (Baker et al., 2006; Millar & Richardson, 2013, Ozesmi & Bauer, 2002). In order to assist in the identification and delineation of wetland features from visible or near infrared imagery, ancillary elevation information, generally from a digital elevation model (DEM), is often used to refine upland/lowland classifications (Ozesmi & Bauer, 2002).

Synthetic aperture radar (SAR) illuminates a target scene using an active sensor system (usually aircraft or satellite-based) which in turn, receives an echo measuring the strength of reflection of the target based on the wavelength of sensor energy. This information is subsequently used to determine landscape attributes such as topography and standing water locations (Li & Zhu, 2005; Ozesmi & Bauer, 2002). Of primary benefit to SAR technology is the capability for the active sensor's energy to penetrate cloud cover; making it suitable for day or night scene acquisition. SAR has been shown to improve wetland identification and classification compared with photo-interpretation techniques; with improvements in the areas of forest canopy penetration and surface water identification (Wdowinski et al., 2008; Whitcomb et al., 2009); specifically, in the C-band (~5.6 cm) and L-band (~23cm) wavelengths. Touzi et al. (2009) notes that the The use of

L-band SAR imagery to identify wetlands is improved with an inundated forest floor since the smooth surface creates a more easily discernable radar backscatter signature than the surrounding rough surface; characterizing the importance of the timing of data acquisition for SAR-based wetland identification (Touzi et al., 2009; Merchant* et al., 2016; Chasmer et al., 2015).

DEM-based soil moisture models, such as the topographic wetness index (TWI), have been commonly used on a variety of elevation sources at varying spatial resolutions (Sorensen R. et al, 2006; Schmidt & Persson, 2003; Lang et al., 2013). While most wetland mapping efforts with LiDAR involving the fusion of ancillary visible red-green-blue (RGB) band or near infrared (NIR) imagery (Maxa & Bolstad, 2009; Wu et al., 2009; Huang et al., 2014), LiDAR point cloud-derived pulse return metrics alone have been found to accurately represent wetland location and vegetation structure (Hopkinson et al., 2006; Maxa & Bolstad, 2009; Millard & Richardson, 2013). Compared to SAR-based detection, Millard (2013) found that LiDAR more accurately identified wetland structure as the geomorphic form of the landscape; closely related to wetland hydrology and structure. Murphy (2009) noted that the use of the LiDAR-based, topographically-driven wet areas mapping model represented wetland areas, particularly in areas of subtle relief, more accurately than other topographically derived soil moisture indices tested, including TWI.

2.5 Review of Manual Wetland Interpretation and Classification

Many jurisdictions, including the province of Alberta, provide a mechanism by which wetlands can be identified and delineated; including via "desktop" methods. Alberta's "Wetland Identification and Delineation Directive; Water Conservation, 2015, No. 4", provides tips and recommendations for [wetland] photo interpretation, adapted from Tiner (1999), noting that interpretation of evergreen and coniferous forests can be aided by looking for evidence of saturated soils or characteristic understory vegetation where the canopy is open, using LiDAR and Wet Areas Mapping datasets. Though the use of only LiDAR-derived bare earth DEM for the generation of predicted flow line locations and LiDAR-derived bare earth DEM and full feature DSM rasters, via discernment of hydrophytic raised bog vegetation for improved wet areas source location identification, this thesis aims to quantify the efficacy of the wet areas mapping algorithm for high precision landscape segmentation from upland to lowland wet areas; of which delineated wetlands are characteristically a subset.

Table 1. Hydrophytic plants used to map wet areas in the field (based on Beckingham et al. 1996).

Plant species	Ecosite	Plant species	Ecosite
Willow (*Salix spp.*)	M, RF, PF	Rush (*Jumcus spp.*)	MA
Cow-parsnip (*Heracleum lanatum*)	M, RF, PF	Sedge (*Carex spp.*)	MA, RF, PF
Marsh reed grass (*Calamagrotis canadensis*)	M, MA, RF	Bulrush (*Scirpus spp.*)	MA
Tall lungwort (*Mertensia paniculata*)	M	Tamarack (*Larix laricina*)	PF, RF
Common horsetail (*Equisetum arvense*)	WNR, MA, RF	Dwarf birch (*Betula pumila*)	PF, RF
Meadow horsetail (*Equisetum pratensa*)	WNR, MA, RF	Black spruce (*Picea mariana*)	PNDF, RF, PF, B
Tufted moss (*Aulacomnium palustre*)	RF	Labrador tea (*Ledum groenlandicum*)	PNDF, RF, PF, B
Brown moss (*Drepanocladus spp.*)	RF, PF	Bog cranberry (*Vaccinium vitis-idaea*)	PNDF, B
Marsh marigold (*Caltha palustris*)	RF	Cloudberry (*Rubus chamaemorus*)	B, PF
Golden moss (*Tomenthypnum nitens*)	RF,PF	Peat moss (*Sphagnum spp.*)	B, RF, PF
Common cattail (*Typha latifolia*)	MA	River alder (*Alnus tenuifolia*)	M

B, bog; M, meadow: MA, marsh: PDNP, poorly drained and nutrient poor; PF, poor fen; RF, rich fen; WNR, wet and nutrient-rich

Following Chisholm (2014), the Canadian Wetland Classification System (CWCS) was chosen for use in this project because it provides a consistent classification system for the two study areas, in Alberta and New Brunswick. The CWCS uses a hierarchy approach to identifying wetlands, beginning with wetland class, then wetland form and finally wetland type. Wetland class is determined by wetland development and the ecosystem in which it exists; wetland form is determined by morphological characteristics, and wetland type is specific to the vegetation or physiological characteristics of the vegetation on the wetland (NWWG, 1997; Zoltai & Vitt, 1995).

Specific features for determining wetland classes are as follows (NWWG, 1997; Zoltai & Vitt, 1995):

1. Bogs: Sphagnum moss is the dominant vegetation; acidic; ombrotrophic.
2. Fens: Dominated by bryophyte vegetation; often minerotrophic; poor fens can be similar to bogs, except for having better decomposition and productivity; thinner forest floor layer than bogs; often deciduous vegetation.
3. Swamps: Contain trees and/or tall shrubs; minerotrophic water; little peat accumulation (often peat contains woody material); drier than marshes, fens and open bogs.
4. Marshes: Do not have trees; contain vascular plants; little peat accumulation; shallow minerotrophic water; fast decomposition,

Wetland forms are numerous, however only six were included in the study area,

as follows (NWWG, 1997):

1. Basin Bog: flat surface, not raised above surrounding terrain
2. Domed Bog: convex surface, raised above surrounding terrain
3. Horizontal Fen: flat surface, containing water that is part of drainage system
4. Drainageway Swamp: drainage paths are somewhat sloped, may or may not have distinct flow
5. Lagg Swamp: between upland and peatland
6. Linked-basin Marsh: confined to shallow depressions, receive both surface and ground water

CHAPTER 3

STUDY AREAS

3.1 Introduction

Two study areas from contrasting forest regions were selected for analysis for this thesis: (i) the Ecosystem Management Emulating Natural Disturbance (EMEND) research project, to represent boreal forest conditions, and (ii) the University of New Brunswick (UNB), to represent temperate forest conditions

3.2 Boreal Forest Study Area: EMEND

The EMEND area is located in the Clear Hills Upland, Lower Foothills Ecoregion of Alberta, approximately 90 km north-west of Peace River, a 160 km^2 project area (56˚46' 13" N, 118˚22'28"W), characteristic of the boreal mixed wood plains was selected for study. The EMEND project refers to a forest research partnership involving the University of Alberta, provincial and federal government departments, and forest companies operating in northwest Alberta. As such, it refers to large-scale variable retention harvest experiment designed to test the effects of residual forest structure on ecosystem integrity and forest regeneration at the forest stand-level.

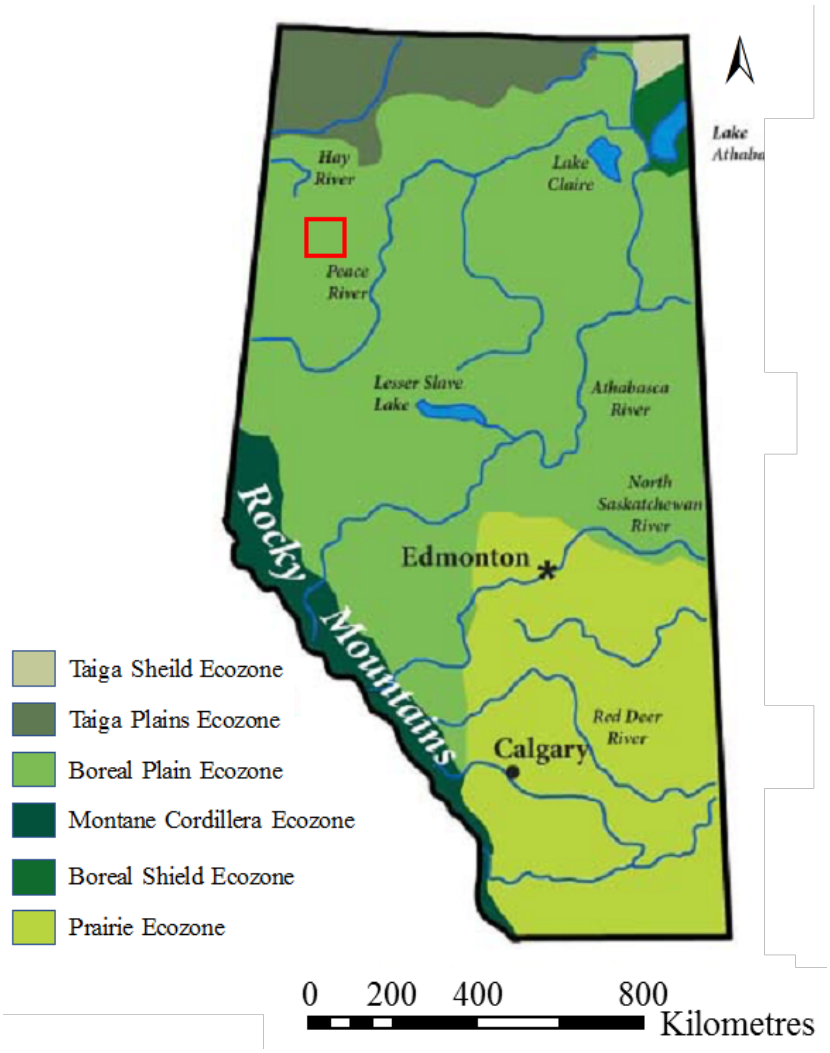

Figure 19. Provincial locator map for the EMEND study area. Extent of EMEND study area shown in red outline.

The EMEND area is representative of boreal forests facing heavy land use pressures by energy and forestry companies. As a result, the land is dissected by road, rail, pipeline and seismic line networks. The flat to lightly rolling terrain formed by continental glaciation during the Ice Age has resulted in a tight mosaic of forest-covered uplands and wetlands (bogs and fans). Eluviation and illuviation of clay fragments produced mineral soils mainly consisting of fine-textured luvisols on glaciolacustrine deposits, with few coarse

fragments (Kishchuk, 2004). Average yearly and monthly (January, July) air temperatures amount to 1.2C, -17.7C and 15.9C. Average yearly precipitation is 431 mm, with 38% accumulating as snow (Kishuck, 2004). Forest overstory primarily consists of spruce (*Picea* sp.), pine (Pinus sp.), and aspen (*Populus* sp.), while low-bush cranberry (*Viburnum edule*), prickley rose (*Rosa acicularis*), alder (*Alnus* sp.) and buffalo berry (*Shepherdia canadensis*) dominate the understory (Hiltz, 2014).

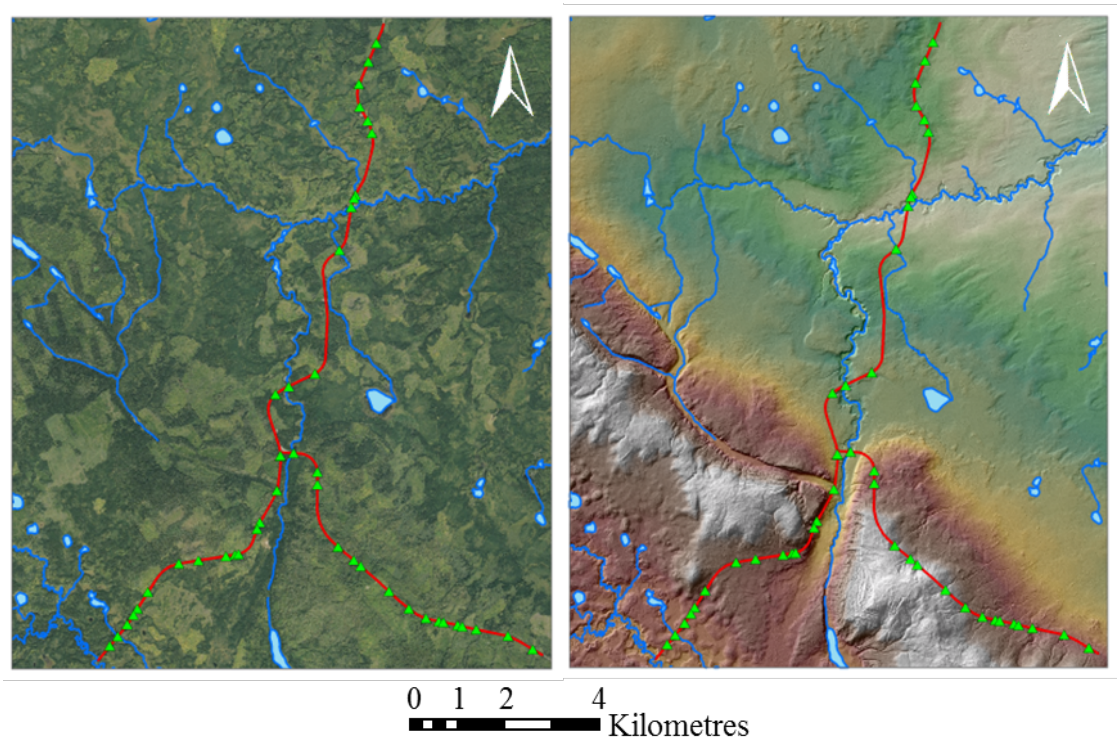

Figure 20. Landscape characteristics of the EMEND study area. Mapped roads (red lines), provincially-mapped water features (light blue polygons) and streams (blue lines) and road-stream crossings (green triangles) overlaid on orthoimage (left) and bare-earth DEM (right). Orthoimage provided by Valtus Imagery Services.

Data Layers Available for the EMEND Study Area

Hydrographic Networks. Collected at 1:500,000 scale, provincially recognized water *Base Waterbody* features (HYDPOL) in the form of lakes and double-line river polygons as well as *Single Line Hydrography Network* features (SLNET) were provided by the Government of Alberta's Sustainable Resource Development, Resource Information Management Branch (RIMB). The HYDPOL layer comprises seamless provincial extent hydrography polygon features collected from various sources of provincial base and resource map data and some federal topographic data, and is intended as a GIS ready hydrography polygon base layer to support business applications and decision making related to water bodies and major water courses in Alberta (Base Waterbody Polygon.xml metadata, 2004). The SLNET dataset contains all captured single line representation of hydrographic features and was designed to provide users with a connected network of single line hydrography (Base Stream and Flow Representation.xml metadata, 2000).

The Alberta Vegetation Inventory (AVI). This photo-derived digital inventory developed to identify the type, extent and conditions of vegetation (AVI online metadata, retrieved August, 2017), was used to develop a binary upland/wetland inventory (AVI-uplands). Derived from the ecosystem classification system developed by Corns and Annas (1986) and Beckingham et al. (1996), the AVI-uplands layer is intended to identify wetlands and uplands at 10 metre resolution. **The "Derived Ecosite Phase v.1" dataset** (DEP v1 Manual 2017). This datalayer provides a framework to group ecological sites and site phases based on Alberta Vegetation Inventory (AVI) and LiDAR-derived datasets.

Bare-earth and full-feature LiDAR DEMs at 1 m resolution. The EMEND area was LiDAR surveyed in August 2008 by Northwest Geomatics Group, using a Leica ALS 50-II LiDAR system, with a stated minimum total point density of 2 points/m^2, with a vertical accuracy of +/- 30cm. Vendor-classified ground returns were interpolated to generate bare earth DEM rasters as well as full feature DSM rasters at 1 metre resolution.

SRTM DEM data at 30 m and 90 m resolution. A 3 arc-second SRTM v4.1 dataset (tile 13_01) covering 5 x 5 degrees, was downloaded from http://srtm.csi.cgiar.org. Using ArcGIS, these data, natively delivered in 3 arc-second spatial resolution, were transformed from the geographic WGS84 coordinate system to projected NAD83 coordinate system at 90 metre spatial resolution. Rodriguez et al. (2005) assessed absolute vertical accuracy of 3 arc-second SRTM data as +/- 9.0 m from GPS reference elevations in North American locations tested.

A 1 arc-second SRTM v3 dataset (tile n56_w119) covering 0.5 x 0.5 degrees, was downloaded from https://earthexplorer.usgs.gov. Using ArcGIS, these data, natively delivered in 1 arc-second spatial resolution, were transformed from the geographic WGS84 coordinate system to projected NAD83 coordinate system at 30 metre spatial resolution. Elkhrachy (2007) assessed overall vertical accuracy of 1 arc-second SRTM data as +/- 5.94 m from GPS reference elevations.

Orthoimage base layers. The Valtus - Views image service, hosted by Valtus Imagery services and accessed through a protected WMS service, was used as the base imagery

layer for this project. Used with permission, and only for qualitative assessments and site descriptive purposes, these layers were not used to inform any analysis.

3.3 Acadian Forest Study Area: UNB Forest

The University of New Brunswick (UNB) Forest is part of the Atlantic Maritime Ecozone (ESWG, 1995). A research and teaching forest managed by the Faculty of Forestry and Environmental management, the UNB Forest is, located at about 150 m above the Saint John River flow channel at Fredericton, New Brunswick. It has grown on undulating to gently rolling terrain with hills and ridges. Soils on top of sandstone and siltstone formations are shallow covered by till grading from ablation to basal (Stobbe, 1940; Wicklund and Langmaid, 1949). The forest vegetation varies in its mixture from sugar maple (*Acer saccharum*), red maple (*Acer rubrum*), white birch (*Betula papyrifera*) and yellow birch (*Betula alleghaniensis*), balsam fir (*Abies balsamea*), black spruce (*Picea mariana*), red spruce (*Picea rubens*), eastern white cedar (*Thuja occidentalis*) and Eastern hemlock (*Tsuga Canadensis*) (ESGW, 1995).

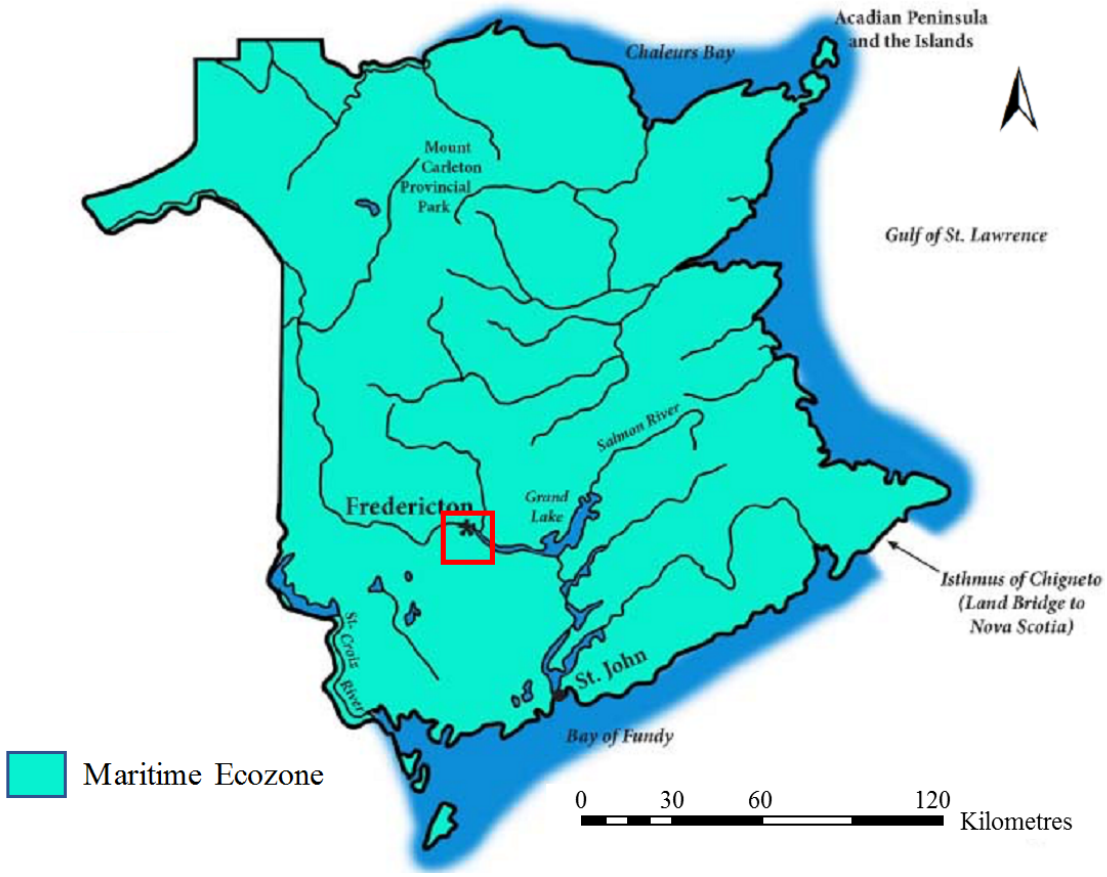

Figure 21. Provincial locator map for the UNB Forest study area. Extent of the UNB Forest study area shown in red outline

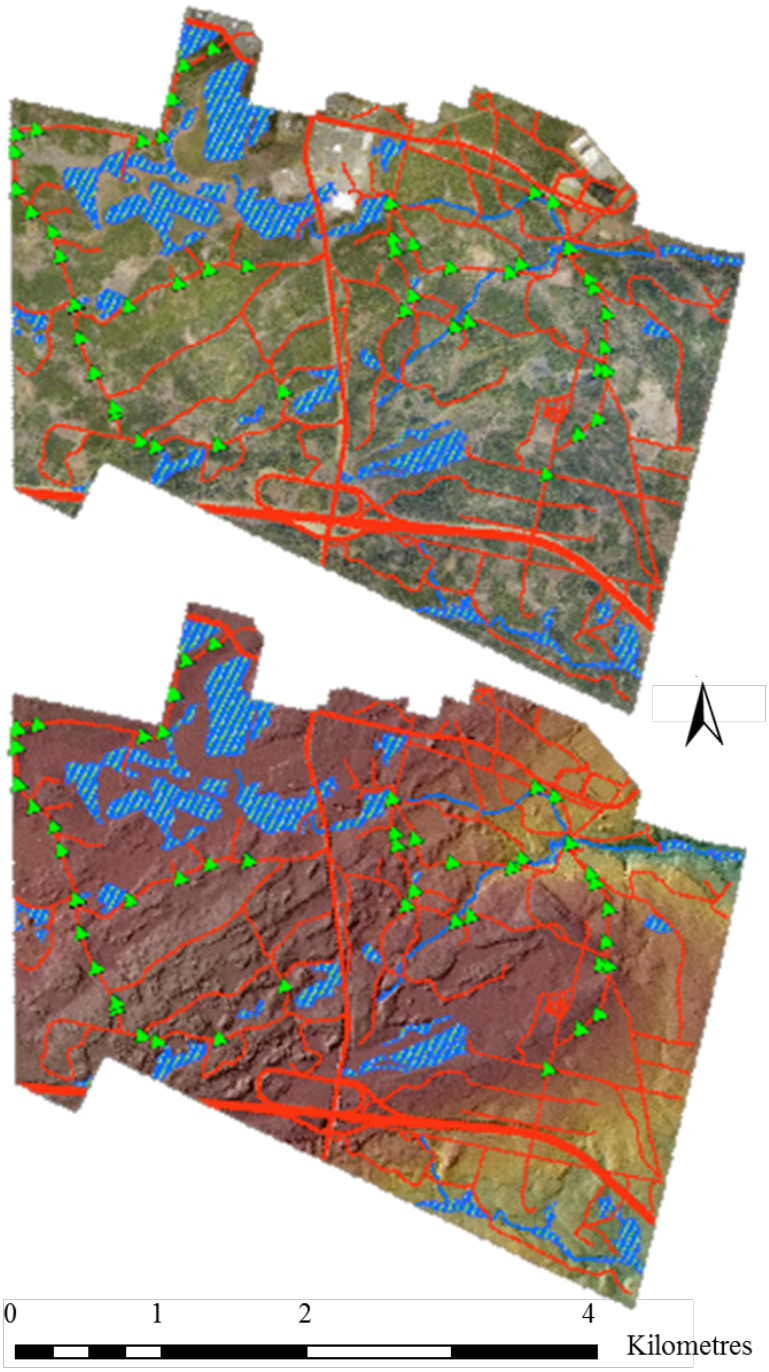

Figure 22. Landscape characteristics of the UNB Forest study area. Mapped roads (red lines), provincially-mapped water features (light blue polygons) and streams (blue lines) and road-stream crossings (green triangles) overlaid on orthoimage (left) and bare-earth DEM (right). Orthoimage provided by GeoNB.

Data layers available for the UNB Forest Study Area

The New Brunswick Hydrographic Network (NBHN). This network defines surface drainage features including rivers, streams, lakes, islands, wetlands, and watershed boundaries for the province of New Brunswick, all delineated from province-wide collections of orthophotos. The NBHN waterbody (polygon) and watercourse (line) geometry contain an inventory of all provincially observed lakes, rivers and streams (NBHN_0000_01_wc.xml metadata). The wetland polygons layer draws on data from a number of reference datasets intended to identify areas where the water table is at or near the surface and the land is covered by shallow water at some time during the growing season (NBHN_0000_01_wl.xml metadata). In addition, the provincial forest inventory database contains forested stands (polygons) that have been classified as wetlands.

Bare-earth and full-feature LiDAR DEMs at 1 m resolution. These data were collected in August 2014 by Leading Edge Geomatics, using a Riegl LMS Q780 LiDAR system, with a stated nominal ground density of 1 point/m^2, with a vertical accuracy of +/- 15cm. Vendor-classified ground returns were interpolated to generate bare-earth DEM and full-feature DSM rasters at 1 m resolution.

SRTM DEM data at 30 m and 90 m resolution. A 3 arc-second SRTM v4.1 dataset (tile 23_02) covering 5 x 5 degrees, was downloaded from http://srtm.csi.cgiar.org. Using ArcGIS, these data, natively delivered in 3 arc-second spatial resolution, were transformed from the geographic WGS84 coordinate system to projected NAD83 coordinate system at 90 metre spatial resolution. Rodriguez et al. (2005) assessed absolute vertical accuracy of 3 arc-second SRTM data as +/- 9.0 m from GPS reference elevations in North American locations tested.

A 1 arc-second SRTM v3 dataset (tile n45_w067) covering 0.5 x 0.5 degrees, was downloaded from https://earthexplorer.usgs.gov. Using ArcGIS, these data, natively delivered in 1 arc-second spatial resolution, were transformed from the geographic WGS84 coordinate system to projected NAD83 coordinate system at 30 metre spatial resolution. Elkhrachy (2007) assessed overall vertical accuracy of 1 arc-second SRTM data as +/- 5.94 m from GPS reference elevations.

Orthoimage base layers. The GeoNB_Basemap_Enhanced_Imagery image service, hosted by Service New Brunswick and accessed through ArcGIS Online, was used as the base imagery layer for this project. Used only for qualitative assessments and site descriptive purposes, these layers were not used to inform any analysis.

CHAPTER 4

LOCATING AND CONFORMANCE TESTING OF MODELED FLOW LINES

4.1 Introduction

The objective of this chapter is to determine, in quantitative terms, the extent to which DEM-derived predicted flow lines conform to GPS-tracked flow channel locations on forested land, and how this varies by DEM spatial resolution and DEM source, i.e., LiDAR DEM at 1, 10 and 30 m versus SRTM at 30 and 90 m spatial resolution. This is done for two geographically contrasting forest locations: EMEND, representing boreal forest conditions on flat terrain; centered on ephemeral and low order intermittent flow channels (Chapter 3.2), and the UNB Forest, representing maritime Acadian forest conditions, centered on intermittent and low order permanent flow channels (Chapter 3.3). The hypothesis is that bare earth LiDAR DEM at 1 m spatial resolution is best for locating and topographically delineating ephemeral flows with low upslope flow contributing areas. However, DEM-registered elevation obstructions across flow channels due to roads, beaver dams, and vegetation overgrowth or debris can artificially modify flow directions and upslope flow accumulation, thereby obscuring DEM-based flow path delineations unless the DEMs are properly hydro-conditioned (Chapter 2). The need for DEM hydro-conditioning increases with DEM resolution due to the increasing number of DEM-registered flow blockages.

4.2 Methodology

GPS tracking of flow lines

Flow lines were GPS-tracked along readily discerned channels, whether dry or water-filled; each revealed by channel-patterning hydrophytic vegetation (e.g., sedges, sphagnum mosses) and/or bare-earth exposure. This was done at the EMEND study area in June, 2012, and the UNB Forest in August, 2017. GPS-tracking was done using hand-held GPS devices (Magellan Mobile Mapper CX and Garmin GPSMAP 60x), with nominal position accuracies of 2-3 m and <10 m respectively, on open terrain. Ephemeral draws were defined by slight vegetation change towards hydric species. Ephemeral to intermittent flow channels were defined by direct flow-channel recognition (bare-ground exposure along channel < 50 cm wide), with no requirement for the presence of water at the time of classification. Permanent flows were defined by moderate to strong channelization > 50 cm wide. The selection of the EMEND field site shown in Figure 23 (right, yellow box) in the lowlands of the larger EMEND area was made such that wetland complexes (Chapters 5, 6 and 7) and their flow connectivities (Chapter 4) could be examined within an area of relatively low relief. The selection of the UNB Forest field site shown in Figure 24 was made where the contrasting influence of more incised, higher order permanent flows and their associated wetlands could be explored.

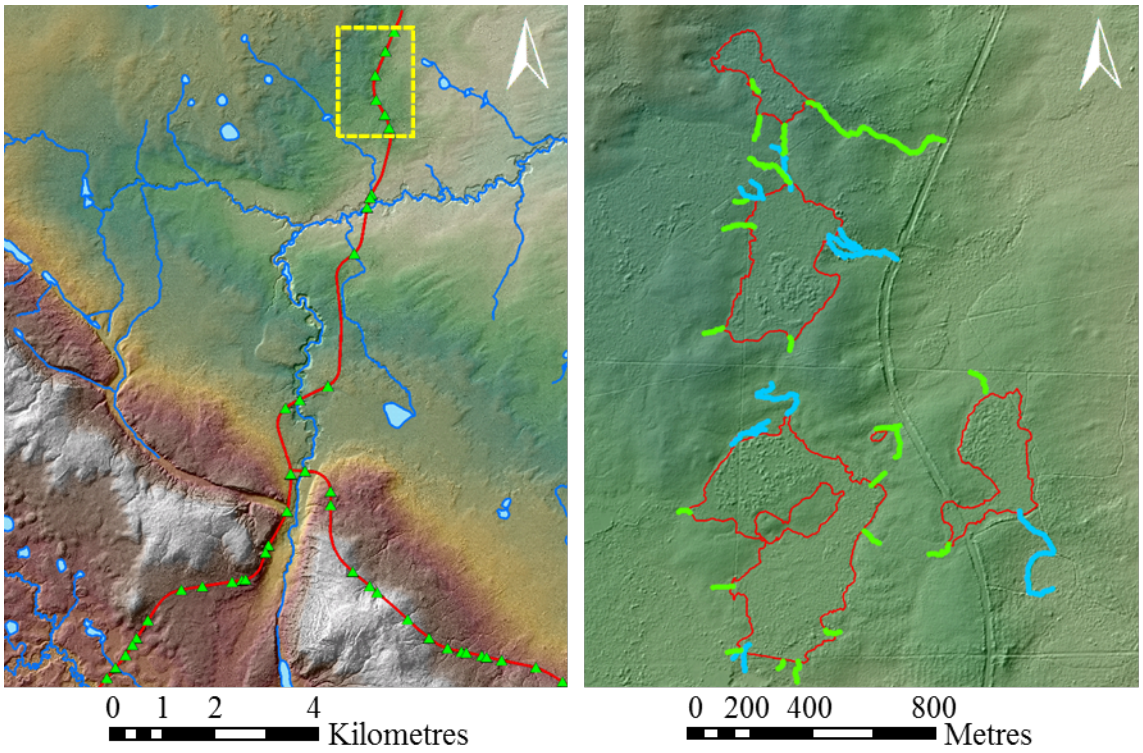

Figure 23. Locator map for EMEND (left), with close-up for yellow box (right). Left: provincial flow lines (blue), roads (red), culverts (green). Right: Field site with GPS-tracked flow lines (ephemeral green; intermittent blue) flow lines and wetland borders (red).

Within the EMEND study area, 3.8 km of flow lines were mapped, with 50% (1.9 km) of the flow-line segments classified as ephemeral, and 50% (1.9 km) of segments classified as intermittent. Within the UNB Woodlot study area, 6.9 km of flow lines were mapped, with 94% (6.5 km) of the flow-line segments classified as permanent, and 6% (414 m) classed as intermittent.

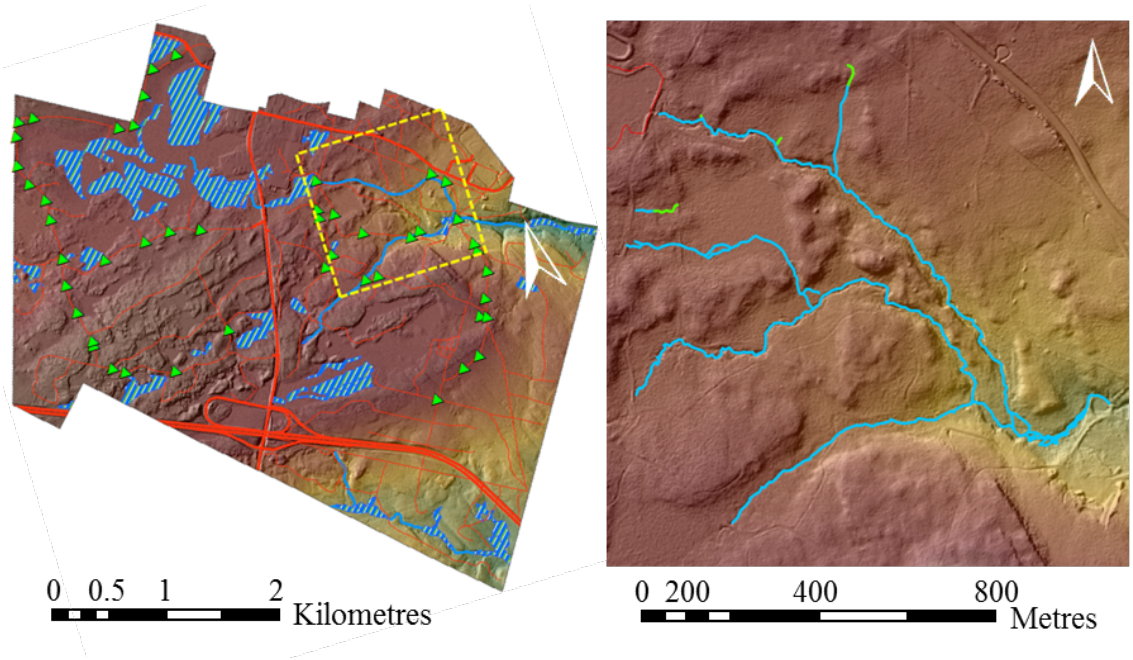

Figure 24. Locator map for UNB Forest (left), with close-up for the yellow box (right) Left: provincial flow lines (blue), roads (red), and wetland features (blue to white hashing). Right: Field site with GPS-tracked flow lines (ephemeral: green; intermittent to permanent: blue).

Predicted flow-line generation for conformance testing

For each of the DEM sources (SRTM 90 m, SRTM 30 m, LiDAR 30 m, LiDAR 10 m, and LiDAR 1 m), input elevation rasters were hydro-conditioned via depression breaching. Predicted flow lines were generated at 0.5, 1, 2, 4, 8 and 16 ha flow initiation thresholds (as outlined in chapter 2). Field-mapped flow segments were termed "captured" (Figure 25) when located within 10 m of DEM-located flow-line.

To ensure consistency in conformance testing, vertices of GPS-tracked and DEM-located flow lines were densified to 1 m intervals and converted to (flow line) sample points, using ESRI's ArcGIS suite. Next, the distances between GPS-tracked and DEM-located nearest flow-line points were determined for each combination of LiDAR 1 m, 10 m and

30 m, SRTM 30 m and 90 m, at flow-line initiation thresholds of 0.5, 1, 2, 4, 8, 12, and 16 ha. Cumulative frequency distributions for the nearest distances between the GPS-track to DEM-delineated flow lines were subsequently generated in Microsoft Excel, at 1 m distance intervals, up to 100 m.

4.3 Results

Figure 25 (top) shows the influence of the upslope channel-initiation threshold on the nearest GPS-tracked to DEM-delineated flow-line point distances by channel type. For EMEND, 78% and 20% of all GPS-tracked flow-line points -respectively classified as intermittent and ephemeral - were located within 10 m of the DEM-delineated flow lines with the 4 ha threshold for upslope channel-initiation area. For the UNB Forest, the corresponding number increases from 87% to 99% of permanent-classified flow-line points as the threshold for upslope channel-initiation area decreases from 16 to 4 ha, respectively. Regarding intermittent-classified flows for the UNB Forest, the occurrence of matched GPS-to-DEM delineated flow-line points increases from 48 to 92% as the threshold for upslope channel-initiation area decreases from 4 to 0.5 ha. Figure 25 (bottom) shows how the GPS-to-DEM flow-line point matching process varies in proportion of the total number of points counted matching, by channel type, and in reference to the upslope channel-initiation area decreases threshold from 16 to 0.5 ha. The EMND versus UNB Forest differences so depicted are mainly due to (i) number of channel types selected for GPS tracking (mostly permanent for the UNB Forest, and limited to ephemeral to intermittent at EMEND), and (ii) terrain type (rugged with bare-

earth channel exposure within the UNB Forest, versus flat with limited bare-earth channel exposure at EMEND).

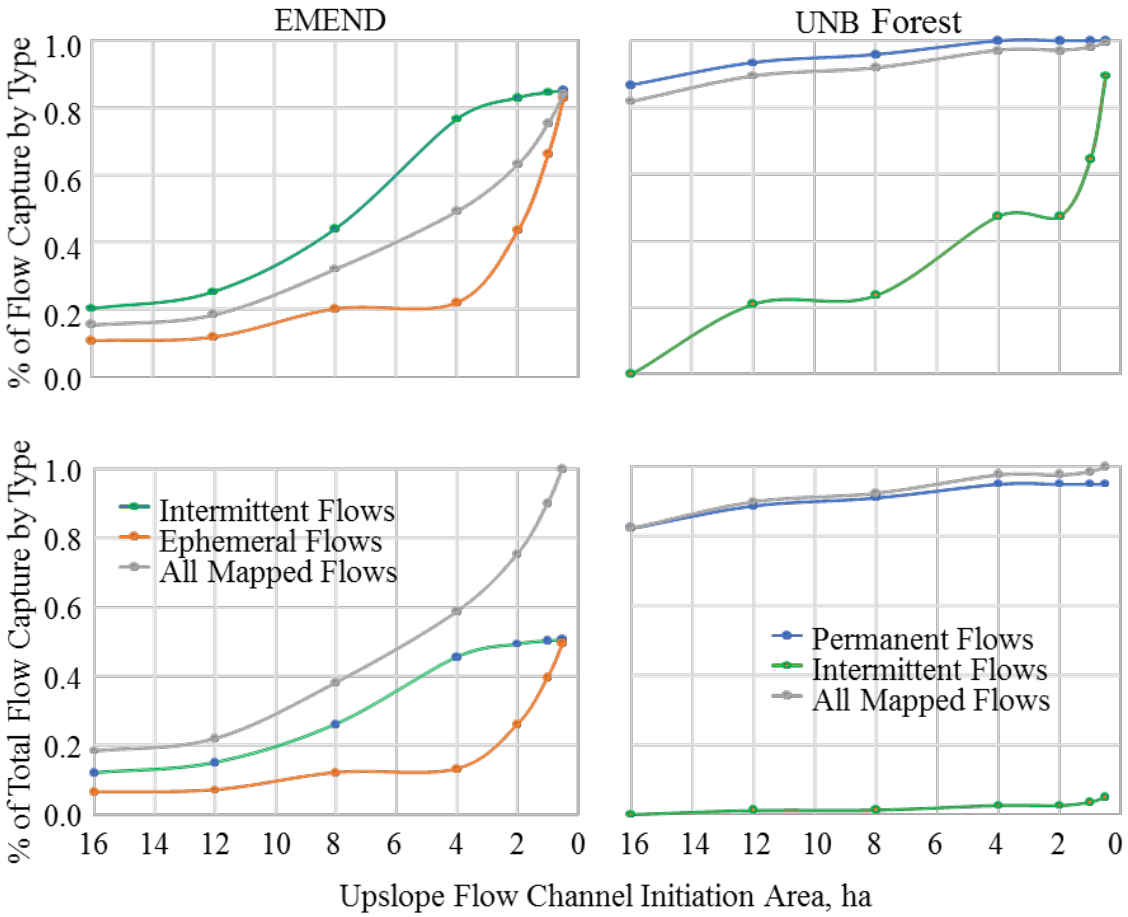

Figure 25. Percent occurrences of modeled flow-line points within 10m of GPS-tracked flow line points, by upslope contributing area, for LiDAR 1m.Upslope flow initiation, decreases left to right from 16 to 0.5 ha. Top: percent of matched occurrences by channel type. Bottom: percent of all < 10 m point-matched occurrences, by channel type. Left EMEND; right UNB Forest.

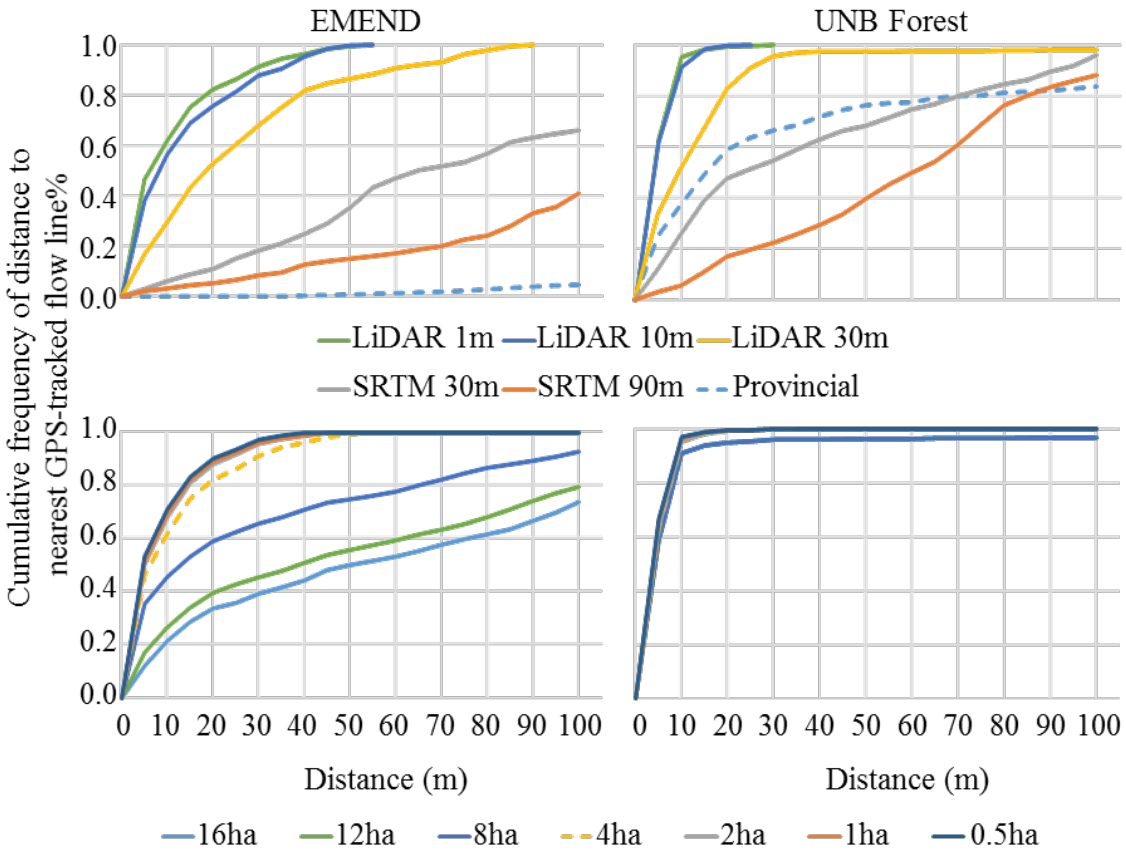

Figure 26. DEM-modelled versus GPS-tracked flow-line distance conformance for EMEND (left) and for the UNB Forest (right) locations, by DEM resolution (top; 4 ha upslope flow initiation area only), and by upslope flow-initiation areas (bottom; 1m bare-earth LiDAR DEM only).

Figure 26 (top) shows the influence of DEM source and spatial resolution on closest GPS-tracked versus DEM-modelled flow-line distance conformance. For example, the flow lines derived from the 30 m LiDAR DEM (down-sampled from the 1 m LiDAR DEM) matched the corresponding GPS tracks better than the lines derived from the 30 m SRTM DEM, by 50 and 41% for the EMEND and UNB Forest locations, respectively.

Figure 26 (bottom) shows that decreasing the threshold for upslope flow-line initiation from 4 to 0.5 ha increases the overall GPS-versus-DEM within 10 m flow-line

conformance with 8% and < 1% increases for the EMEND and UNB Forest locations. For EMEND, however, modelled to GPS-tracked conformance decreases by 22%, 42% and 46% as the threshold for upslope flow initiation is set to increase from 4 to 8, 12 and 16 hectares respectively. At the UNB Forest study area (lower right), there is little change in this regard, with 96 to 92% of the GPS- and DEM-mapped flow-lines remaining within 10 m of each other as the flow-initiation threshold increases from 0.5 to 16 ha.

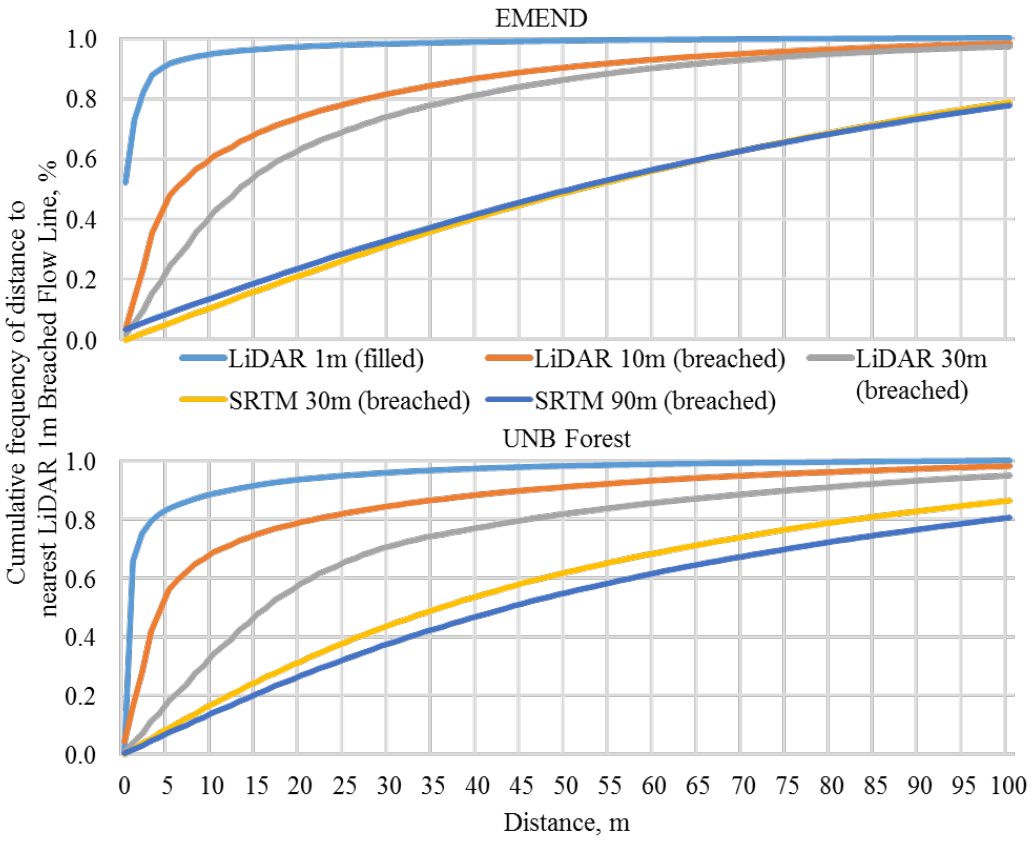

Figure 27. DEM-modelled flow-line distance conformance relative to "Optimal" flow line delineation (LiDAR 1m, 4 ha, Breached) for EMEND (top) and for the UNB Forest (bottom) locations.

Figure 27 assesses the variation of modelled flow lines, all at 4 ha flow contributing area, as they relate to conformance relative to the "optimal" flow network delineations (LiDAR

1m-based with breached hydro-conditioning) shown in Figure 25, with 84% of all LiDAR 1m (filled) flow lines within 5 m of breached counterparts and steady declines in conformance with increasing DEM resolution, even when breaching hydro-conditioning methods are applied.

4.4 Discussion

The above results show that the best DEM-derived flow-line delineations are achieved when using LiDAR DEMs of 1 m resolution (Figure 26). To capture permanent and intermittent flow channels, it is best to set threshold for upslope flow-initiation area at 4 ha. The DEM-delineation of GPS-tracked ephemeral flow channels also leads to within 10 m flow-line matching, but requires reducing the upslope flow-initiation area to 1 ha and 0.5 ha (Figure 25). The extent of this conformance, however, could not be achieved without using the WAM-developed DEM breaching algorithm in Chapter 2. Without the implementation of the depression breaching algorithm, overall GPS-to-DEM flow-line matching deteriorates considerably due to an overall inability to DEM-delineate flow-lines connectivity across un-breached DEM flow blockages such as roads with culvert installations, across non-flooded beaver dams, and elevation noise that dampens the meandering of flow lines within floodplains (Chapter 2). Decreasing the DEM resolution lowers the breaching requirement but at the cost of lowering the GPS-to-DEM flow-line delineation conformance (Figure 27).

The primary benefit of DEM-based flow-line delineation using laser-based altimetry methods (i.e., LiDAR) is the ability to classify and interpolate a “bare-earth” surface. Although still imperfect, LiDAR-derived bare-earth elevation surfaces produce better and

more detailed ground elevation representation then can be attained with other less canopy-penetrating digital surface models (DSMs), such as the SRTM-DEMs. In detail, the vertical SRTM data accuracy is ±5.94 m (Elkhrachy, 2017), i.e., considerably lower than the LiDAR based vertical accuracies of ±30 and ±15 cm for the EMEND and UNB Forest LiDAR data, respectively. In addition, the SRTM data do not reflect bare-earth elevations where the ground is forest covered, and much of the topographically defining flow-line locations can only be crudely represented by straight lines either along or diagonal to the 30 and 90 m grid cells.

Since the above GPS-to DEM-based flow-line derivations were not done across areas with similar ephemeral to permanent flow-channel coverage, no inferences should be drawn from EMEND versus UNB Forest flow-line conformance results by upslope flow-initiation area. For the most part, the differences are simply due to focusing only on small flat versus rugged terrain conditions within the much larger EMEND and UNB Forest areas. White et al. (2015) noted that area dissections into subsequently smaller upslope flow-initiation requirements yields a geometric increase in channel density such that

$$\log_{10}(\text{stream density, ha}^{-1}) = 2 - 0.5 \log_{10}(\text{flow threshold, ha}).$$

That being the case, care must be taken to ensure that contrasting study areas each contain a similar mix of permanent/intermittent/ephemeral and channel types.

Figure 27 explores both (i) the differences in conformance levels associated with filling versus breaching of LiDAR 1m DEMs and; (ii) the influence of DEM spatial resolution on modeled flow line conformance. Although 84% of all flow lines generated by filling were within 5 m, the remaining 16% of modeled flow lines show significant deviation

from breached flow lines with 8% of modeled flows > 20 m. As illustrated in Chapter 2, Figure 7, these zones of greater disparity tend to be associated with large impoundments where more advanced hydro-conditioning techniques, such as road-specific breaching allow improvements to the topographically-modeled flow paths. Between the EMEND and UNB Forest study areas, similar trends are evident; with decreasing conformance as DEM spatial resolution increases. Interestingly, the influence of DEM source technology is also apparent, with both SRTM 30 m and SRTM 90 m modeled flow lines attaining similar conformance levels, regardless of their differences in spatial resolution.

CHAPTER 5

DEM-BASED WETLAND DELINEATION

5.1 Introduction

In principle, it should be possible to locate wetlands in forested landscapes from digital bare-earth elevation models (DEMs). Generally, wetlands occur in depressions, tend to be relatively flat, or come in the form of raised bog (or peat plateaus) on otherwise level land. With LiDAR-generated bare-earth DEMs, these features to come in full view, as shown in Chapter 2. There are, however, difficulties in determining whether the last laser pulse returns of the LiDAR point cloud data actually represent true bare-earth elevations. This is particularly the case for forested areas and wetlands with dense ground vegetation cover. Across wetlands, raised bogs appear as somewhat elevated cone clusters in hill-shaded 1 m LiDAR DEMs, due to their raised mats of thick peat. As a result, the topographically-derived wet areas mapping process interprets raised bogs and peat plateaus to be well drained uplands. Bare-earth DEMs must therefore be hydro-conditioned to allow the DEM-based flow accumulation process to work properly towards and away from with wetlands with raised bogs. This hydro-conditioning is necessary in order to conform to the following wetland classification requirements in principle: (i) wetland soils need to be hydric, i.e., are subject to very poor to poor drainage, with water tables at or near the surface year-round; (ii) wetland vegetation needs to be hydrophytic, i.e., is able to grow in soils with severe to total soil aeration restrictions; (iii) wetlands need to be in water-accumulating and -retaining areas with topographic and pedologically defined flow restrictions. For example, fine-textured soils located within depressions have

low to no permeability and therefore remain wet year-round, although the water table within these depressions may fluctuate according to the hydrological balance between water inflow, outflow, and evapotranspiration.

The objective of this chapter is to demonstrate that LiDAR-generated point cloud data can be used to locate wetlands in a systematic fashion. The hypothesis is that (i) hydrophytic vegetation characteristics can be DEM-located and -delineated across LiDAR-DEMs by their low and fine- to-coarse-textured surface. In doing so, the DEM-delineation needs to be guided reliably to automatically select depressions and flat low-lying areas, with each requiring at least 4 ha of upslope flow-contributing areas (Murphy et al., 2009). This chapter illustrates and analyzes the process of DEM-based wetland delineation by examining the effects of DEM resolution and DEM source (LiDAR or SRTM). Two case study areas are chosen to conduct this analysis: one within the boreal forest zone in Northern Alberta at EMEND north of Peace River Alberta, and one within the maritime Acadian Forest zone within the UNB Forest in Fredericton, New Brunswick. The results of this delineation are systematically compared with the corresponding GPS-tracked borders within the context of: (i) incorporating the hydropytic DTW=0 seeding process on LiDAR 1m DEMs (Chapter 2); (ii) changing DEM resolutions using LiDAR-derived DEMs at 1, 10 and 30 m resolution, and SRTM-DEM resolutions at 30 and 90 m resolution, and; (iii) increasing the DTW threshold for the DEM-derived wetland borders from 10 cm to 2 m.

The resulting changes in false positive and false negative wetland area classification and the resulting nearest point distances between the GPS- and DEM-tracked wetland borders are documented in terms of varying the DTW thresholds from 10 cm to 2 m.

5.2 Methodology

GPS-tracking of wetland borders

Select wetland borders were GPS-tracked during the summers of 2012 and 2017 using hand-held GPS devices (Magellan Mobile Mapper CX and Garmin GPSMAP 60x) with position accuracies of 2-3 m and < 10 m in open terrain, for the EMEND and UNB Forest areas respectively. The borders of the ground-validated wetlands, i.e., bogs, swamps and fens, were tracked based on abrupt transitions from hydrophytic to non-hydrophytic vegetation, from hydric to mesic soil moisture regimes, and from flat to rising elevation. Soil pits were dug, and soil moisture readings including depth-to-water were taken to confirm the transition from hydric to soil moisture regimes (Beckingham et. al. 1996; Gunter et al (2004); Murphy et al. (2009) and each site classified according to the Canadian Wetland Classification System (CWCS).

Within the EMEND study area, 5 wetlands ranging from 0.1 to 23.8 ha were GPS-tracked (Figure 28). Mean wetland size was 6.7 ha, with 47.1 ha mapped in total. These wetlands consisted of three raised bogs surrounded by horizontal fens, one swamp and one small linked-basin marsh. Within the UNB Woodlot Forest, 5 bogs ranging from 1.0 to 5.4 ha (Figure 29) were GPS-tracked. These wetlands consisted of 4 marshes and one basin bog. Mean wetland size was 3.6 ha, with 14.4 ha mapped in total.

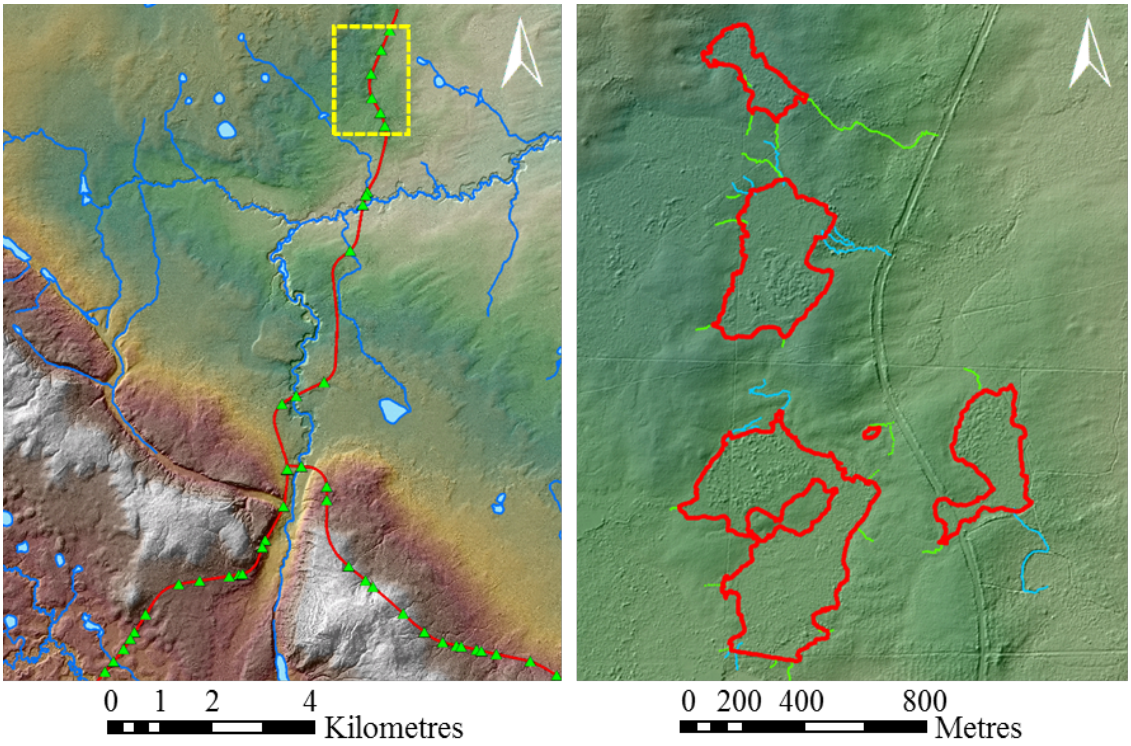

Figure 28. Locator map for EMEND study area wetland border tracking. Left: Locator map for EMEND area, showing provincially mapped stream channels (blue), road (red), and culvert installations across roads (green), with yellow box outlining the GPS-tracked wetland area. Right: Close-up of the field site with GPS-tracked wetlands in red, with ephemeral and intermittent flow-lines in green and blue, respectively.

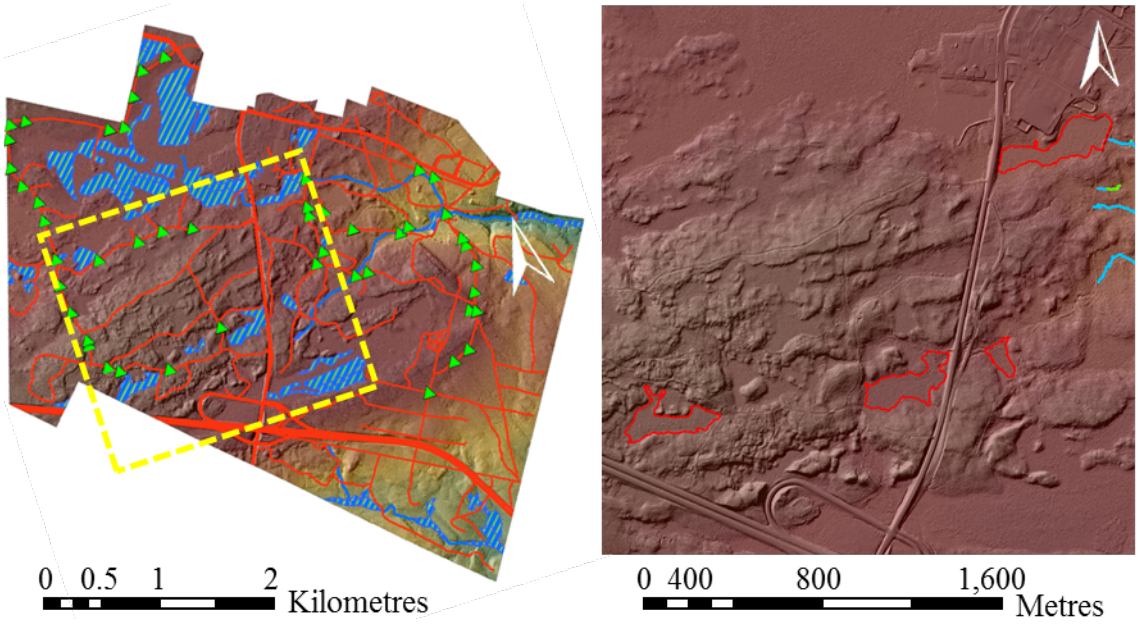

Figure 29. Locator map for UNB Forest study area wetland border tracking. Left: Locator map for UNB Forest area, showing provincially mapped stream channels (blue), wetlands (hashed blue), roads (red), and culvert installations across roads (green), with yellow box outlining of GPS-tracked wetland area. Right: Close-up of the field site with GPS-tracked wetlands in red, with intermittent and permanent flow lines in green and blue, respectively.

DEM-based wetland border delineation

For each of the DEM sources (SRTM 90 m, SRTM 30 m, LiDAR 30 m, LiDAR 10 m, and LiDAR 1 m), predicted flow lines were generated at 0.5, 1, 2, 4, 8 and 16 a upslope flow-initiation area thresholds for the DTW derivation algorithm, as described in Chapter 2. This involved using the 1 m bare-earth DEMs with and without hydrophytic DTW = 0 seeding (HDS). For each DTW raster output, the continuous DTW surface was classified in two-class "wet/dry" representations using DTW thresholds of < 25 cm to < 200 cm, in 25 cm intervals. The resulting DTW-classified wetland borders were overlaid on the GPS-

tracked wetland borders, for selecting the optimal wetland-border defining DTW threshold, and for determining the extent of false negative and false positive wetland areas inside and outside the GPS-tracked borders, respectively. The nearest point distances between the GPS-tracked and DTW-modeled wetland borders were determined systematically along 1 m intervals along DTW-modeled wetland boundaries. These points were also classified by noting whether they lay along false-negative or a false-positive wetland areas inside or outside the GPS-tracked wetland borders. The resulting nearest GPS- to DTW-modeled border distances were compiled and evaluated in terms of (i) boxplots with their 10 th, 25 th, 50 th, 75 th and 90th percentile distributions, and (ii) the correlations of among the GPS- to DTW-modeled border distances, by DTW-border threshold.

5.3 Results

The GPS-wetland border tracking results are overlaid in Figure 30 and Figure 31 on the orthoimages and color shaded relief 1 m DEMs of the EMEND and UNB Forest areas, respectively. In general qualitative terms, these tracks follow the image- and DEM-recognized wetland locations, with the areas inside border locations generally more homogeneous in vegetation composition and terrain conditions than the areas outside the border locations. Compared to the UNB Forest wetlands (Figure 31), raised bogs occur more frequently inside the EMEND study area as noted by the textured clusters within the wetland borders (Figure 30, right).

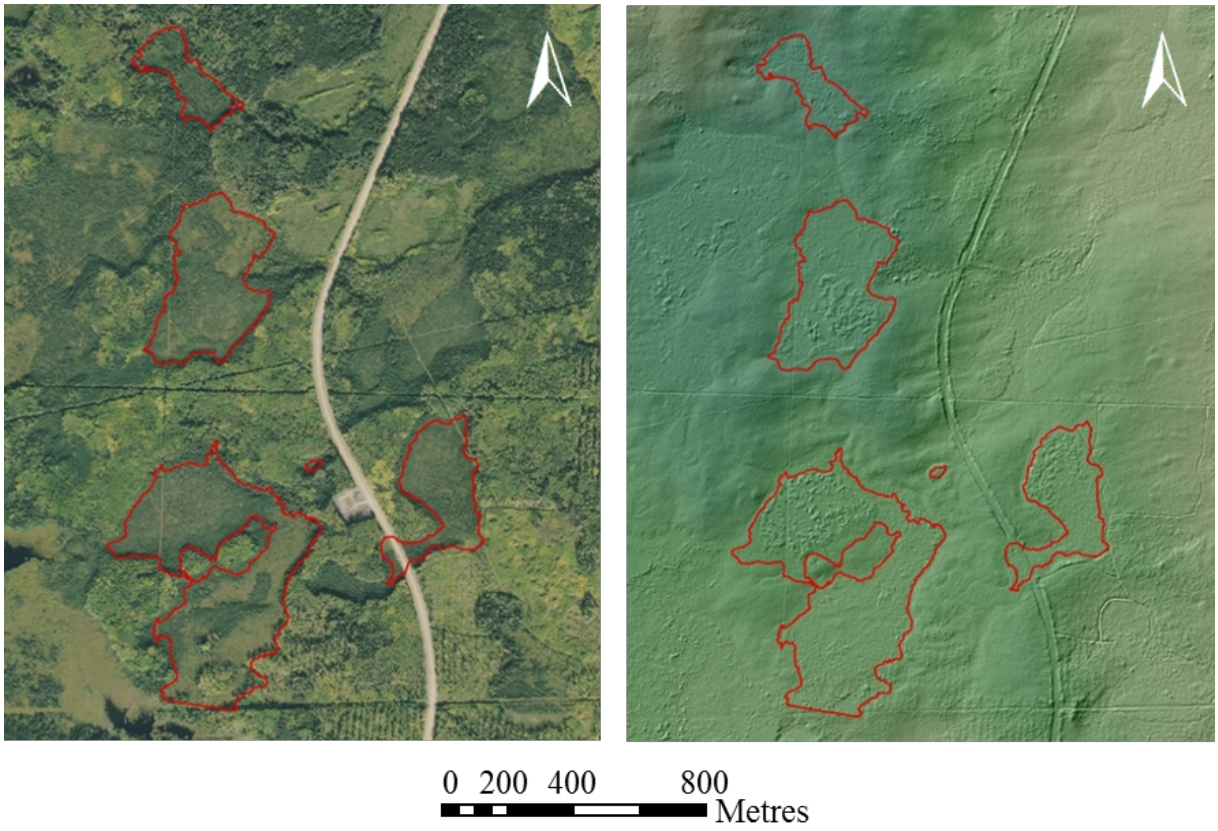

Figure 30. Bare Earth LiDAR DEM topographic pattern within wetlands at the EMEND study area. Overlay of the GPS-tracked wetland borders (red) at EMEND on surface orthoimage (left) and color shaded relief bare-earth LiDAR DEM (right, 1 m resolution).

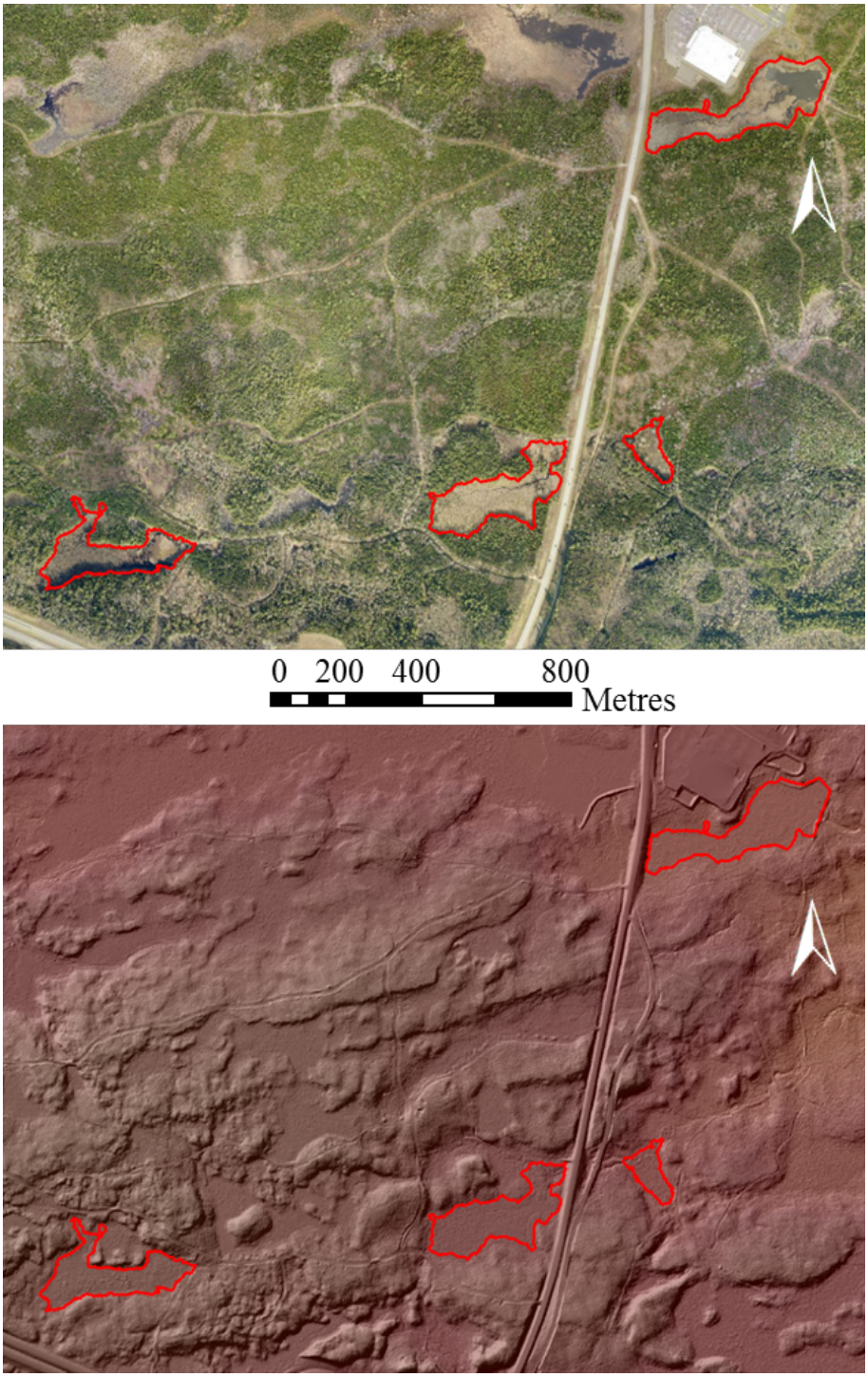

Figure 31. Bare Earth LiDAR DEM topographic pattern within wetlands at the EMEND study area. Overlay of the GPS-tracked wetland borders (red) at EMEND on surface orthoimage (top) and color shaded relief bare-earth LiDAR DEM (bottom, 1 m resolution).

The extent of hydrophytic DTW=0 seeding (HDS) and its subsequent influence on the DTW-based wetland border delineation process is illustrated in Figure 32 and Figure 33 for the EMEND and UNB Forest areas respectively. Due to the greater presence of raised bog features, the HDS influence is much stronger within the EMEND than the UNB Forest areas. Due to this HDS seeding, the DTW-delineations of the wetland borders are not only complete in terms of properly contouring the orthoimage and shaded relief-discerned wetland features, but also capture the gradual transitioning from the wetlands to their surrounding uplands. Within these DTW-graded transitions, the DTW < 25 cm HDS-delineated wetland borders are not only closest to the GPS-tracked borders, but also correspond well to the image-extent captured wetlands that were not GPS-tracked.

The influence on hydrophytic DTW=0 seeding (HDS) on the DTW-based wetland border delineation is further demonstrated in Figure 34 and Figure 35 for the EMEND and UNB Forest areas respectively. Without HDS, the extent of wetland areas are clearly under-represented, and more notably so for the EMEND than the UNB Forest areas. As a result, the gradual transitioning from the wetlands to their surrounding uplands, when delineated without HDS, is under-represented as well for the GPS-tracked and non-tracked wetlands in Figure 34 (left) and Figure 35 (top).

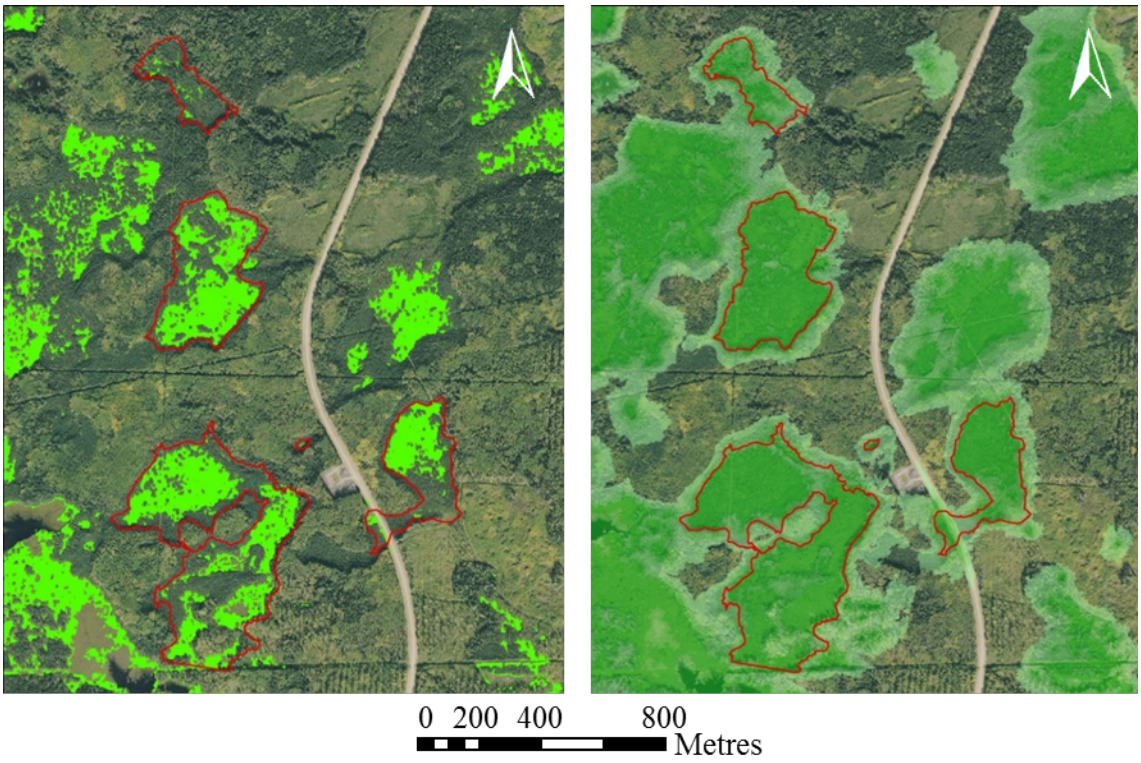

Figure 32. Hydrophytic seeded DTW for the EMEND study area. Left: EMEND hydrophytic DTW= 0 seed locations (bright green). Right: hydrophytically seeded DTW <10, <25, <50, <100 cm distribution (shaded dark to light green) generated from the 1 m LiDAR DEM. Background: orthoimage.

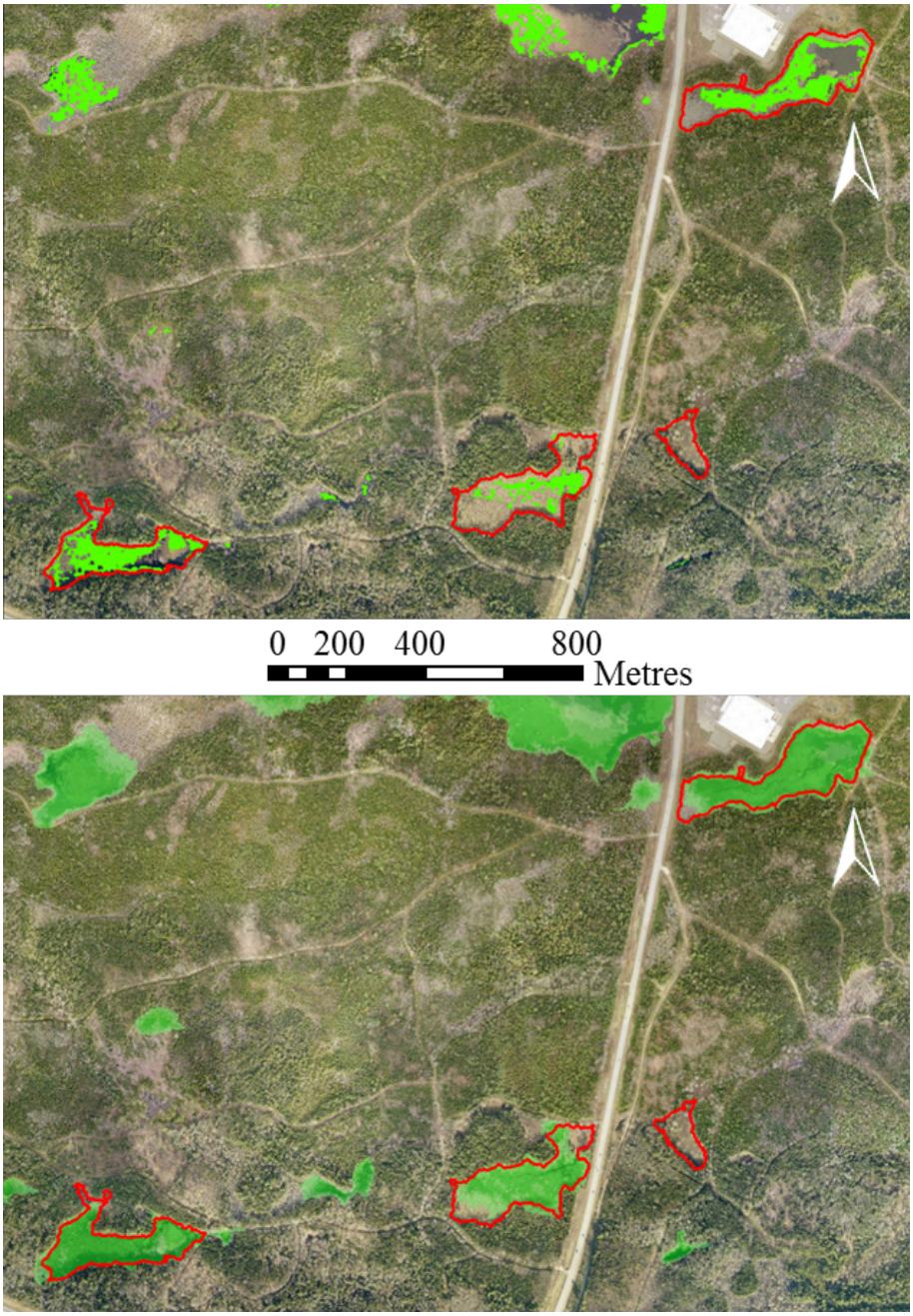

Figure 33. Hydrophytic seeded DTW for the UNB Forest study area. Left: UNB Forest hydrophytic DTW= 0 seed locations (bright green). Right: hydrophytically seeded DTW <10, <25, <50, <100 cm distribution (shaded dark to light green) generated from the 1 m LiDAR DEM. Background: orthoimage.

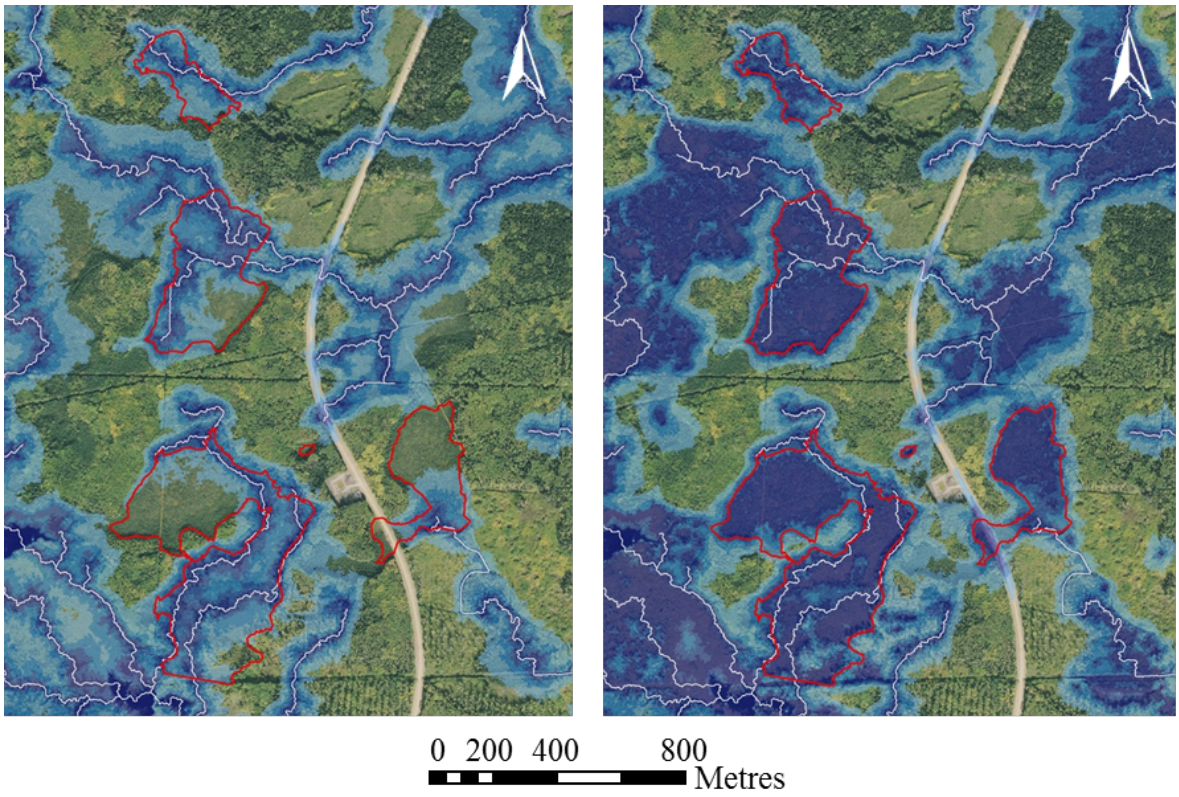

Figure 34. Influence of Hydrophytic Seeding on WAM results for the EMEND study area. EMEND overlay of GPS-tracked wetland borders (red) and DEM-delineated flow lines (white) on DEM-generated cartographic <10, <25, <50 and <100 cm depth-to-water pattern, shaded dark to light blue, respectively, without (left) and with (right) hydrophytic DTW=0 seeding. Note that wetland border conform best to the DTW < 25 cm area. Background: orthoimage.

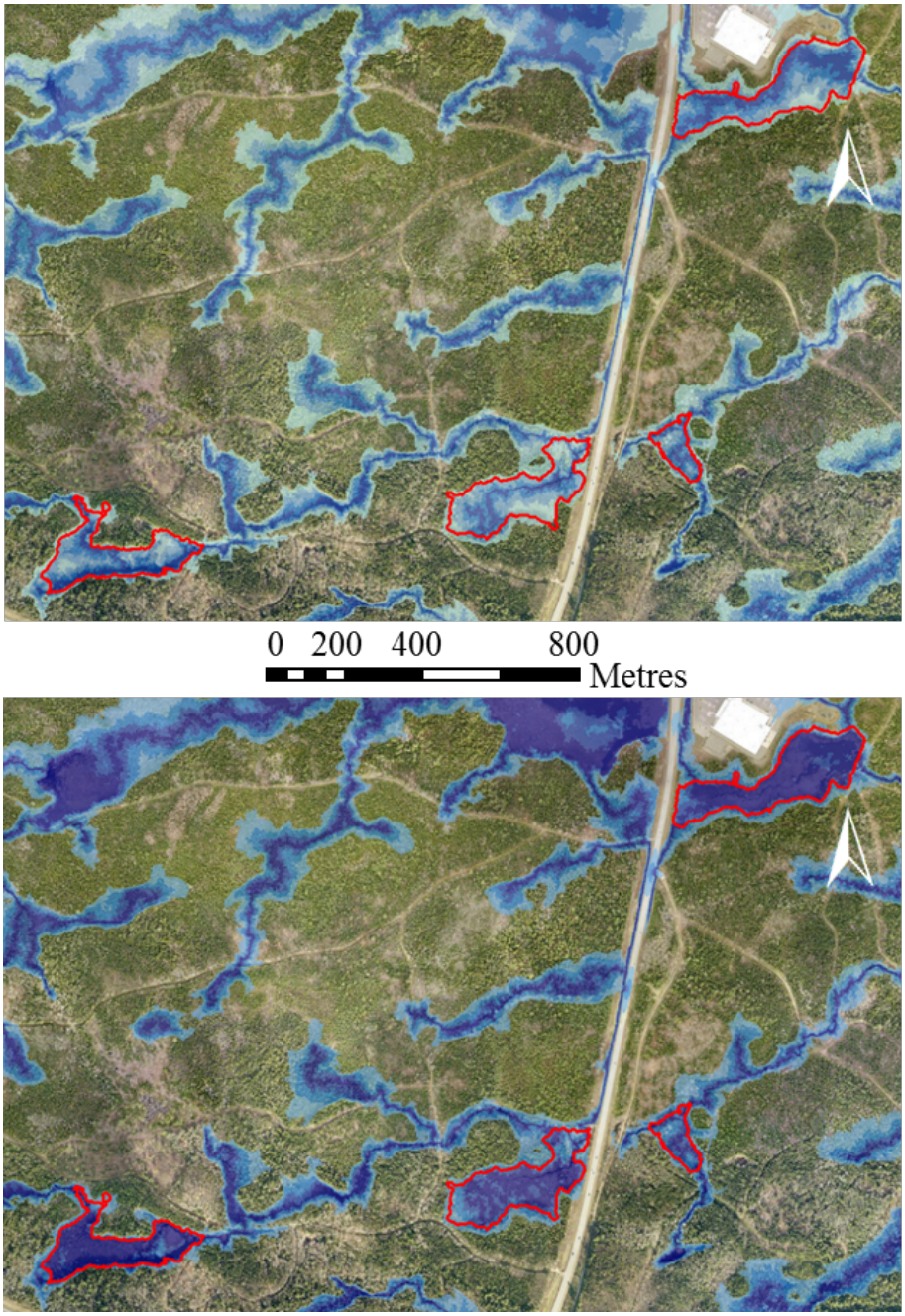

Figure 35. Influence of Hydrophytic Seeding on WAM results for the UNB Forest study area. UNB Forest overlay of GPS-tracked wetland borders (red) and DEM-delineated flow lines (white) on DEM-generated cartographic <10, <25, <50 and <100 cm depth-to-water pattern, shaded dark to light blue, respectively, without (left) and with (right) hydrophytic DTW=0 seeding. Note that wetland border conform best to the DTW < 25 cm area. Background: orthoimage.

Analyzing the GPS-versus 1 m LiDAR DEM-derived wetland border delineations more closely by varying DTW border threshold reveals that the nearest point distances between the GPS- and DEM-border delineations are the tightest for false-positive DTW-inferred wetland segments inside the GPS-tracked borders (Figure 36 - left). As the DTW-threshold increases from 25 cm to 2 m, the nearest inside false-positive distances start to level off with the nearest outside false-negative distances. Figure 36 (right) also show this by way of the correlation pattern between the nearest point distances generated with the DTW > 25 cm threshold on the y axis, and with the DTW ≤ 25 cm threshold on the x axis: here there are few points with distances > 20 m inside the GPS-tracked borders for the DTW ≤ 25 cm threshold, but the inside numbers increase steadily while the outside numbers decrease with each DTW > 25 cm class.

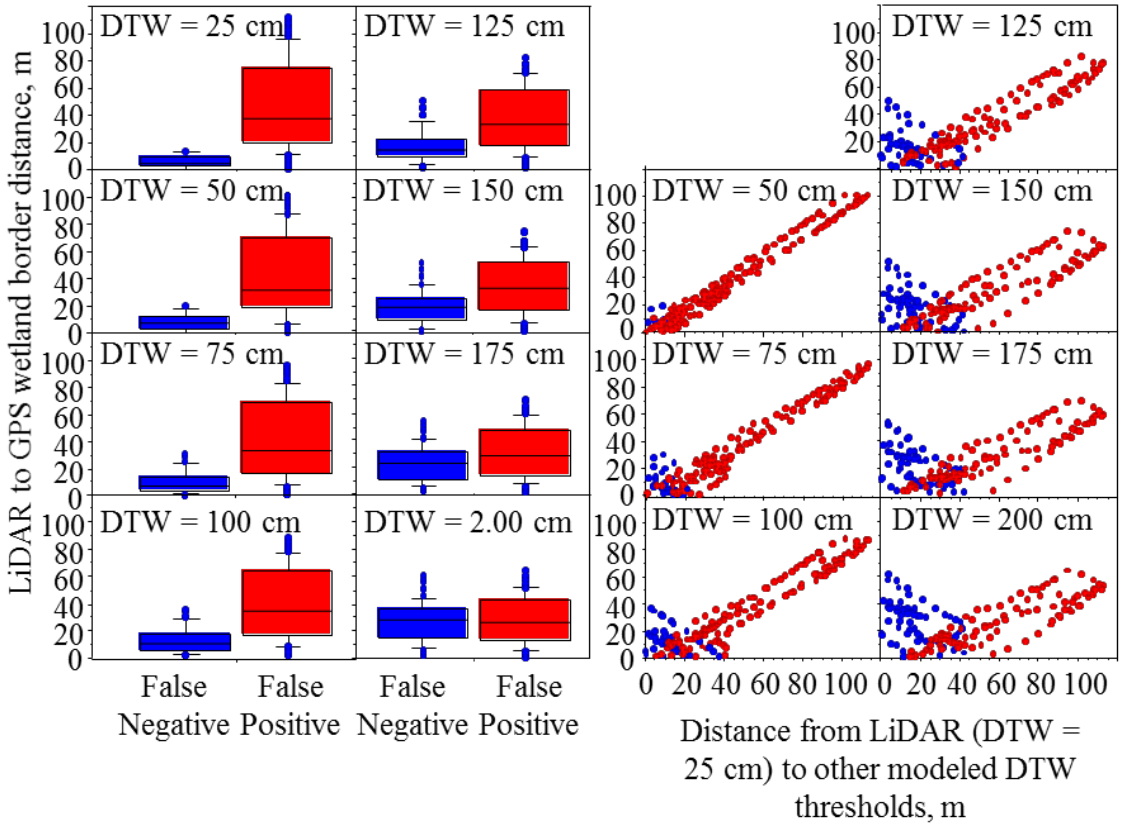

Figure 36. Boxplots (left) and scattergrams (right) of distances between DTW- and the GPS-tracked wetland borders. Generated by varying the DTW-defining wetland borders from 25 cm to 2 m, and grouped by false negative and false positive wetland areas inside (blue) and outside (red) the GPS –tracked borders.

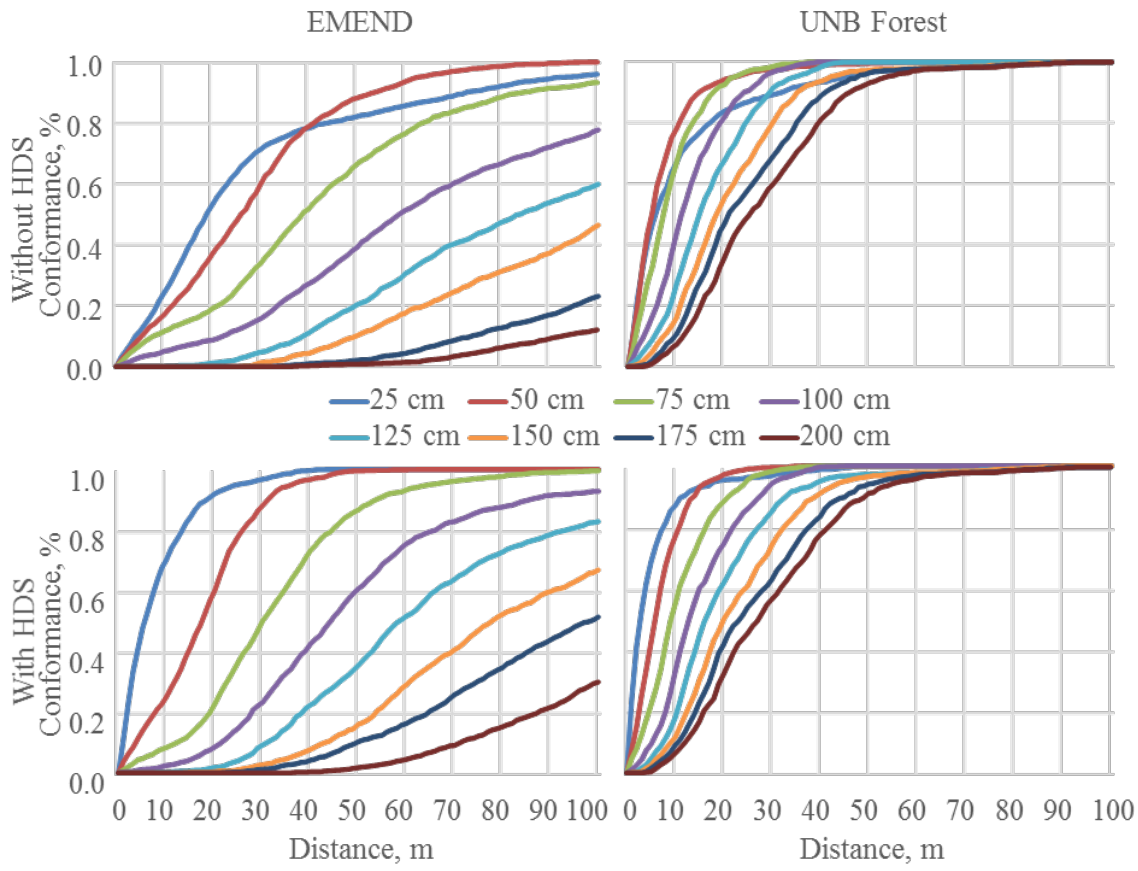

Figure 37 Conformance plots of GPS-tracked versus HDS non-HDS integrated WAM. Cumulative distance conformance for 1 m LiDAR DEM wetland borders by wetland-area defining DTW thresholds from 25 cm to 2 m without (top) and with (bottom) hydrophytic DTW seeding, assuming 4 ha for minimum upslope flow initiation area. EMEND left; UNB Forest right.

Figure 37 demonstrates how the wetland–border GPS-tracked versus the 1 m HDS-processed LiDAR- DEM delineated conformance levels vary by DTW thresholds from 10 cm to 2 m by plotting the percentage of the cumulative nearest point distances between the GPS-tracked and DEM-delineated wetland borders, for the EMEND and UNB Forest study areas. These plots suggest that the DTW = 25 cm appears to be optimal, with GPS-tracked versus DEM-delineated border distances conforming to ±12 and ±8 m for the EMEND and UNB Forest study areas, eight times out of 10.

While Figure 32 to Figure 37 refer to the close correspondence between the GPS-tracked and 1 m LiDAR-DEM delineated wetland borders, Figure 38 and Figure 39 depict how the DEM-based flow-channel and wetland-border delineations vary in comparison with the GPS-tracked borders by DEM resolution, for the EMEND and UNB Forest areas respectively. This is done in the following sequence: 1 m LiDAR-DEM with HDS, 1m LiDAR-DEM without HDS, 10 m LiDAR-DEM, 30 m LiDAR-DEM, 30 m SRTM, 90 m SRTM, all based on using the 4 ha threshold area for upslope flow-line initiation. The DEM-generated flow channels and associated wet-areas so delineated follow a similar pattern by location and flow direction. However, this is not the case for capturing the extent of actual wetland borders and areas. Essentially, only the HDS-seeded and the 1 m LiDAR DEMs with the DTW $\leq$= 25 cm threshold fills the GPS-tracked wetland borders in a reproducible manner across both the EMEND and UNB Forest areas.

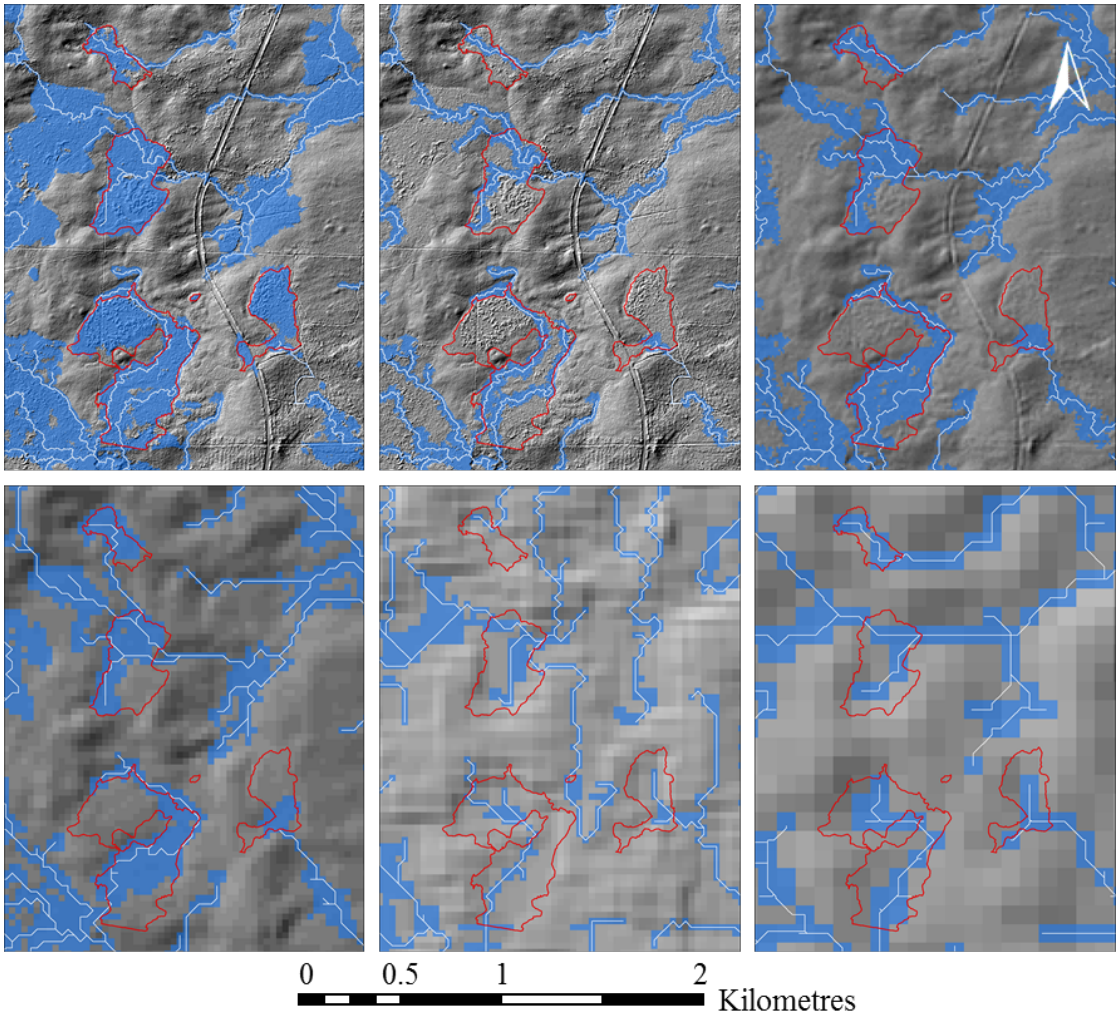

Figure 38. EMEND study area: binary DTW < 25 cm distribution, with > 4 ha of upslope flow accumulation areas, by DEM source, and with the GPS-tracked wetland borders overlaid (red). Top left and middle: LiDAR 1m, with and without hydrophytic DTW seeding. Top right: LiDAR-DEM10m. Bottom left: LiDAR-DEM 30m, Bottom middle: SRTM 30m, Bottom right: SRTM 90m.

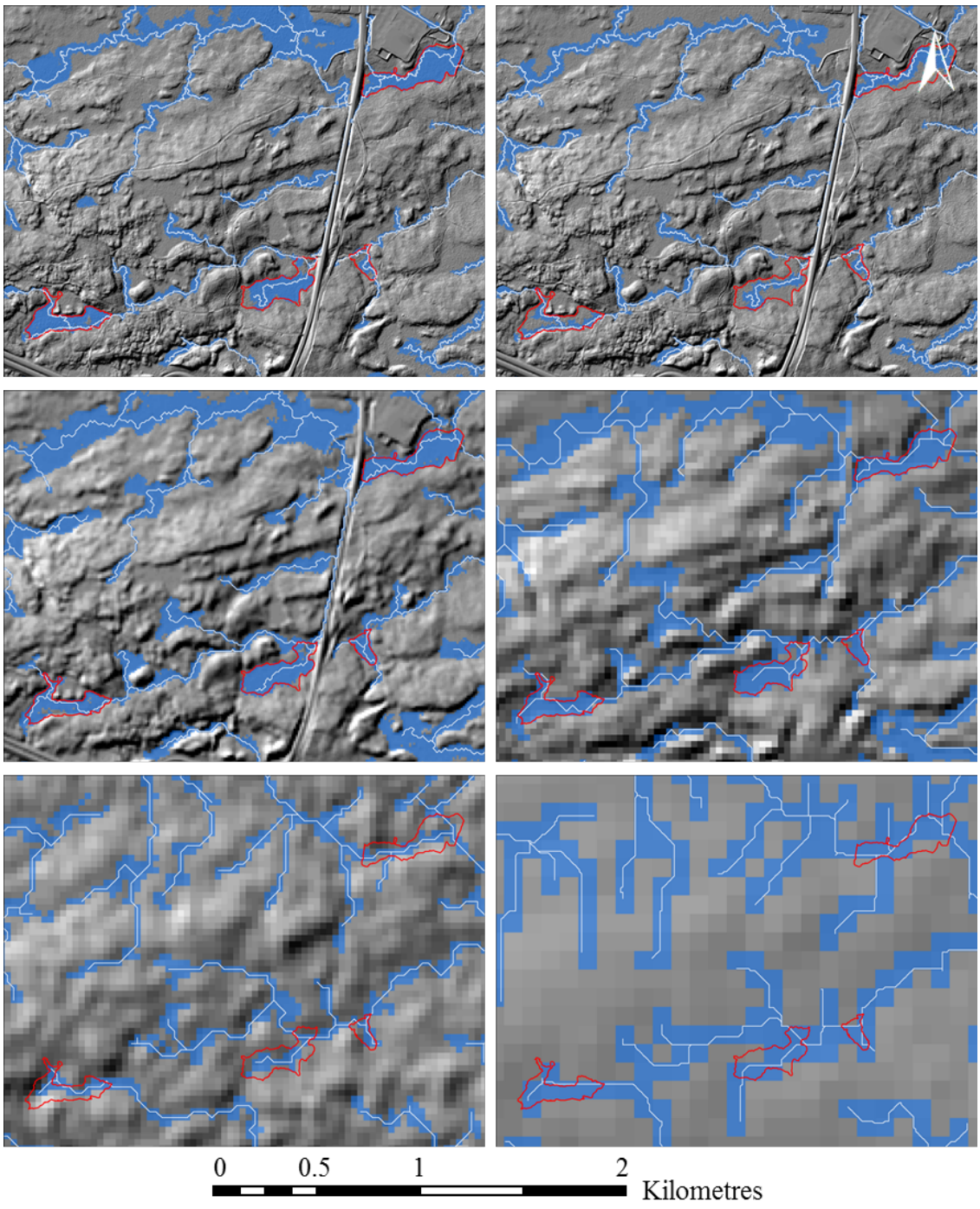

Figure 39. UNB Forest study area: binary DTW < 25 cm classification, with > 4 ha of upslope flow accumulation areas, by DEM source, and with the GPS-tracked wetland borders overlaid (red). Top: LiDAR, with (left) and without (right) hydrophytic DTW seeding, Middle left: LiDAR-DEM10m, Middle right: LiDAR-DEM 30m, Bottom left: SRTM 30m, Bottom right: SRTM 90m.

5.4 Discussion

As shown, all DEM sources and spatial resolutions used can be used to locate the GPS-tracked wetlands, but the precision of DEM-delineating the exact locations of the wetland borders and their inside areas not only drops with decreasing DEM resolution, but also requires careful DEM hydro-conditioning by way of hydrophytic DTW=0 seeding. The fact that this seeding can be realized using LiDAR point cloud data only is of practical significance, because it simplifies the overall process that is normally used in delineating wetland borders through a combination of varying remote sensing techniques and ancillary data requirements (Chapter 2).

Nevertheless, the above wetland border delineation process does not come without caveats, mainly due to the difficulty of determining the bare-earth elevations underneath dense laser-pulse reflecting ground vegetation. In this regard, Hopkinson (2005) noted that both ground return elevation accuracy under aquatic vegetation (i.e. cat tails) and low shrubs (< 2 m) had the largest relative height error estimates on rasterized LiDAR bare earth surfaces of all land cover types sampled, with associated bare-earth detection errors of 11 cm and 12 cm respectively. Without special processing consideration, this error results in a "false earth" DEM model across landscape portions that are not only covered by dense vegetation, but also by appreciable plant litter accumulations in the form of, e.g., deep forest floor layers and peat accumulations. Down-sampling of bare earth LiDAR DEM data from 1 to 10 and 30 m generally maintains these "false earth" wetland-related artifacts. With SRTM-based DEMs, this is a mute issue because of the limited SRTM vertical accuracy at ±5.94 m (Elkhrachy, 2017).

In part, the hydrophytic DTW=0 seeding process for better capturing the extent of wetland borders addresses the issue of "false earth" elevation representation in terms of placing the extent of the cartographically determined water table (DTW) as a flat elevation entity across each DEM-delineated HDS zone. Care must be taken, however, that hydrophytic DTW=0 seeding process does not generate false positives across the landscapes where the DEM-captured elevation texture is similar to what is found raised bog features, as illustrated by, e.g.,Figure 30. Typical candidates for generating such false positives are associated with re-generating forest stands. Most of such occurrences, however, can be eliminated in at least two ways: (i) through orthoimage and forest inventory overlays, (ii) noting the slope position and DTW variations within incorrectly seeded hydrophytic DTW=0 areas.

Based on the qualitative visual inspection of HDS-DEM delineation for several non-GPS-tracked wetlands across the EMEND and UNB Forest areas in Figure 32 to Figure 35, it can be concluded that the above methodology could be useful across much wider areas and terrain conditions. In this regard, selected EMEND study area serves as a flat terrain example, while the selected UNB Forest study area serves as a rugged terrain example.

Chapter 6

WETLAND LOCATION CONFORMANCE TESTING

6.1 Introduction

This chapter describes how the DEM-based wetland border delineations vary quantitatively in conformance with GPS-tracked wetland borders by DEM resolution from 1 to 90 m, by DEM source technology (LiDAR versus SRTM generated), by upslope area flow initiation threshold (0.5 to 16 ha), by cartographic depth-to-water contouring from < 10 cm to 2 m, by boreal versus maritime forest zone, and with and without hydrophytic DTW=0 hydro-conditioning. The objectives of this chapter are to (i) systematically quantify the areal extent to which the wetland delineations in Chapter 5 conform to the GPS-tracked wetland borders at the EMEND and UNB Forest areas by DEM type, resolution and wetland-defining thresholds; (ii) determine DEM-based wetland delineation DTW thresholds that are most suitable for each of the two study areas and; (iii) evaluate how the optimal quantification varies by DEM layer type and by study area.

The general hypothesis is that bare-earth DEMs can be used to locate wetlands reliably, but careful hydro-conditioning of high-resolution DEMs; particularly by way of hydrophytic DTW=0 seeding, is needed to reliably determine the locations, areas and flow configurations of wetlands across forested landscapes.

6.2 Methodology

Wetland-area conformance testing

Using the GPS-tracked wetland borders in Chapter 5 as ground-truthed borders, a 50 m buffer zone around each GPS-tracked wetland feature was defined and classified as non-wetland area (Figure 40). This buffer distance was established to minimize the influence of adjacent non-tracked wetland features on the conformance of the subset of GPS-tracked features, while allowing for sufficient assessment of potential false positive areas beyond GPS-tracked borders. The combined wetland containing area was used to determine the mix of false negative and false positive wetland areas generated by varying the DEM-based wetland-emulating DTW threshold from < 0.25 to < 2.0 m for each of the six DEM sources: SRTM 90 m, SRTM 30 m, LiDAR 30 m, LiDAR 10 m, and LiDAR 1 m with and without hydrophytic DTW=0 seeding. Also varied was the threshold for upland flow-initiation area from 0.5 to 16 hectares. The resulting permutations of all false & true positive and false & true negative DEM-delineated wetland areas were mapped and systematically evaluated in reference to the GPS-tracked and 50 m buffered wetland areas through quantitative confusion matrix assessment. The extent of GPS- to DEM-delineation conformance was summarized using standard proportionate agreement and Cohen's Kappa (Cohen, 1960) which indexes the resulting areal conformance outcomes in relation to random chance agreement. This assessment was also used to gauge the extent of conformance of the DEM-based wetland delineations in reference to (i) two Alberta's vegetation index layers (i.e., AVI-Upland and DEP, Chapter 3), and two wetland layers for New Brunswick (SNB and DNR, Chapter 3), with focus on the EMEND and UNB Forest locations.

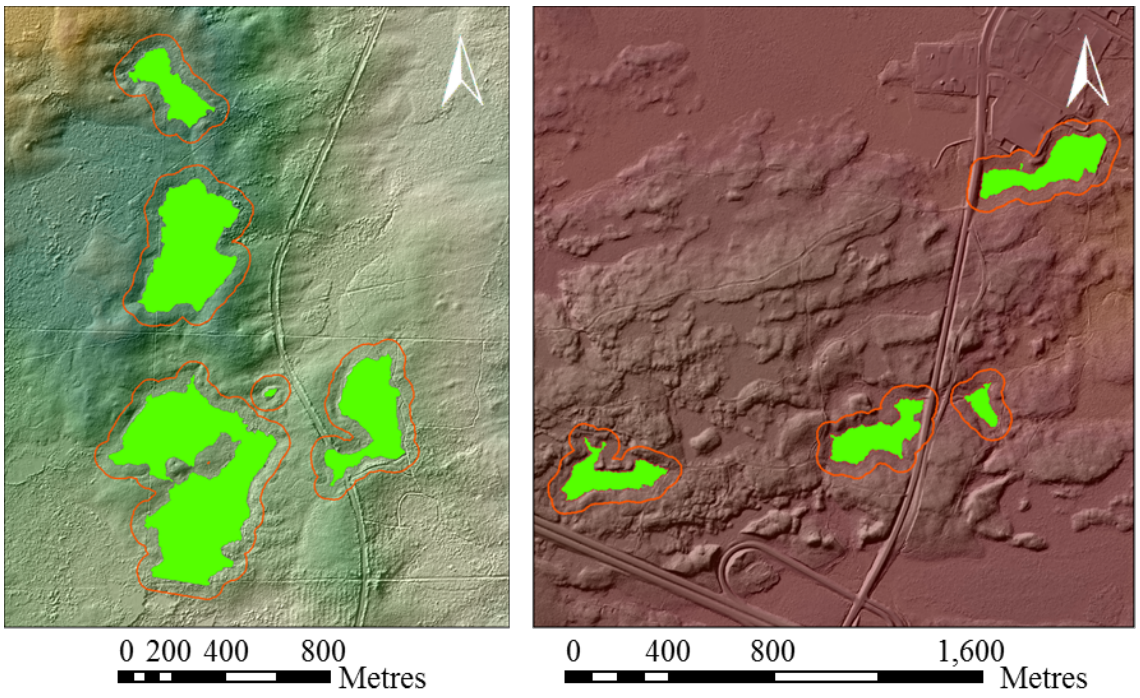

Figure 40. GPS versus DEM wetland delineation conformance testing for the EMEND (left) and UNB Forest (right) study areas. Green areas: GPS tracked. Red lines: 50 m buffer lines around green areas. Combined area serves to limit the evaluation extent of DEM-delineated false positive and false negative wetland areas. Background: shaded relief of 1m LiDAR DEMs.

6.3 Results

The mapping of all false & true positive and false & true negative DEM-delineated wetland areas in reference to the GPS-tracked and 50 m buffered wetlands is illustrated in Figure 41 and Figure 42 for the EMEND and UNB Forest study areas, by varying the wetland-defining DTW threshold for the 1 m HDS-flattened LiDAR DEM from 25 to 100 cm. Results shown, using the 25 cm rather than 100 cm DTW threshold produces superior DEM-delineation results by substantially lowering the extent of false negative (false wet) while eliminating all false positive (false dry) wetland areas. The corresponding percentage areas are listed in Table 2 leading to following total true assessment change

from DTW = 100 cm to DTW = 25 cm: for EMEND, proportionate agreement (overall classification accuracy) increases from 60% to 84%; For UNB Forest, proportionate agreement from 74% to 90%. Proportionate agreement for all tested WAM solutions is shown in Table 2. The higher conformance levels of the UNB Forest versus EMEND areas can be attributed to the more rugged area for the former, which also leads to the formation of more easily recognized and less overgrown flow channels and wetland borders, which – in turn – improves the visual recognition and hence GPS-tracking of the same in the field.

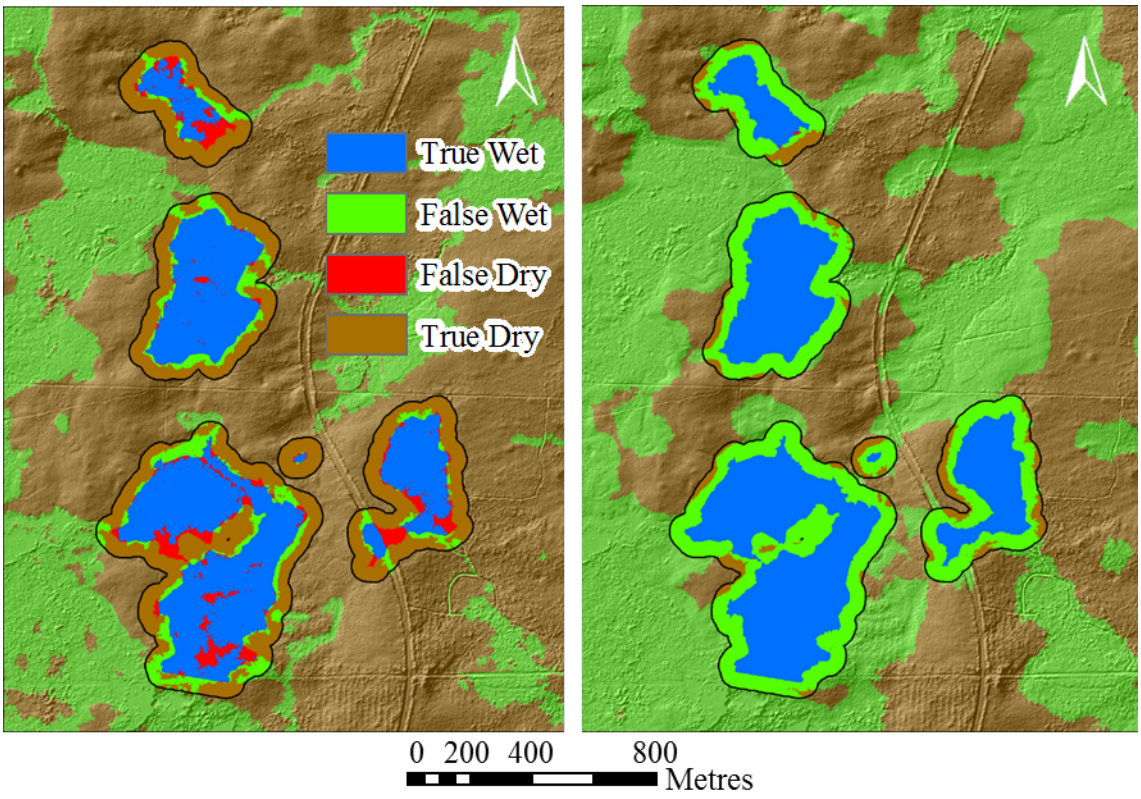

Figure 41. Quantifying the presence of false & true positive and false & true negative DEM-delineated wetland areas, using GPS-tracked wetland areas (true wet blue, true dry brown) as reference for the EMEND study area. Based on 1m HDS-flattened LiDAR DEM, with DTW-defined wetland borders set at 25 (left) and 100 cm (right). The upland area threshold for minimum flow accumulation is set at 4 ha. The area inside the black border is used for the confusion matrix assessment shown. Background: shaded relief of 1m LiDAR DEM.

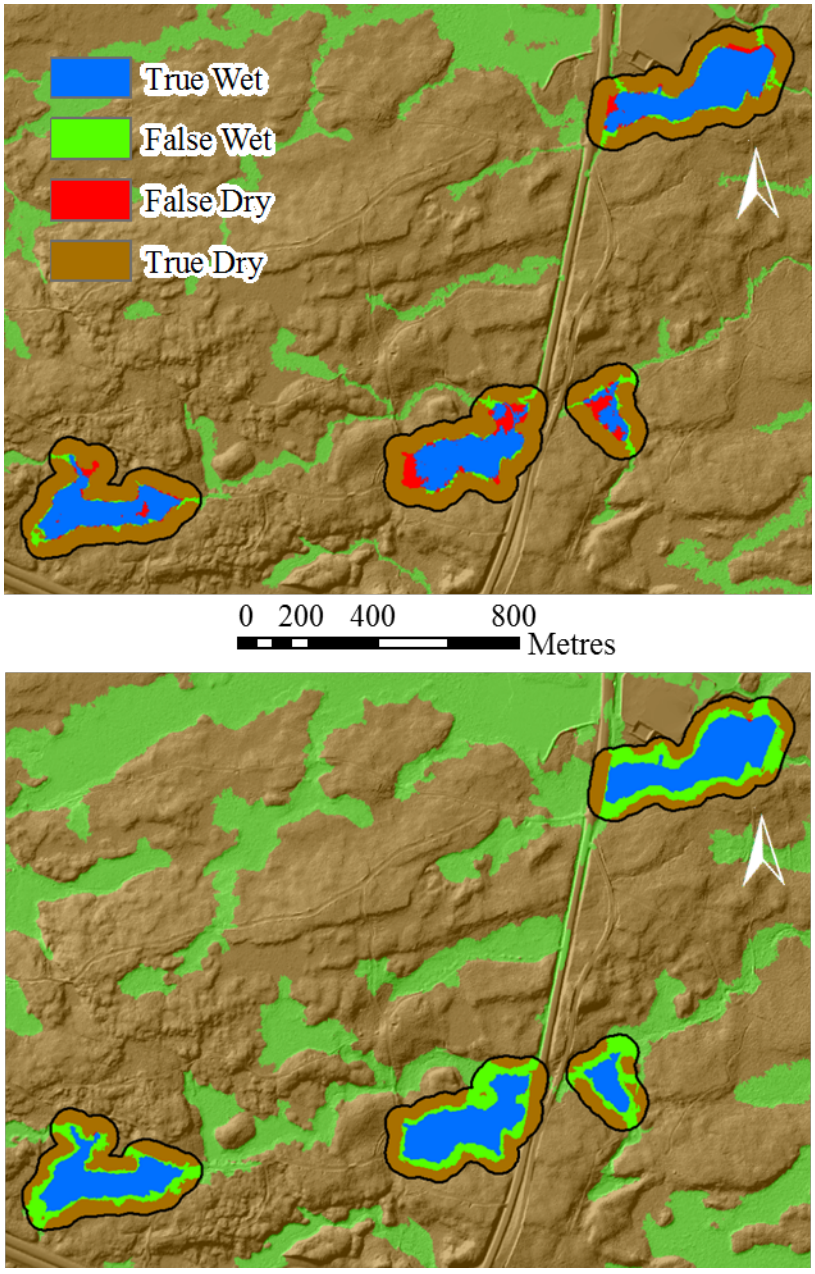

Figure 42. Quantifying the presence of false & true positive and false & true negative DEM-delineated wetland areas, using GPS-tracked wetland areas (true wet blue, true dry brown) as reference for the UNB Forest study area. Based on 1m HDS-flattened LiDAR DEM, with DTW-defined wetland borders set at 25 (top) and 100 cm (bottom). The upland area threshold for minimum flow accumulation is set at 4 ha. The area inside the black border is used for the confusion matrix assessment shown. Background: shaded relief of 1m LiDAR DEM.

Table 2. Proportionate agreement example for the GPS-tracked and DEM-delineated wetland areas regarding the EMEND and UNB Forest study areas. (LiDAR DEM 1m, HDS, 4ha), extending to 50 m beyond the GPS-tracked wetland border.

	EMEND		**UNB Forest**	
	25 cm	**100 cm**	**25 cm**	**100 cm**
True Wet	0.46	0.52	0.31	0.36
True Dry	0.37	0.07	0.59	0.38
Total True	*0.84*	*0.60*	*0.90*	*0.74*
False Wet	0.10	0.40	0.05	0.25
False Dry	0.06	0.00	0.05	0.00
Total False	*0.16*	*0.40*	*0.10*	*0.26*

The permutation results of the confusion matrix assessment pertaining to the DEM- versus GPS- wetland area delineation comparisons are compiled in Table 3 in form of the Cohen's Kappa numbers, for the EMEND and UNB Forest study areas. These numbers vary from 0, i.e., no conformance other than through chance to 0.78, i.e., overall DEM-GPS delineation conformance increases to 78% of perfect conformance. For convenience, the table entries are colour-coded using Lardis & Koch's (1977) Kappa conformance criteria: 0 – 0.2 = slight (red), 0.21 – 0.4 = fair (orange), 0.41 – 0.6 = moderate (yellow), 0.61 – 0.8 = substantial (green) and 0.81 – 1.0 = near perfect (none present). This was to provide a quick visual conformance assessment as the thresholds that define the DTW extent of wetland delineation varies from 10 to 200 cm, and the minimum upslope areas for flow-channel initiation increase from 0.5 to 16 ha. Optimal combinations by DEM source are shown with underlines, and overall optimal (highest classification accuracy) highlighted by dotted border. WAM combinations within 1 standard deviation of optimal (highest Kappa) for each DEM source shown in bold. A

proportionate agreement summary table for all WAM permutation classification accuracy results is provided in Table 5.

The following observation can be made: highest proportionate agreement of GPS-versus DEM-delineations are achieved by using the 1 m LiDAR DEM with the HDS process in place for both the EMEND and UNB Forest study areas. In this regard, the HDS process is obligatory for the EMEND study area, while providing only a small but consistent improvement for the UNB Forest study area. The choice of minimum upslope areas for flow-channel initiation is also important, but there is greater flexibility with slightly improved conformances obtained with the 4 hectare threshold. This result is in keeping with the expectation that traditional delineation of flow channels generally stops at this limit, thereby marking the overall transition of ephemeral to intermittent channels to permanent flow channels.

Surprising is the gradually improvement of the GPS- versus DEM-wetland delineation at EMEND towards higher DEM resolution without using the HDS process. This can be attributed to two observations. (i) without the HDS process, the water table predictions underneath the wetlands are solely influenced by the sometimes problematic (Chapter 2) local modeled bare earth elevation. As such, the DTW-delineation process falls short of reaching the wetland borders especially where elevations vary inside these borders as in raised bogs. (ii) as the DEM resolution varies from 1 to 10 m, more of the elevation changes within the wetland borders become flattened, hence allowing the 90 m SRTM DEMs to provide the best possible conformance without the HDS process in place.

In reference to the DEM- versus provincial wetland layers for Alberta and New Brunswick, the HDS-processed 1 m LiDAR DEM with 4 hectare upslope area for flow

channel initiation general results very similar to what is documented for the EMEND and UNB Forest areas in Table 3 (bottom lines). This implies that the HDS-processed 1 m LiDAR DEM not only applies to the two study areas of this Thesis, but can also be applied elsewhere with reasonable Kappa conformance confidence at 62 to 73%. The lower Kappa number for SNB forest wetland layer is due to the fact that this layer is a subset of that more comprehensive SNB wetland layer.

Table 3. Cohen's Kappa for assessing the wetland border classification. Assessed by upslope flow initiation area and DTW threshold, study area, DEM source and resolution.

Flow		EMEND						UNB Forest					
Init.,	DTW,	LiDAR				SRTM		LiDAR				SRTM	
ha	m	1 m (HS)	1 m	10 m	30 m	30 m	90 m	1 m (HS)	1 m	10 m	30 m	30 m	90 m
0.5	0.1	0.54	0.07	0.21	0.13	0.18	0.16	0.65	0.33	0.60	0.45	0.21	0.12
	0.25	0.52	0.17	0.28	**0.27**	0.22	0.26	0.71	0.56	0.64	0.50	0.24	0.19
	0.5	0.31	0.17	0.20	0.19	0.29	0.36	0.60	0.61	0.50	0.41	0.27	0.22
	0.75	0.15	0.11	0.11	0.08	0.32	0.41	0.47	0.49	0.38	0.31	0.27	0.22
	1	0.05	0.05	0.04	0.04	0.31	0.42	0.37	0.39	0.31	0.23	0.27	0.22
	1.25	0.02	0.02	0.01	0.01	0.28	0.43	0.30	0.31	0.24	0.17	0.23	0.20
	1.5	0.00	0.00	0.00	0.01	0.25	0.42	0.24	0.25	0.19	0.12	0.19	0.17
	1.75	0.00	0.00	**0.00**	0.00	0.21	0.40	0.19	0.20	0.14	0.09	0.15	0.13
	2	0.00	0.00	**0.00**	**0.00**	0.17	0.38	0.15	0.16	0.11	0.06	0.13	0.11
1	0.1	0.57	0.07	0.19	0.14	0.19	0.14	0.66	0.32	0.60	0.51	0.24	0.14
	0.25	0.58	0.15	0.27	0.25	0.23	0.24	0.75	0.57	0.67	0.54	0.28	0.23
	0.5	0.38	0.19	0.18	0.23	0.31	0.34	0.65	0.66	0.54	0.45	0.33	0.29
	0.75	0.20	0.14	0.11	0.15	0.35	0.39	0.52	0.56	0.43	0.34	0.33	0.31
	1	0.09	0.07	0.05	0.08	0.38	0.42	0.43	0.46	0.34	0.26	0.35	0.31
	1.25	0.03	0.04	0.02	0.03	**0.38**	0.44	0.35	0.38	0.27	0.19	0.32	0.29
	1.5	0.01	0.02	0.00	0.01	0.36	0.44	0.29	0.31	0.21	0.13	0.26	0.27
	1.75	0.00	0.00	0.00	0.00	0.34	0.43	0.23	0.25	0.16	0.09	0.21	0.22
	2	0.00	0.00	**0.00**	**0.00**	0.31	0.42	0.18	0.20	0.13	0.07	0.19	0.18
2	0.1	0.59	0.06	0.18	0.12	0.16	0.13	0.66	0.27	0.56	0.53	0.26	0.14
	0.25	0.62	0.13	0.26	0.22	0.21	0.22	0.78	0.52	0.71	0.58	0.32	0.23
	0.5	0.45	0.17	0.18	0.17	0.27	0.31	0.70	0.69	0.57	0.46	0.37	0.30
	0.75	0.26	0.13	0.12	0.17	0.30	0.37	0.57	0.63	0.46	0.36	0.37	0.32
	1	0.12	0.06	0.09	0.11	0.35	0.40	0.47	0.52	0.37	0.27	0.40	0.33
	1.25	0.05	0.02	0.04	0.07	0.34	0.43	0.39	0.44	0.30	0.20	0.37	0.32
	1.5	0.02	0.00	0.02	0.03	0.35	0.43	0.32	0.36	0.24	0.14	0.32	0.29
	1.75	0.00	0.00	0.00	0.02	0.36	0.43	0.26	0.29	0.19	0.10	0.26	0.25
	2	0.00	0.01	**0.00**	0.01	0.35	0.43	0.21	0.23	0.16	0.07	0.23	0.21
4	0.1	0.61	0.07	0.18	0.12	0.09	0.13	0.66	0.27	0.55	0.54	0.27	0.13
	0.25	0.67	0.18	**0.30**	0.24	0.12	0.21	**0.78**	0.52	**0.72**	0.61	0.33	0.22
	0.5	0.51	**0.24**	0.27	0.23	0.20	0.30	0.73	**0.70**	0.59	0.49	0.38	0.29
	0.75	0.31	0.22	0.21	0.20	0.26	0.36	0.62	0.68	0.48	0.37	0.39	0.33
	1	0.16	0.17	0.15	0.15	0.31	0.41	0.52	0.57	0.39	0.28	**0.42**	**0.34**
	1.25	0.07	0.11	0.09	0.13	0.33	0.44	0.43	0.48	0.32	0.21	0.40	0.33
	1.5	0.03	0.06	0.05	0.07	0.35	0.46	0.35	0.40	0.25	0.14	0.35	0.32
	1.75	0.01	0.04	0.03	0.04	0.36	0.46	0.28	0.32	0.20	0.10	0.30	0.28
	2	0.00	0.02	0.01	0.02	0.35	0.46	0.23	0.26	0.17	0.07	0.27	0.24

Table 3. (continued) Cohen's Kappa for assessing the wetland border classification. Assessed by upslope flow initiation area and DTW threshold, study area, DEM source and resolution.

Flow		EMEND						UNB Forest					
Init.,	DTW,	LiDAR				SRTM		LiDAR				SRTM	
ha	m	1 m (HS)	1 m	10 m	30 m	30 m	90 m	1 m (HS)	1 m	10 m	30 m	30 m	90 m
8	0.1	0.61	0.06	0.15	0.10	0.06	0.13	0.64	0.21	0.48	0.53	0.19	0.12
	0.25	0.69	0.15	0.27	0.21	0.09	0.21	0.75	0.69	0.69	**0.62**	0.27	0.20
	0.5	0.52	0.22	0.24	0.22	0.15	0.31	0.72	0.61	0.64	0.50	0.29	0.26
	0.75	0.32	0.23	0.21	0.19	0.20	0.37	0.65	0.65	0.53	0.37	0.31	0.30
	1	0.17	0.20	0.17	0.15	0.26	0.42	0.56	0.60	0.43	0.29	0.35	0.31
	1.25	0.17	0.12	0.12	0.12	0.28	0.45	0.47	0.54	0.35	0.23	0.35	0.32
	1.5	0.03	0.13	0.07	0.07	0.31	0.47	0.39	0.47	0.29	0.16	0.29	0.31
	1.75	0.01	0.11	0.04	0.05	0.33	0.47	0.32	0.40	0.23	0.12	0.29	0.29
	2	0.00	0.07	0.01	0.04	0.33	**0.48**	0.27	0.33	0.19	0.09	0.27	0.26
12	0.1	0.61	0.06	0.12	0.09	0.04	0.12	0.63	0.17	0.40	0.46	0.14	0.11
	0.25	0.70	0.14	0.24	0.20	0.07	0.19	0.73	0.35	0.60	0.61	0.19	0.18
	0.5	0.53	0.20	0.25	0.17	0.10	0.27	0.70	0.53	0.62	0.52	0.24	0.27
	0.75	0.34	0.23	0.19	0.19	0.13	0.33	0.64	0.58	0.56	0.38	0.27	0.31
	1	0.18	0.22	0.15	0.17	0.21	0.37	0.56	0.56	0.46	0.30	0.29	0.32
	1.25	0.08	0.18	0.16	0.14	0.25	0.42	0.49	0.51	0.37	0.24	0.30	0.33
	1.5	0.03	0.14	0.11	0.08	0.27	0.44	0.41	0.45	0.31	0.17	0.26	0.33
	1.75	0.01	0.12	0.07	0.05	0.29	0.46	0.34	0.39	0.24	0.12	0.21	0.31
	2	0.00	0.11	0.04	0.05	0.30	0.46	0.28	0.34	0.20	0.10	0.17	0.27
16	0.1	0.61	0.05	0.09	0.08	0.02	0.11	0.63	0.16	0.32	0.36	0.14	0.09
	0.25	**0.70**	0.10	0.19	0.17	0.06	0.17	0.73	0.31	0.51	0.43	0.19	0.15
	0.5	0.55	0.14	0.24	0.17	0.07	0.25	0.70	0.45	0.52	0.52	0.24	0.21
	0.75	0.36	0.16	0.20	0.21	0.11	0.31	0.64	0.49	0.48	0.43	0.27	0.24
	1	0.19	0.17	0.18	0.20	0.18	0.37	0.55	0.46	0.47	0.34	0.29	0.25
	1.25	0.09	0.18	0.20	0.18	0.23	0.42	0.48	0.43	0.42	0.27	0.30	0.26
	1.5	0.04	0.17	0.16	0.12	0.25	0.44	0.42	0.39	0.34	0.20	0.26	0.26
	1.75	0.01	0.15	0.12	0.13	0.29	**0.46**	0.35	0.34	0.28	0.15	0.21	**0.24**
	2	0.00	0.12	0.10	0.09	0.29	0.47	0.30	0.29	0.23	0.11	0.17	0.22
AVI Upland		0.62						0.73					
DEP		0.65						0.46					

Table 4 summarizes the "optimal" wetland-delineation thresholds (DEM solution, DTW, upslope flow initiation area) based on the Table 3 results by DEM resolution.

These optimal solutions were used to generate the nearest distance conformance plots in Figure 43, together with the corresponding conformance plots for the two Alberta and two New Brunswick wetland pertinent data layers (Figure 43– dashed line). In detail, Figure 43 shows tighter wetland delineation conformances for the UNB Forest that the EMEND

area across DEM resolution. With respect to the provincial data layers, there is ± 20 m distance conformance for the New Brunswick wetland layer, and ± 35 m distance conformance for the Alberta Derived Ecosite and AVI layers, eight times out of 10 in each case. In comparison, the best-fitting DTW = 25 cm contour increases in conformance from ±44 m (LiDAR-DEM 1 m) to ±13m (LiDAR-DEM 1 m, HDS), eight times out of ten. At 90%, this precision increases from ±72 m to ±17 m, eight times out of ten.

Table 4. Optimal model predictor variables by study area. Summary table of optimal wetland conformance solutions, by DEM source for the EMEND and UNB woodlot study areas, also showing the range of optimal solutions between study areas, by DEM source.

		EMEND	UNB Woodlot	Inter-Site Range
LiDAR 1m (HDS)	ha	4	4	0
	cm	25	25	0
LiDAR 1m	ha	4	4	0
	cm	25	50	25
LiDAR 10m	ha	4	4	0
	cm	25	25	0
LiDAR 30m	ha	0.5	8	7.5
	cm	25	25	0
SRTM 30m	ha	1	4	3
	cm	125	100	25
SRTM 90m	ha	8	4	4
	cm	200	100	100

Overall classification accuracy by way of proportionate agreement, which does not include the probability of correct classification due to random chance (Cohen's Kappa) is included in Table 5 below for all WAM permutations tested, with a summary of proportionate agreement for optimal solutions by DEM type in Table 6.

Table 5. Proportionate agreement (overall classification accuracy) of WAM classifications relative to GPS-tracked wetland borders. Assessed by upslope flow initiation area and DTW threshold, by study area, DEM source and resolution. Shades from red (lower proportionate accuracy) to green (higher proportionate accuracy) for EMEND (left) and UNB Forest (right) study areas.

Flow		EMEND						UNB Forest					
Init.,	DTW,	LiDAR				SRTM		LiDAR				SRTM	
ha	m	1 m (HS)	1 m	10 m	30 m	30 m	90 m	1 m (HS)	1 m	10 m	30 m	30 m	90 m
0.5	0.1	0.77	0.54	0.60	0.56	0.59	0.58	0.82	0.67	0.80	0.72	0.60	0.56
	0.25	0.76	0.58	0.64	0.64	0.61	0.63	0.86	0.78	0.82	0.75	0.62	0.60
	0.5	0.65	0.59	0.60	0.59	0.65	0.68	0.80	0.80	0.75	0.70	0.63	0.61
	0.75	0.57	0.55	0.55	0.54	0.66	0.71	0.73	0.75	0.69	0.65	0.63	0.61
	1	0.53	0.52	0.52	0.52	0.66	0.71	0.69	0.70	0.65	0.61	0.63	0.61
	1.25	0.51	0.51	0.50	0.50	0.64	0.71	0.65	0.66	0.62	0.59	0.62	0.60
	1.5	0.50	0.50	0.50	0.50	0.62	0.71	0.62	0.63	0.59	0.56	0.59	0.59
	1.75	0.50	0.50	0.50	0.50	0.61	0.70	0.60	0.60	0.57	0.54	0.57	0.57
	2	0.50	0.50	0.50	0.50	0.58	0.69	0.58	0.58	0.56	0.53	0.57	0.55
1	0.1	0.79	0.53	0.59	0.57	0.60	0.57	0.83	0.66	0.80	0.75	0.62	0.57
	0.25	0.79	0.58	0.63	0.63	0.62	0.62	0.87	0.78	0.84	0.77	0.64	0.61
	0.5	0.69	0.60	0.59	0.61	0.66	0.67	0.83	0.83	0.77	0.72	0.66	0.64
	0.75	0.60	0.57	0.56	0.57	0.68	0.69	0.76	0.78	0.71	0.67	0.67	0.65
	1	0.54	0.54	0.53	0.54	0.69	0.71	0.71	0.73	0.67	0.63	0.67	0.66
	1.25	0.52	0.52	0.51	0.51	0.69	0.72	0.68	0.69	0.63	0.60	0.66	0.65
	1.5	0.50	0.51	0.50	0.51	0.68	0.72	0.64	0.66	0.61	0.57	0.63	0.63
	1.75	0.50	0.50	0.50	0.50	0.67	0.72	0.62	0.62	0.58	0.55	0.61	0.61
	2	0.50	0.50	0.50	0.50	0.66	0.71	0.59	0.60	0.56	0.53	0.59	0.59
2	0.1	0.79	0.53	0.59	0.56	0.58	0.57	0.83	0.64	0.78	0.77	0.63	0.57
	0.25	0.81	0.57	0.63	0.61	0.60	0.61	0.89	0.76	0.85	0.79	0.66	0.62
	0.5	0.72	0.59	0.59	0.59	0.64	0.66	0.85	0.84	0.79	0.73	0.68	0.65
	0.75	0.63	0.56	0.56	0.58	0.65	0.68	0.79	0.81	0.73	0.68	0.69	0.66
	1	0.56	0.53	0.54	0.55	0.68	0.70	0.74	0.76	0.69	0.63	0.70	0.66
	1.25	0.52	0.51	0.52	0.54	0.67	0.71	0.70	0.72	0.65	0.60	0.69	0.66
	1.5	0.51	0.50	0.51	0.52	0.68	0.72	0.66	0.68	0.62	0.57	0.66	0.64
	1.75	0.50	0.50	0.50	0.51	0.68	0.72	0.63	0.65	0.59	0.55	0.63	0.63
	2	0.50	0.50	0.50	0.50	0.68	0.71	0.61	0.62	0.58	0.54	0.62	0.60
4	0.1	0.80	0.54	0.59	0.56	0.54	0.56	0.83	0.63	0.78	0.77	0.64	0.57
	0.25	0.84	0.59	0.65	0.62	0.56	0.60	0.89	0.76	0.86	0.80	0.67	0.61
	0.5	0.75	0.62	0.63	0.61	0.60	0.65	0.86	0.85	0.80	0.74	0.69	0.64
	0.75	0.66	0.61	0.60	0.60	0.63	0.68	0.81	0.84	0.74	0.68	0.69	0.66
	1	0.58	0.58	0.58	0.58	0.66	0.71	0.76	0.79	0.70	0.64	0.71	0.67
	1.25	0.53	0.56	0.55	0.56	0.66	0.72	0.72	0.74	0.66	0.60	0.70	0.67
	1.5	0.51	0.53	0.53	0.53	0.67	0.73	0.68	0.70	0.63	0.57	0.67	0.66
	1.75	0.50	0.52	0.51	0.52	0.68	0.73	0.64	0.66	0.60	0.55	0.65	0.64
	2	0.50	0.51	0.50	0.51	0.67	0.73	0.62	0.63	0.58	0.54	0.64	0.62

Table 5. (continued) Proportionate agreement (overall classification accuracy) of WAM classifications relative to GPS-tracked wetland borders. Assessed by upslope flow initiation area and DTW threshold, by study area, DEM source and resolution. Shades from red (lower proportionate accuracy) to green (higher proportionate accuracy) for EMEND (left) and UNB Forest (right) study areas.

Flow		EMEND						UNB Forest					
Init.,	DTW,	LiDAR				SRTM		LiDAR				SRTM	
ha	m	1 m (HS)	1 m	10 m	30 m	30 m	90 m	1 m (HS)	1 m	10 m	30 m	30 m	90 m
8	0.1	0.81	0.53	0.57	0.55	0.53	0.56	0.82	0.61	0.74	0.76	0.60	0.56
	0.25	0.84	0.58	0.63	0.61	0.54	0.60	0.88	0.84	0.84	0.81	0.63	0.60
	0.5	0.76	0.61	0.62	0.61	0.58	0.65	0.86	0.81	0.82	0.75	0.64	0.63
	0.75	0.66	0.61	0.61	0.59	0.60	0.69	0.83	0.82	0.76	0.69	0.66	0.65
	1	0.59	0.60	0.58	0.57	0.63	0.71	0.78	0.80	0.72	0.65	0.67	0.65
	1.25	0.58	0.56	0.56	0.56	0.64	0.73	0.74	0.77	0.68	0.61	0.67	0.66
	1.5	0.51	0.57	0.54	0.53	0.65	0.73	0.70	0.73	0.64	0.58	0.65	0.66
	1.75	0.51	0.55	0.52	0.53	0.67	0.74	0.66	0.70	0.61	0.56	0.64	0.64
	2	0.50	0.53	0.50	0.52	0.66	0.74	0.63	0.67	0.60	0.54	0.64	0.63
12	0.1	0.81	0.53	0.56	0.54	0.52	0.56	0.81	0.59	0.70	0.73	0.57	0.55
	0.25	0.85	0.57	0.62	0.60	0.54	0.59	0.87	0.67	0.80	0.81	0.60	0.59
	0.5	0.77	0.60	0.62	0.59	0.55	0.64	0.85	0.76	0.81	0.76	0.62	0.63
	0.75	0.67	0.61	0.59	0.59	0.57	0.66	0.82	0.79	0.78	0.69	0.64	0.66
	1	0.59	0.61	0.58	0.59	0.60	0.69	0.78	0.78	0.73	0.65	0.65	0.66
	1.25	0.54	0.59	0.58	0.57	0.62	0.71	0.74	0.76	0.69	0.62	0.65	0.67
	1.5	0.52	0.57	0.56	0.54	0.63	0.72	0.71	0.73	0.65	0.58	0.63	0.67
	1.75	0.51	0.56	0.54	0.53	0.65	0.73	0.67	0.70	0.62	0.56	0.60	0.65
	2	0.50	0.55	0.52	0.52	0.65	0.73	0.64	0.67	0.60	0.55	0.58	0.64
16	0.1	0.81	0.52	0.54	0.54	0.51	0.55	0.81	0.58	0.66	0.68	0.57	0.54
	0.25	0.85	0.55	0.59	0.59	0.53	0.59	0.87	0.65	0.75	0.71	0.60	0.57
	0.5	0.77	0.57	0.62	0.59	0.53	0.63	0.85	0.73	0.76	0.76	0.62	0.60
	0.75	0.68	0.58	0.60	0.60	0.56	0.66	0.82	0.74	0.74	0.71	0.64	0.62
	1	0.60	0.59	0.59	0.60	0.59	0.68	0.78	0.73	0.74	0.67	0.65	0.62
	1.25	0.55	0.59	0.60	0.59	0.62	0.71	0.74	0.71	0.71	0.63	0.65	0.63
	1.5	0.52	0.59	0.58	0.56	0.62	0.72	0.71	0.69	0.67	0.60	0.63	0.63
	1.75	0.51	0.58	0.56	0.56	0.64	0.73	0.68	0.67	0.64	0.57	0.60	0.62
	2	0.50	0.56	0.55	0.54	0.65	0.73	0.65	0.65	0.61	0.55	0.58	0.61
AVI Upland		0.81						0.87					
DEP		0.82						0.73					

Table 6 provides a summary of proportionate agreement of optimal WAM classifications relative to GPS-tracked wetland borders by DEM source for the EMEND and UNB Forest study areas. In agreement with the Kappa estimates of Table 3, highest proportionate agreement at both the EMEND and UNB Forest study areas at 85% and 89% respectively, are identified using LiDAR 1m with HDS, with a low inter-site range of 4%. Highest

inter-site range of proportionate agreement is identified using the LiDAR 1 m without HDS (23%) between the EMEND and UNB Forest study areas.

Table 6. Summary table of proportionate agreement of optimal WAM solutions for the EMEND and UNB Forest study areas, by DEM source.

	EMEND	UNB Woodlot	Inter-Site Range
LiDAR 1m (HDS)	0.85	0.89	0.04
LiDAR 1m	0.62	0.85	0.23
LiDAR 10m	0.65	0.86	0.21
LiDAR 30m	0.64	0.81	0.17
SRTM 30m	0.69	0.71	0.02
SRTM 90m	0.74	0.67	0.07

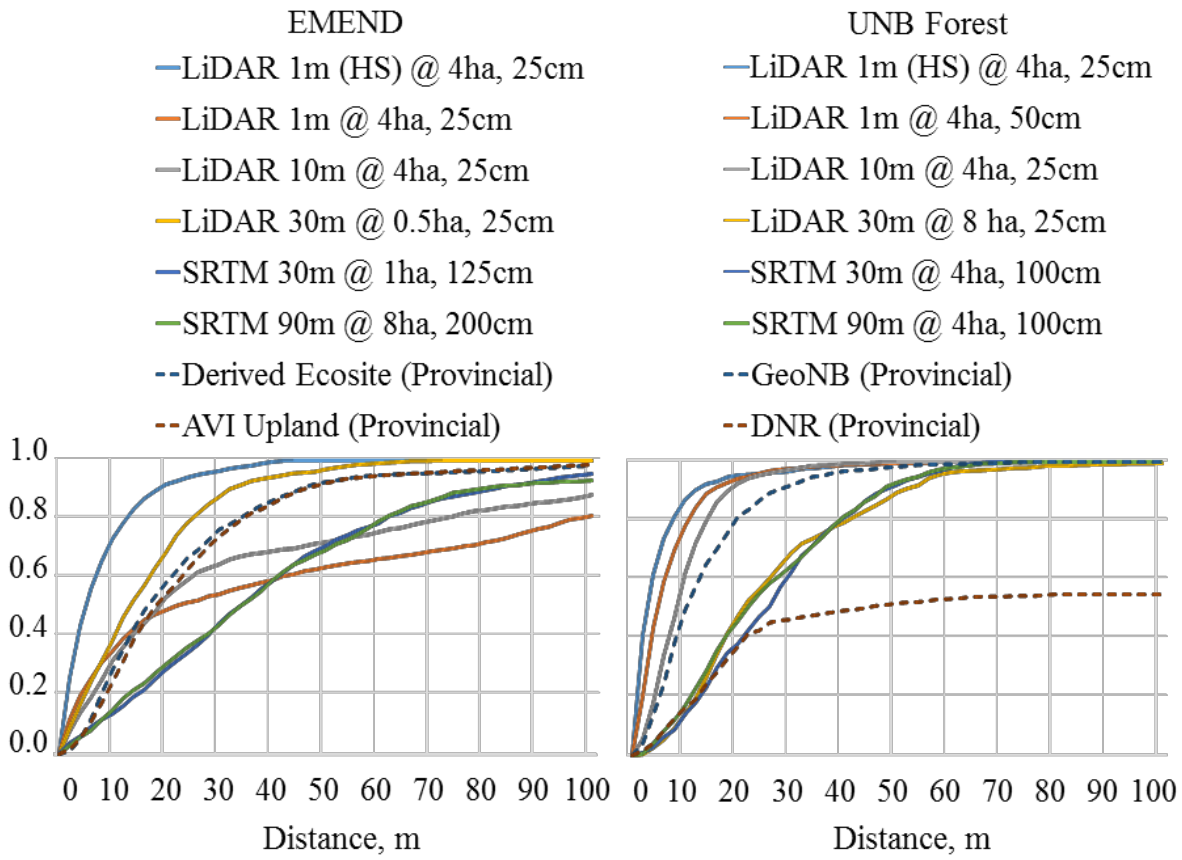

Figure 43. Cumulative frequency of nearest point distances between GPS-tracked and DEM-delineated wetland borders, using the optimal DEM delineation combinations listed in Table 3, for the EMEND (left) and UNB Forest study areas (right). Also included are the corresponding conformance results using two Alberta and two New Brunswick wetland pertinent data layers (bottom of Table 5).

6.4 Discussion

Figure 43 and Table 6 show that the HDS-processed 1 m LiDAR DEM using flow-line initiation of 4 ha and DTW <= 25 cm as defining threshold for wetland location are statistically "optimal" based on all permutations tested, as shown for the select study areas for EMEND and the UNB Forest. Without the HDS process, DEM- delineated wetland conformance decreased especially for the EMEND study area, but increased again with decreasing DEM resolution, mainly due to increased elevation smoothing across flat

terrain. For the UNB forest, DEM-wetland delineation decreased gradually with decreasing resolution, mainly due to elevation over smoothing across rugged terrain

While these results are specific to the two study areas, the results are sufficiently reproducible but only when using the HDS-processed DEMs for DEM-based wetland delineation. This being so, the same could be applied elsewhere with similar ground-truth conformance results. In part, this is already supported by the above conformance comparison between the HDS-based DEM- wetland delineations and the provincial wetland layers (SNB) or wetland related analogues (DEP). This possibility is further explored in chapter 7.

While the conformance of the HDS-based DEM- wetland delineation process can be considered "substantial" by way of Cohen's Kappa, there is obviously room for improvement through further research. Likely improvements will come about by finding further seeds for within-wetland DTW=0 zonation and further reducing the occurrence of false HDS positives outside obvious wetland areas.

Even with further DEM-based wetland improvements, it is important to note that direct field delineations by professional wetland delineators is an absolute necessity to avoid surprises when considering the lay of the land any particular wetland in terms of the precise wetland border locations, variations in vegetation composition within and across the wetland, and its hydrological function with emphasis on inflow and outflow locations, amounts and rates.

Chapter 7

WETLAND LOCATOR VALIDATION

7.1 Introduction

While the results described in chapters 4 to 6 are study-area specific, this chapter describes how the modeled DEM-based wetland delineation of this thesis applies to the EMEND and UNB Forest areas as a whole, without a conformance-restricting buffer zone in reference to modeled or delineated provincial wetland-informing data layers for Alberta (DEP hydric/subhydric classes) and New Brunswick (SNB wetlands) introduced in chapter 3. The hypothesis is that application of the "optimal" WAM solution as defined in chapter 6 leads to similar conformance levels relative to provincial wetland layers across a larger area. If so, then the methodology procedures as described above can be said to be validated, and can therefore be of practical use for assessing wetland numbers, areas, wetland to upland transitioning, and wetland-to-wetland connectivity across wider regions in a geographically and hydrologically comprehensive manner. To this effect, the wetland data layers so produced should be of practical use in forest management and planning, with additional guidance given to professional wetland delineators in term of planning, field-tracking and evaluation of survey operations.

7.2 Methodology

The "optimal" DEM-delineation procedure, as defined in chapter 6, refers to using 1 m HDS processed LiDAR 1m, with 4 hectare upstream contributing area threshold for flow line initiation, and with wetland extent limited to DTW <= 25 cm depth. This procedure was area-conformance tested using the Derived Ecosite Phase 1 (DEP) hydric/subhydric

class data layer for Alberta, and the SNB wetland layer for New Brunswick (SNB), centered around the EMEND and UNB Forest study areas. In order to comparably assess model conformance between study areas, the UNB Forest study area was expanded such that EMEND and UNB Forest areas possessed similar extents with 16,597 and 20,163 hectares respectively. Area-conformance testing was done by locating and delineating false negative, false positive and correct classification of DEM-delineated wetland relative to DEP and SNB data layers areas using ArcGIS. This was followed by examining the resulting zones using the confusion matrix approach, reporting the percent occurrences of false positive and false negative area occurrences, and evaluating these occurrences in terms of conformance above random chance using Cohen's Kappa index and overall conformance by way of assessment of proportionate agreement.

7.3 Results

Figure 44 and Figure 45 present close-ups of DEP (hydric/subhydric classes) and SNB wetland outlines overlaid on the 1m HDS-processed LiDAR-DEM DTW <= 25 cm (optimal) delineation, suggesting a general qualitative agreement with the optimal DEM-based wetland delineation process, but with the DTW-zonation process providing more detail than what is provided by provincially mapped wetland features.

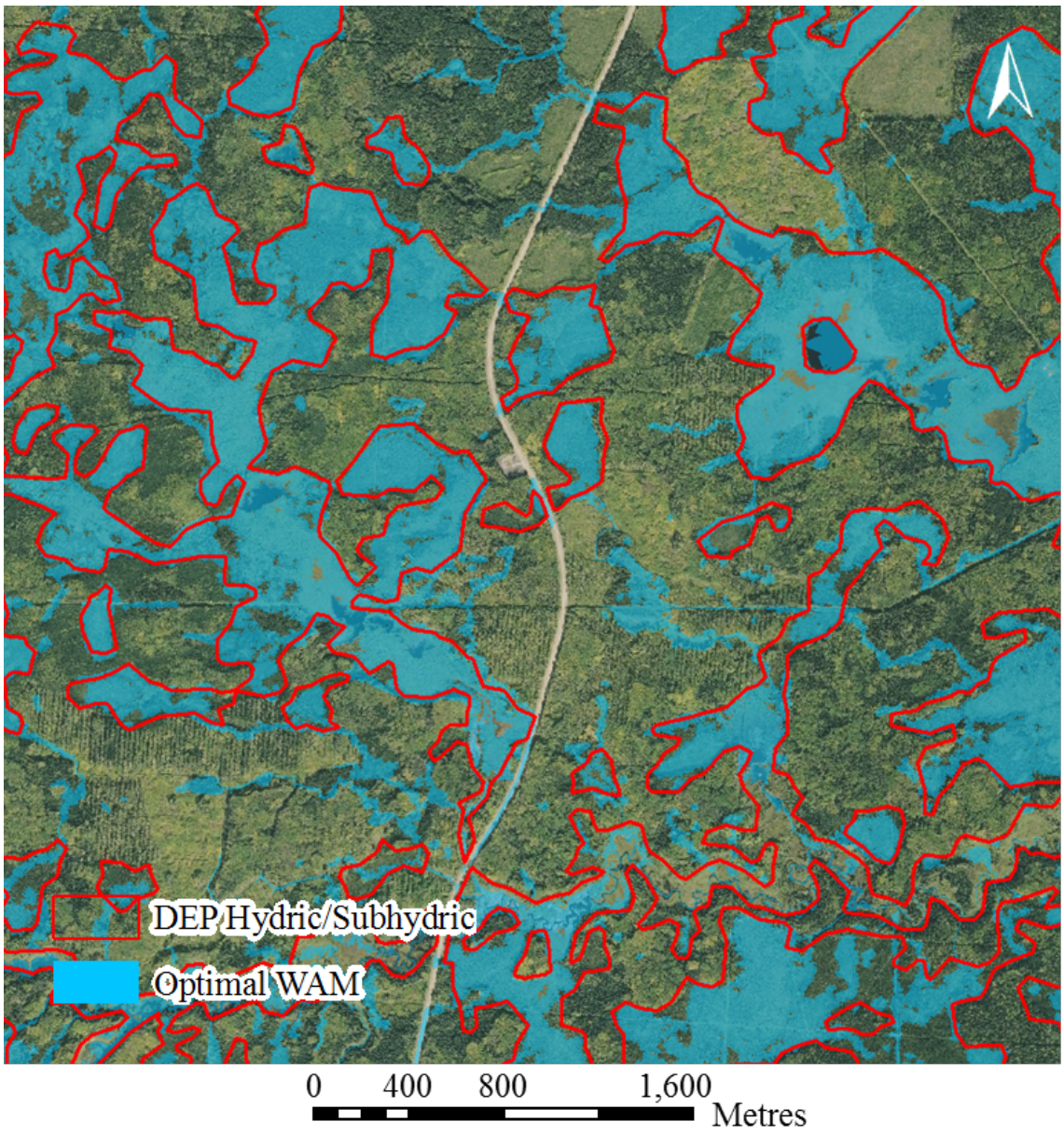

Figure 44. Close-up of DEP hydric/subhydric class outlines overlaid on the 1m HDS-processed LiDAR-DEM DTW <= 25 cm (optimal) delineation for the EMEND area.

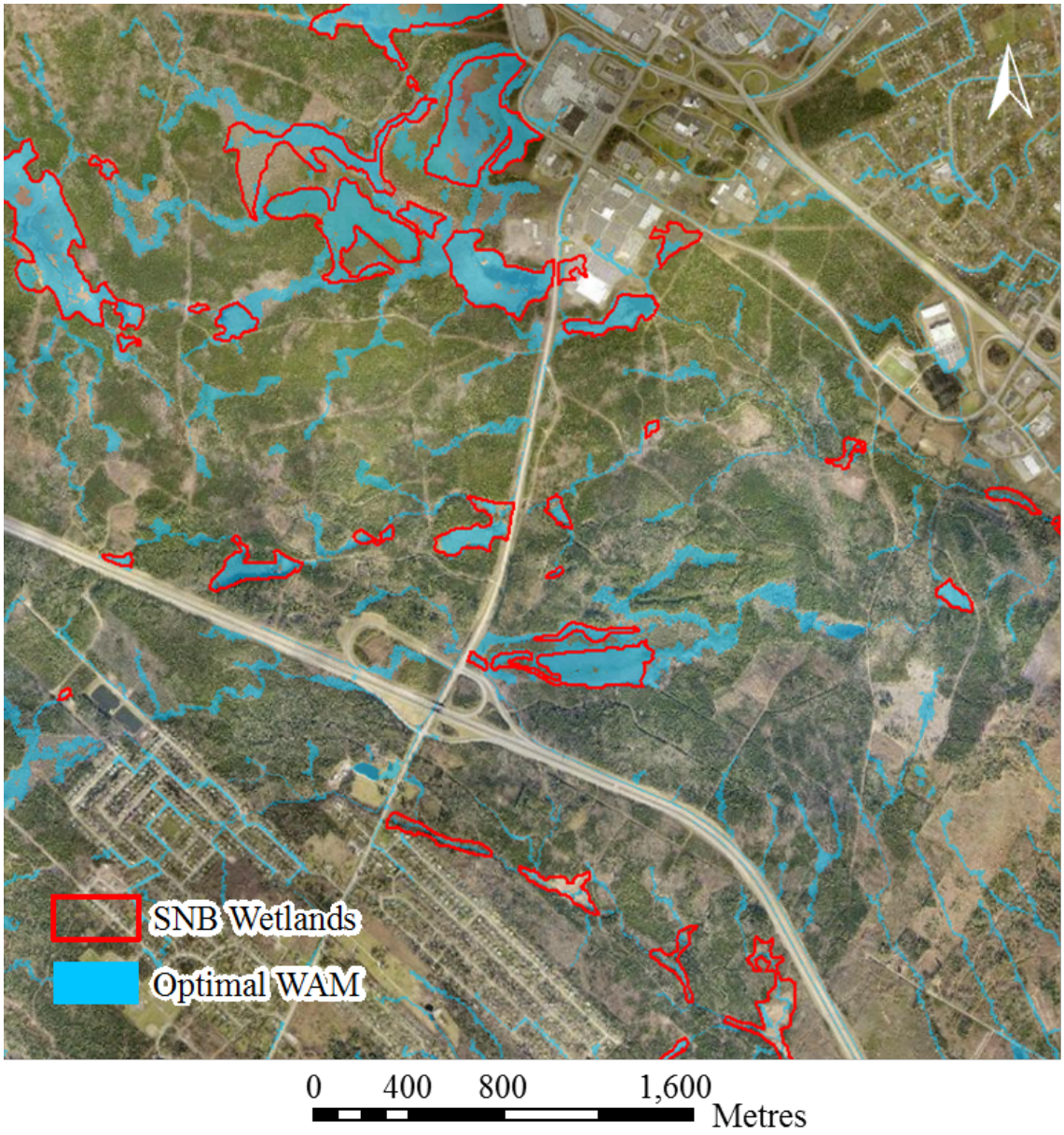

Figure 45. Close-up of SNB Wetlands outlines overlaid on the 1m HDS-processed LiDAR-DEM DTW <= 25 cm (optimal) delineation for the UNB Forest area.

The distributions of the false negatives and false positives generated using the DTW <= 25 cm zonation relative to the provincial wetland features is shown in Figure 46 and Figure 47 across the entire EMEND and UNB Forest areas. The areas so mapped are quantified by way of the conformance evaluation matrix in Table 7, showing the percentage areas identified as either correct, false positive or false negative relative to provincial DEP/SNB layers within the expanded study areas. Proportionate agreement for the EMEND area dropped by 3%, to 82% when assessing conformance based on the DEP layer instead of GPS-tracked locations as in chapter 6, while proportionate agreement at the expanded UNB Forest study area increased by 3% to 92% when assessing conformance based on SNB wetland layer.

Table 7. Proportionate agreement between modeled Provincial (DEP/SNB) and modeled optimal WAM for EMEND and UNB Forest study areas.

	EMEND	**UNB Forest**
True Wet	0.28	0.04
True Dry	0.54	0.88
False Wet	0.07	0.07
False Dry	0.11	0.01
Proportionate Agreement	0.82	0.92
Cohen's Kappa	0.62	0.42

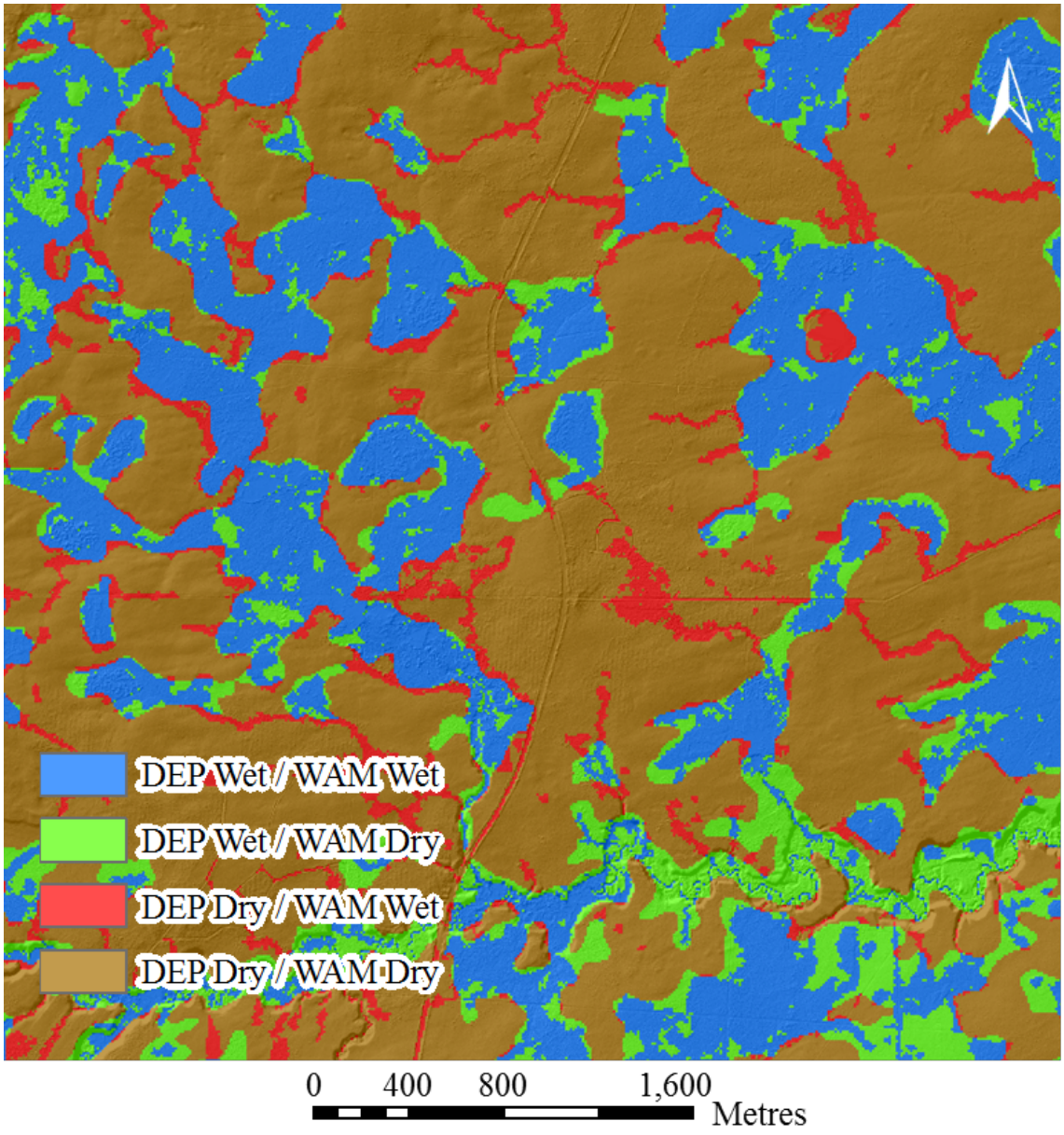

Figure 46. Area-based conformance assessment of the 1m LiDAR 1m (4ha SCA & HSD) wetland delineation procedure in reference to the Derived Ecosite Phase 1 (DEP) hydric/subhydric data layer for the EMEND area.

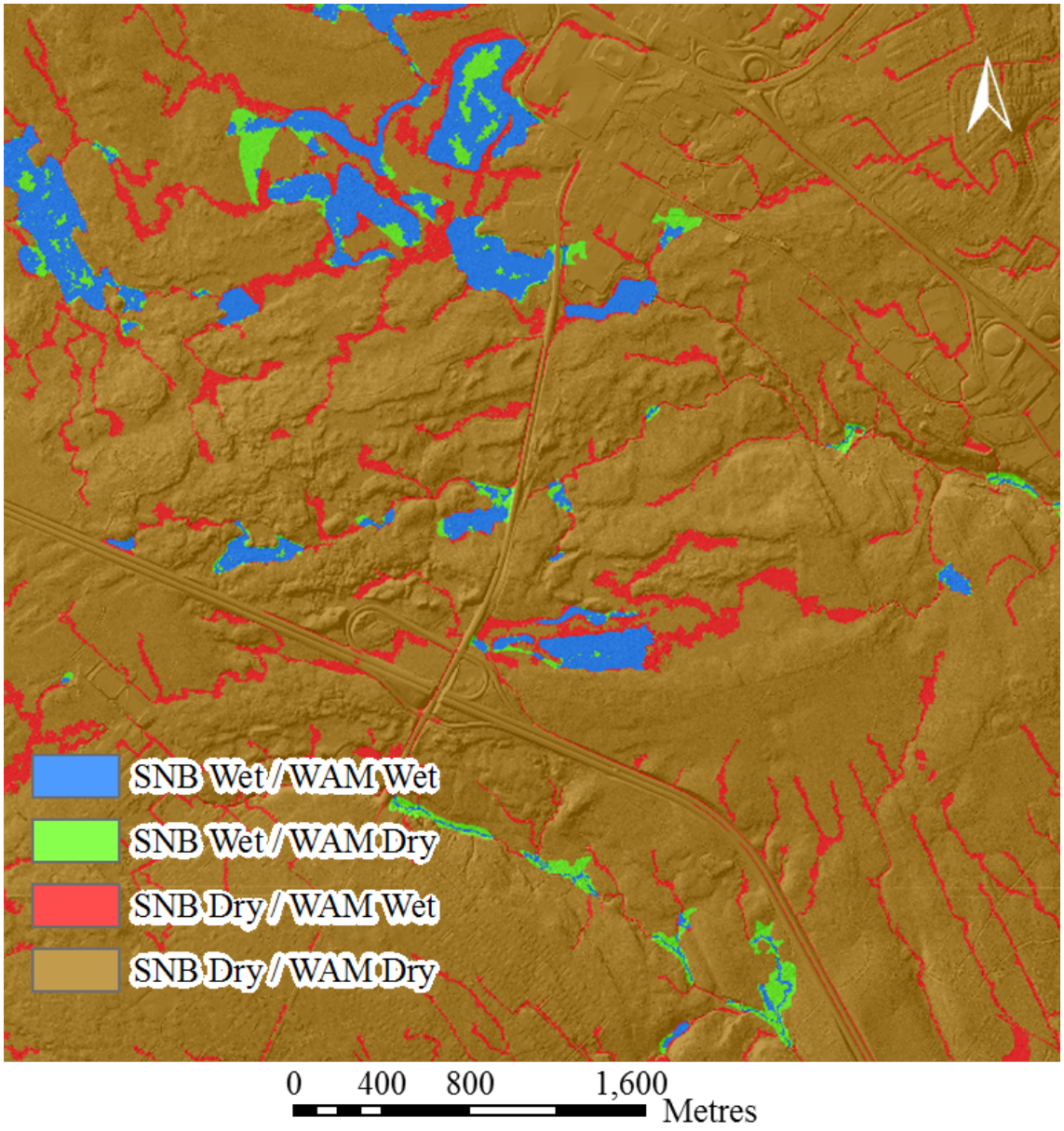

Figure 47. Area-based conformance assessment of the 1m LiDAR 1m (4 ha flow initiation & HSD) wetland delineation procedure in reference to the SNB wetlands layer for the UNB Forest.

To assess the model sensitivity of model output to DTW threshold, the change in conformance percentages by varying the DEM-based wetland defining DTW zonations from 10 to 200 cm were calculates as shown in Figure 48, with clear differences between the EMEND and UNB Forest areas. For EMEND, the best DEM-based wetland comparison with the DEP data layers is obtained with the DTW <= 25 cm zonation at a conformance level of 82% correct. For the UNB Forest, the best DEM-based wetland comparison with the SNB's wetland layer is obtained with the DTW = 10 cm zonation, at 92% correct. Also, the percentage of false negative correspondences between the DEM-based wetland delineation and the provincial wetland features is lower for the UNB Forest than for EMEND area. This is mainly due to scale difference in wetland-delineation methodologies: based on general vegetation type indexing across Alberta versus image-based wetland delineation across New Brunswick. The area percentages of false positives remain about the same across both areas while steadily increasing with increasing wetland-defining DTW zonations from 10 to 200 cm. This DTW increasing trend reflects that generally wetland-to-upland transitioning from poorly drained to well drained areas, such that – in general - areas with 25 cm < DTW ≤ 50 cm are imperfectly drained, areas with 50 cm < DTW ≤ 100 cm are moderately well drained, and areas with 100 cm < DTW≤ 200 cm and beyond are well drained.

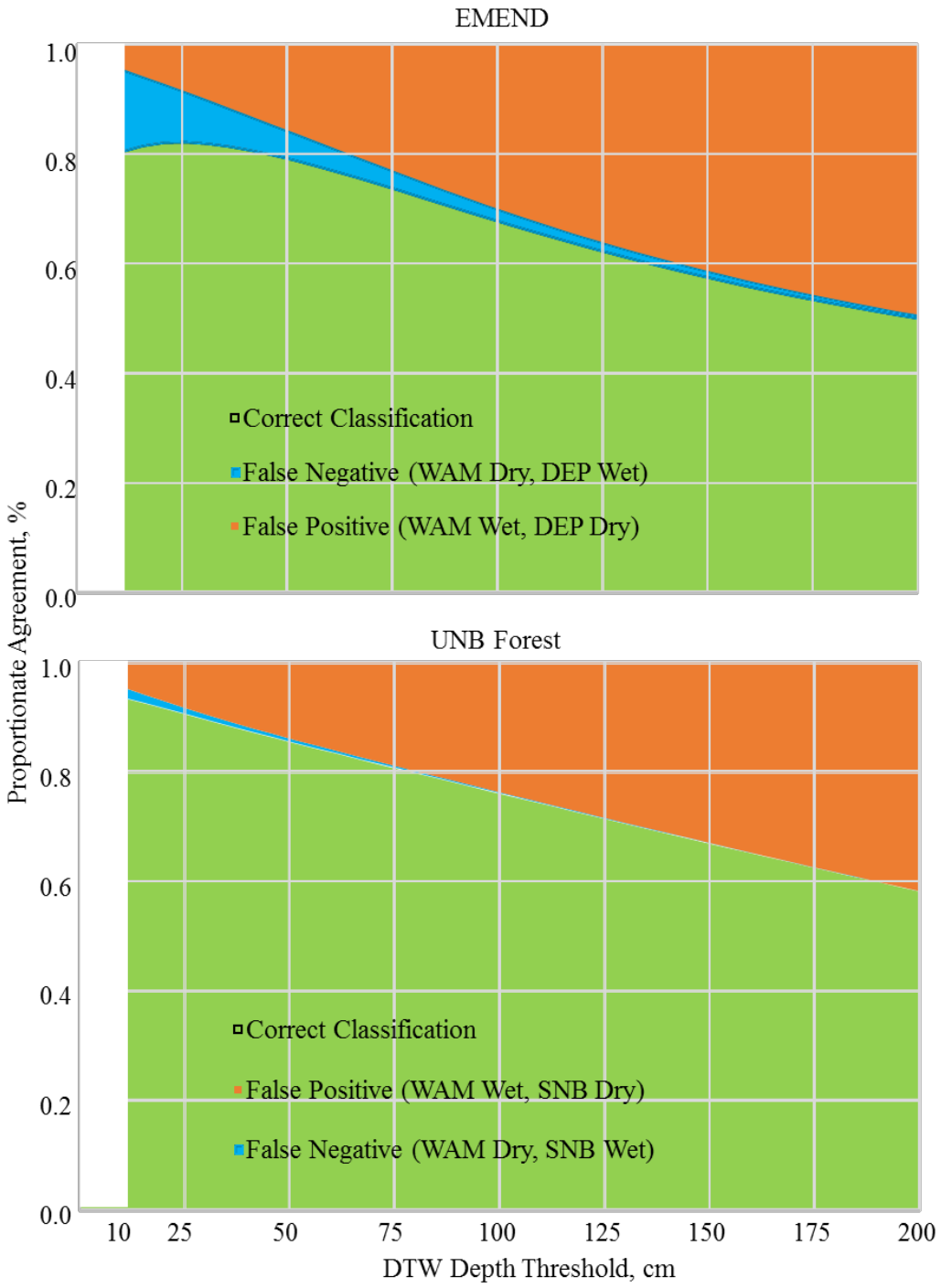

Figure 48. False positive/ false negative DEM-based wetland area conformance tests using the "optimal" delineation procedure (LiDAR DEM 1m, HS, 4ha), with the wetland –defining DTW zone varying from 0 to 200 cm. Top: EMEND area using the Provincial Derived Ecosite Phase v1 (DEP) layer as reference. Bottom: UNB Forest, using the wetland layer of Service New Brunswick as reference.

7.4 Discussion

Through the calibration of successive approximations, it was possibly to achieve a conformance level between GPS-tracked and LiDAR-DEM projected wetland locations better than 80%, based on selecting following thresholds (chapters 4, 5 and 6): (i) DTW <= 25 cm for wetland border delineation, (ii) minimum slope flow accumulation area = 4 ha and (iii) wetland flatting by setting DTW = 0 across wetlands based on DEM-recognizable hydrophytic vegetation patterns (HDS).

Validating this process towards GPS-tracked wetland locations not included in the GPS-tracking effort dropped the conformance level towards 70%. In addition, the wetlands so located form a subset of the Alberta's Derived Ecosite Phase 1 (DEP) hydric/subhydric data layer with an overall conformance level of 82%. For the New Brunswick wetlands layer, the conformance level with SNB wetlands amounts to 92% (Table 7).

The wetland delineation process of this thesis not only lines up well with Alberta's DEP coverage for the EMEND area, but also provides a more detailed differentiation between actual wetland and upland locations (Figure 46). The same is also generally true for New Brunswick's wetland layer (Figure 47). In comparison, the resulting Cohen's Kappa index values amounting to 0.62 and 0.42 (Table 7) for the EMEND and the UNB Forest areas. Hence, the conformance level between the 1 m HDS-processed LiDAR DEM-delineated wetlands and the corresponding wetland features within the provincial data layers is substantially better than by random chance alone.

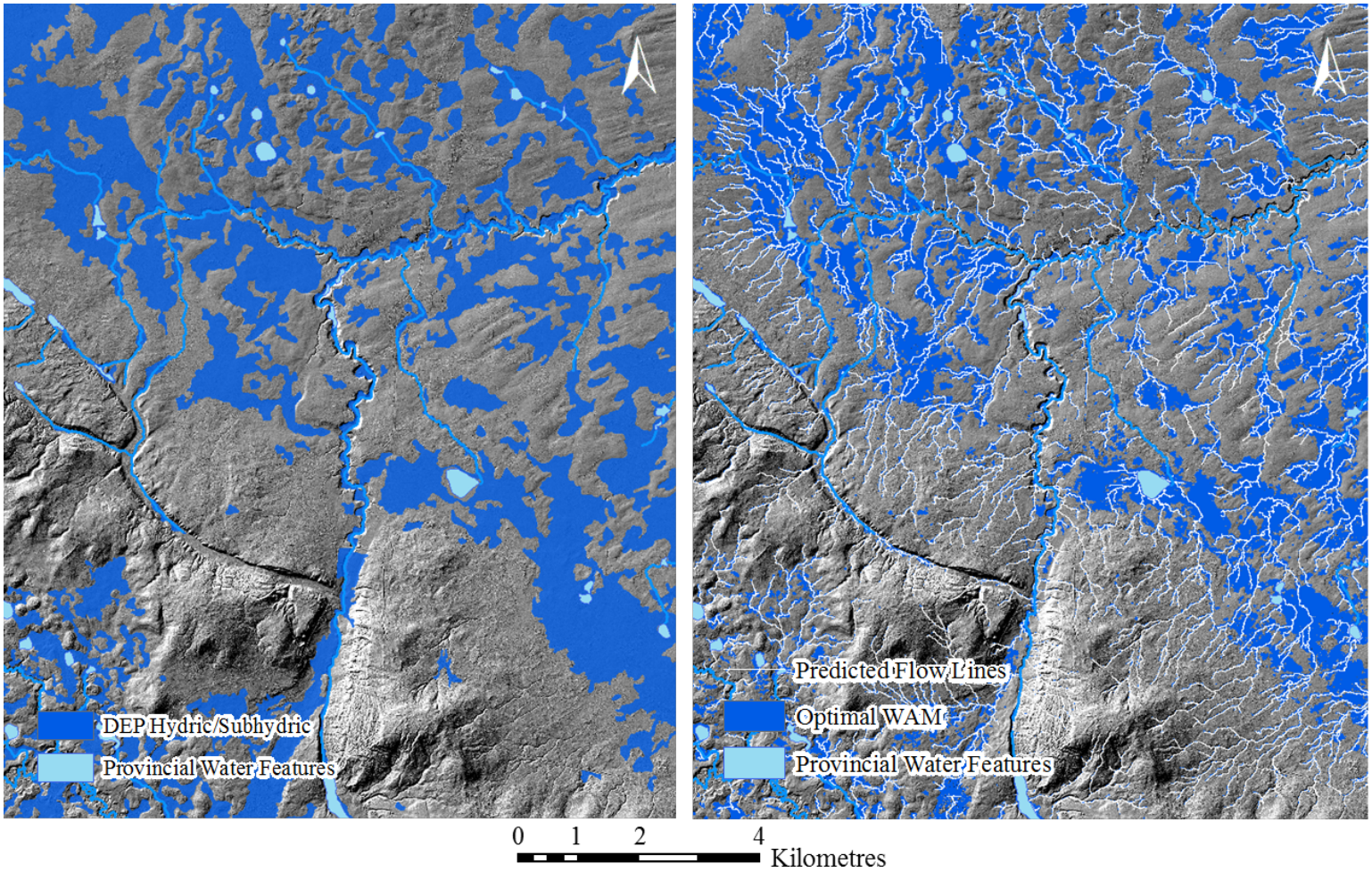

Figure 49. Comparing the 1m LiDAR 1m (4 ha flow threshold & HSD) wetland and flow channel delineation outcomes (right) in reference to the Derived Ecosite Phase 1 (DEP) hydric/subhydric class data layer for the EMEND area (left).

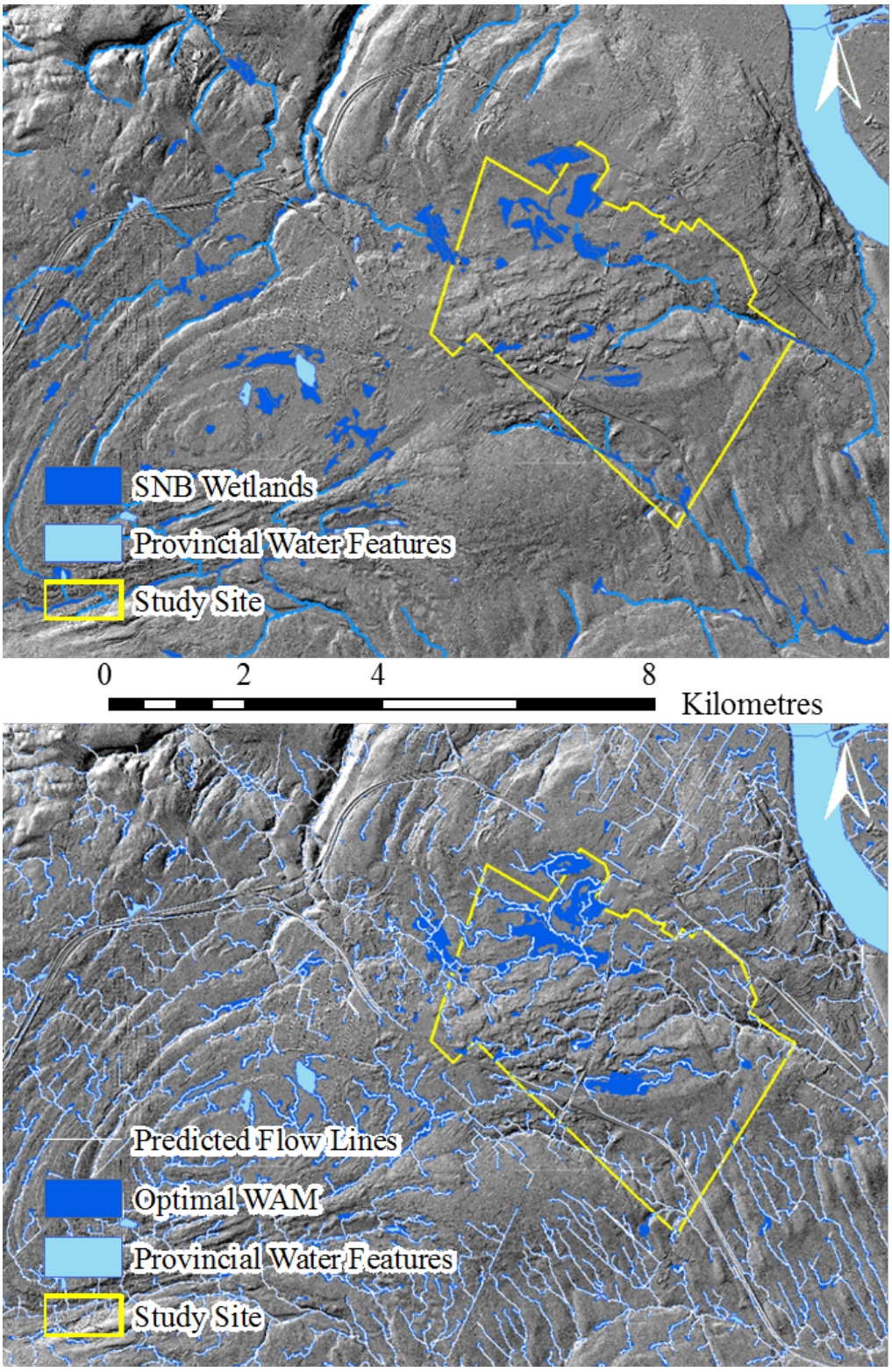

Figure 50. Comparing the LiDAR 1m (4 ha flow threshold & HSD) wetland and flow channel delineation outcomes (bottom) to reference SNB wetlands layer (top) for the UNB Forest area.

Overall, Figure 49 and Figure 50 provide a certain degree of confidence that the above 1m LiDAR-DEM delineations for wetlands and flow channels represent a significant improvement over currently available wetland and flow-channel data layers, at least within the confines of the two study areas of this thesis, while providing a consistent modeled result.

Whether further improvements can be achieved is subject to additional research pertaining to perhaps even more DEM-informed means to seed DTW=0 locations across the wetland components of forested landscapes while at the same time reducing false positive and false negative wetland portions occurrences.

To achieve even higher conformance levels, one needs to address additional limitations. For example, the delineation of any particular wetland may over time change due to hydrological reasons. This is particularly so where wetland-upland transitions are very gradual, especially across flat terrain, and whether the soil underneath depressions are water permeable or not. Prevailing changes in weather conditions also play a role, by gradually changing vegetation composition along the wetland to upland transitions. Hence, the above recommended thresholds for DEM-based wetland delineation may need to be reviewed as these may change across climate, soil and drainage conditions, and time.

Chapter 8

SUMMARY, CONCLUSIONS, SUGGESTIONS FOR FURTHER WORK AND PRACTICAL APPLICATIONS

8.1 Summary

This thesis examined the conformance of DEM-derived flow channels as well as wetland borders and areas within the context of: (i) varying DEM types (LiDAR versus SRTM) with DEM resolutions from 1 to 90 m, (ii) varying upslope flow accumulation areas from 0.5 to 16 ha, (iii) varying the DEM-derived cartographic depth-to-water (DTW) thresholds, and (iv) varying forest zone (boreal in northern Alberta versus maritime in central New Brunswick).

It was found that best delineation results for ephemeral, intermittent and permanent flow channels (chapter 4) were obtained using LiDAR DEMs at 1 m resolution and applying the D8 algorithm to determine flow directions and continuous ridge-to-shore flow accumulation patterns across the areas of interest, i.e. the EMEND and the UNB Forest areas. For this purpose, the 1 m LiDAR DEMs had to be hydro-conditioned by breaching all DEM-captured artificial and natural flow blockages. GPS-tracked ephemeral flow channels generally required the 1 ha threshold for upslope flow accumulation, whereas intermittent streams required 4 ha. The next best distance conformance between GPS-tracked and modelled flow channel location was achieved using the 10 m resampled LiDAR DEMs, but the detailed flow-channel delineation comparison registered a

considerable increase in nearest channel tracks from the 1 m to the 10 m resampled 1 m LiDAR DEM, i.e., 20 m, eight times out of 10.

DEM-derived wetland borders also conformed best to the GPS-tracked wetland borders using the 1 m LiDAR DEM following border delineation threshold settings: DTW < 25 cm after flattening the water table elevation across the wetland by setting DTW=0 at each DEM-recognized hydrophytic vegetation location (chapters 5, 6 and 7). The modelled versus GPS-tracked distance to wetland border and area were checked by varying DEM type (LiDAR, SRTM), resolution (1 to 90 m), and upslope flow accumulation for channel initiation (0.5 to 16 ha). It was found that distances between the modelled and GPS-tracked wetland borders stayed within ±10 m for the EMEND and UNB Forest areas, 7.2 and 8.4 times out of ten.

While the optimal wetland locator and DEM-based wetland border (Chapter 4) and area (chapter 5 and 6) delineation thresholds were found to be the same for both study areas, flow-channel and wetland-border conformances were tighter for the UNB Forest than the EMEND study area. This is mainly due to differences in terrain type: rugged (UNB Forest study area) versus flat (EMEND study area). The difference in climate-related vegetation conditions could also be important, especially in terms a greater prevalence of vegetation-covered ephemeral flow channels within the EMEND than in the UNB Forest study area.

The optimal procedure for DEM-based wetland-area delineation was quantitatively validated across the entire EMEND and UNB Forest areas (chapter 7). This validation produced 82% and 92% conformance levels (proportionate agreement) for the EMEND and UNB Forest areas, respectively, using LiDAR DEMs at 1m resolution, DTW < 25

cm, setting the minimum upslope flow initiation area at 4 ha, and using the hydrophytic DTW = 0 seeding process (HDS) for water-table flattening across the wetland areas. The wet-areas so delineated provide geographic and hydrologically comprehensive data layers regarding the positioning of each wetland within its surrounding area, and this includes the wetland-to wetland flow-channel connections across the areas so delineated.

8.2 Original Research Claims

This thesis show-cases how DEMs of varying technology source (LiDAR/SRTM) and resolution can be optimized to improved DEM-based flow-channel and wetland-border-area delineations in Alberta and New Brunswick, at least for the EMEND and UNB Forest areas.

This was achieved by formulating a qualitative and quantitative delineation, verification and validation process, and by exploring the effects of DEM type and spatial resolution on optimal DEM-based threshold settings pertaining to DEM spatial resolution, upslope flow initiation areas, DEM-derived DTW zonations, and the DTW = 0 placement of DEM-detected hydrophytic vegetation patterns (HDS).

It was found that the inclusion of the DEM-detected hydrophytic vegetation patterns (HDS) strongly improved the conformance of the DEM-based wetland border and area delineation process for both study areas, but more so for the EMEND area than the UNB Forest, likely due to differences in study-area specific terrain types (i.e. flat versus rugged).

The results show that the methodologies as used with recommended threshold settings are generalizable. In turn, this should be helpful for actual wetland delineation and planning processes.

8.3 Suggestions for Further Work

The work followed the process of generating improved wetland delineation results from LiDAR DEMs through successive approximations, with the HDS procedure being the main step forward to increase generality of the DEM-based wetland delineation approach. More work can be done in this direction through: (i) improving HDS model quality by a systematic reduction in false positives (ii) expanding the field sample size both at the two established study areas and at other areas of varying topography, geography, climate and vegetation patterns. (iii) comparisons of DTW-modeled wetland borders relative to those discerned from other remote-sensing technologies.

8.4 Practical Applications

Given the reasonably high conformance levels between the LiDAR-DEM located and delineated wetlands and GPS-tracked wetland borders, it is reasonable to suggest that the above methodology can assist jurisdictional wetland delineations to produce geographically connected and hydrologically informative wetland layers. To that purpose, the process identifies where to locate wetlands of at least > 1 hectare in size, and how to focus on further wetland details through GPS-tracking and/or using surface orthoimages and LiDAR DEM (bare earth, full feature, and images) overlays. In addition, the methodology allows for a quick estimation of overall wetland area percentages, and position of each wetland within its DEM-modeled flow network and associated DTW

distribution pattern. Knowing the hydro-topographic context so generated is important for gauging the hydrologically functioning of each wetland in terms of it's ecological, cultural, recreational, and commercial values case-by-case. For example, knowing the upstream flow contributing area via the overland flow and DTW-defining flow accumulation algorithm in combination with weather-related stream discharge modelling has the potential for the estimation of overall amount of water entering and leaving each wetland day-by-day based on past, current and daily-projected weather reports. Where wetlands are located in depressions, one can determine the amount of water needed to fill the wetland depression up to the elevation of its DEM-located pour point of the depression.

Knowing the percentage area and existing water-storage capacity of wetlands allows one to improve hydrological estimates for amounts of water stored and not stored within the context of determining water conservation needs or downslope flooding potentials. The number and extent of wetlands together with type of wetland specifications are important criteria for general and specific-specific wetland-obligatory habitat conservation considerations. Knowledge of hydro-topographic wetland extent and flow-channel connectivity in urban and sub-urban settings is vital for many architectural and engineering considerations regarding the proper placement of structure and the management of storm water flow from engineering as well as recreational and aesthetic considerations. In forestry, knowing the extent of each specific wetland and its flow-channel connections permits for increased accuracy in area-wide silvicultural investment and forest operations planning, dealing with, e.g., block layout and access, site preparation, seedling selection for planting, and stand tending needs.

References

Agren A. M., Lidberg W., Stomgren M., Ogilvie J., Arp P.A., 2014. Evaluating digital terrain indices for soil wetness mapping – a Swedish case study. *Hydrological Earth Sciences, 18*, 3623-3634.

Anderson M.G. and Burt T.P., 1978. The role of topography in controlling throughflow generation. *Earth Surface Processes and Landforms, 3(4),* 331-344.

Baker, C., Lawrence, R., Montagne, C., & Patten, D., 2006. Mapping Wetlands and Riparian Areas Using LANDSAT ETM Imagery and Decision-Tree-Based Models. *Wetlands, 26(2),* 465–474.

Band, L.E., 1986. Topographic partition of watersheds with digital elevation models. *Journal of Water Resources 22,* 15–24.

Beckingham, J.D., Corns, I.G.W. & Archibald, J.H., 1996. Field Guide to Ecosites of West-Central Alberta. Special Report 9. Canadian Forest Service, Northern Forestry Centre, Edmonton.

Beven, K.J.; Kirkby, M. J., 1979. A physically based, variable contributing area model of basin hydrology. *Hydrolological Science Bulletin, 24,* 43–69.

Burt, T. P., and Butcher, D. P., 1986. Development of topographic indices for use in semi-distributed hillslope runoff models, in Geomorphology and Land Management, edited by O. Slaymaker and D. Balteanu, pp. 1–19, Gebruder Borntraeger, Stuttgart, Germany

Campbell, D. M. H., 2012. TRAIL : Optimizing trail locations by terrain conditions and other considerations, at high resolution. Master's thesis. University of New Brunswick, Fredericton, New Brunswick.

Chasmer, L., Montgomery, J., Hopkinson, C., and Petrone, R., 2015. A Physically-based terrain morphology and vegetation structural classification for wetlands of the Boreal Plains, Alberta Canada. *Canadian Journal of Remote Sensing 42*, 521–540.

Cohen, J., 1960. A coefficient of agreement for nominal scales. *Educational and Psychological Measurement, 20(1),* 37-46.

Corns, I.G.W. and R.M. Annas, 1986. *Field guide to forest ecosystems of West-Central Alberta.* Northern Forestry Center, Canadian Forestry Service, Edmonton, AB. p251.

Costa-Cabral, M. C. and Burges, S. J., 1994. Digital elevation model networks (DEMON): A model of flow over hillslopes for computation of contributing and dispersal areas. *Water Resources Research, 30(6),* 1681-1692

Cowardin, L. M., & Myers, V. I., 1974. Remote Sensing for Identification and Classification of Wetland Vegetation. *The Journal of Wildlife Management, 38(2),* 308–314.

Dahl, T.E., 2006. Status and Trends of Wetlands in the Conterminous United States 1998 to 2004. Washington, D.C.: U.S. Department of the Interior, Fish and Wildlife Service Publication, p112.

Darras, S., Michou, M., Sarrat, C., 1999. IGBP-DIS Wetland Data Initiative: a First Step Towards Identifying a Global Delineation of Wetlands. IGBP-DIS Office, Toulouse, France.

Dias G., 2002. Delineating wetlands using multitemporal RADARSAT. Prepared for Randy Milton, Manager of Wetlands and Coastal Habitat, Nova Scotia Department of Natural Resources, Spring 2002.

Dixom B., Uddameri V., 2016. GIS and Geocomputation for Water Resource Science and Engineering. American Geophysical Union, February 2016, 978-1-118-35413-1.

Dunne T., and Black R. D., 1970. Partial Area Contributions to Storm Runoff in a Small New England Watershed. *Water Resource Research. 6(5),* 1296-1311.

Elkhrachy I., 2017. Vertical accuracy assessment of SRTM and ASTER Digital Elevation Models: A case study of Najran city, Saudi Arabia. Ain Shams Engineering Journal. Available online 29 January 2017.

Fernandez-Prieto, D., Arini, O., Borges, T., Davidson, N., Finlayson, M., Grassl, H., MacKay, H., Prigent, C., Pritchard, D., Zalidis, G., 2006. The GlobWetland Symposium: Summary and Way Forward. Proceedings Glob- Wetland: Looking at Wetlands from Space, October 2006, Frascati, Italy.

Gardiner, T. W., K. C. Sasowsky, and R. L. Day, 1991. Automated extraction of geomorphic properties from digital elevation data, Z. *Geomorphol. Suppl., 80*, 57–68.

Garroway K., Hopkinson C., Jamieson R., 2011. Surface moisture and vegetation influences on LiDAR intensity data in an agricultural watershed. *Canadian Journal of Remote Sensing, 37(3),* 275-284.

Gillin C. P., Bailey S. W., McGuire K. J., and Prisley T., 2015. Evaluation of Lidar-derived DEMs through Terrain Analysis and Field Comparison. *Photogrammetric Engineering & Remote Sensing*, 81(5), 387-396.

Glaser P. H., and Janssens J. A., 1986. Raised bogs in eastern North America: transitions in landforms and cross stratigraphy. *Canadian Journal of Botany*, 64(2), 395-415.

Goodrich D. C. and Woolhiser D. A. 1991. Catchment Hydrology. Reviews of Geophysics, Suppliment. U.S. *National Report to International Union of Geodesy and Geophysics*. Pp 202-209.

Heine, R.A., Lant, C.L., Sengupta, R.R., 2004. Development and comparison of approaches for automated mapping of stream channel networks. *Ann. Assoc. Am. Geogr. 94*, 477–490.

Hirano A., Madden M., Welch R., 2003. Hyperspectral image data for mapping wetland vegetation. *Wetlands 23(2),* 436-448.

Hopkinson, C., Chasmer, L., Lim, K., Treitz, P., & Creed, I., 2006. Towards a universal lidar canopy height indicator. *Canadian Journal of Remote Sensing, 32(2),* 139–152.

Hopkinson, C., Chasmer, L., Sass G., Creed I.F., Sitar M., Kalbfleisch W., and Treitz P., 2005. Vegetation class dependent errors in lidar ground elevation and canopy height

estimates in a boreal wetland environment. *Canadian Journal of Remote Sensing 31(2),* 191-206.

Huang C., Peng Y., Lang M., Yeo I-Y., McCarthy G., 2014. Wetland inundation mapping and change monitoring using Landsat and airborne LiDAR data. *Remote Sensing of Environment, 141,* 231-242.

Jenson, S.K. Domingue, J.O., 1988. Extracting topographic structure from digital elevation data for GIS analysis. *Photogrammetric Engineering & Remote Sensing, 54(11),*1593-1600.

Julien P. Y., Saghafian B. and Ogden F. L. 1995. Raster-based hydrologic modeling of spatially-varied surface runoff. *Journal of the American water resources association. 31(3*), 523-536.

Kaasalainen S., Hyyppa H., Kukko A., Litkey P., Ahokas E., Hyyppa J., Lehner H., 2008. Radiometric calibration of LiDAR intensity with commercially available reference targets. *IEEE Transactions on Geoscience and Remote Sensing. 47(2)*, 588-598.

Kirkby M.J., and Chorley R. J., 1976. Throughflow, Overland Flow and Erosion. *International Association of Scientific Hydrology. Bulletin. 12(3),* 5-21

Klemas, V., 2011. Remote sensing of wetlands: case studies comparing practical techniques. *Journal of Coastal Research, 27(3),* 418-427.

Knight, J. F., Tolcser, B. P., Corcoran, J. M., & Rampi, L. P., 2013. The effects of data selection and thematic detail on the accuracy of high spatial resolution wetland classifications. *Photogrammetric Engineering and Remote Sensing, 79(7),* 613–623.

Kumar L., Priyakant S., Subhashni T., 2013. Improving image classification in a complex wetland ecosystem through image fusion techniques. *Journal of Applied Remote Sensing 8(1).*

Landis J.R., Kosh G. G., 1977. The measurement of observer agreement for categorical data. *Biometrics. 33(1),* 159-174.

Lang M., and McCarthy G., 2009. LiDAR intensity for improved detection of inundation below forest canopy. *Wetlands 29(4),*1166-1178.

Lehner, B., Do¨ll, P., 2004. Development and validation of a global database of lakes, reservoirs and wetlands. *Journal of Hydrology 296 (1-4),* 1-22.

Li, Z., & Zhu, Q. (2005). Digital Terrain Modeling - Principles and Methodology (p. 318). Boca Raton: CRC Press.

Liang, C., MacKay, D.S., 2000. A general model of watershed extraction and representation using globally optimal flow paths and up-slope contributing areas. *Int. J. Geogr. Inf. Sci. 14,* 337–358.

Lindsay, J.B., 2016. Efficient hybrid breaching-filling sink removal methods for flow path enforcement in digital elevation models. *Hydrological Processes, 30(6),* 846–857

Lindsay, J.B., Creed, I.F., 2005. Removal of artifact depressions from digital elevation models: towards a minimum impact approach. *Hydrol. Process. 19*, 3113–3126.

Lindsay, J.B., Dhun, K., 2015. Modelling surface drainage patterns in altered landscapes using LiDAR. *Int. J. Geogr. Inf. Sci. 3*, 1–15.

Mark, D.M. 1988. "Network models in geomorphology", Modelling in Geomorphological Systems, John Wiley.

Maxa M., Bolstad P., 2009. Mapping northern wetlands with high resolution satellite images and LiDAR. *Wetlands 29(1),* 248-260.

Maxa, M., & Bolstad, P. (2009). Mapping Northern Wetlands with High Resolution Satellite Images and LiDAR. *Wetlands, 29(1),* 248–260.

Meng, F.-R., Castonguay, M., Ogilvie, J., Murphy, P.N.C. & Arp, P.A. 2006. Developing a GIS-based flow-channel and wet-areas mapping framework for precision forestry planning. International Precision Forestry Symposium (eds P.A. Ackerman, D.W. La¨ngin & M.C. Antonides), pp. 43–55. Stellenbosch University, Stellenbosch.

Merchant*, M., Adams, J., Berg, A., Baltzer, J., Quinton, W., and Chasmer, L., 2016. The contributions of C-band SAR multipolarization data and polarimetric decompositions to subarctic boreal peatland mapping. IEEE Journal of Selected Topics in Applied Earth Observations and Remote Sensing. 10, 1467–1482.

Millard, K., & Richardson, M., 2013. Wetland mapping with LiDAR derivatives, SAR polarimetric decompositions, and LiDAR–SAR fusion using a random forest classifier. *Canadian Journal of Remote Sensing, 39(04),* 290–307.

Montgomery, D. R. and W. E. Dietrich. 1992. Channel initiation and the problem of landscape scale. *Science, 255*, 826-830.

Montgomery, D.R., and E. Foufoula-Georgiou. 1993. Channel network source representation using digital elevation models. *Water Resources Research, 29(12*), 3925-3934

Moore I. D., Gessler P. E., Neilsen G. A., and Peterson G. A., 1993. Soil Attribute Prediction Using Terrain Analysis. *Soil Science Society of America Journal, 57(2),* 443-452.

Moore, I. D. and R. B. Grayson. 1991. Terrain-based catchment partitioning and runoff prediction using vector elevation data. *Water Resources Research, 27(6)*, 1177-1191

Moore, I. D., R. B. Grayson and A. R. Ladson. 1991. Digital terrain modelling: A review of hydrological, geomorphological, and biological applications. *Hydrological Processes, 5(1),* 3-30.

Morris. D. G., and Heerdegen R. G. 1988. Automatically derived catchment boundaries and channel networks and their hydrological applications. *Geomorphology, 1(2),* 131-141.

Murphy, P. N. C., Ogilvie, J., Connor, K., and Arp, P. A., 2007. Mapping Wetlands: A comparison of two different approaches for New Brunswick, Canada. Wetlands, 27(4), 846,-854.

Murphy P. N. C., Ogilvie J, Meng F-R, Arp P. 2008. Stream network modelling using lidar and photogrammetric digital elevation models: a comparison and field verification. *Hydrol. Proc. 22(12),* 1747-1754.

Murphy, P. N. C., Ogilvie, J., & Arp, P., 2009. Topographic modelling of soil moisture conditions: A comparison and verification of two models. European Journal of Soil Science, 60(1), 94–109.

NWWG., 1997. The Canadian Wetland Classification System. (B. G. Warner & C. D. A. Rubec, Eds.) (2nd ed.). Waterloo, ON: Wetlands Research Center.

O'Callaghan, J. F., and Mark, D. M., 1984. The extraction of drainage networks from digital elevation data". Computer Vision, Graphics and Image Processing, 28, 328-344

Ozesmi S. L., Bauer M, E., 2002. Satellite remote sensing of wetlands. *Wetland ecology and management, 10*, 381-402.

Pan, F., C. D. Peters-Lidard, M. J. Sale, A. W. King. 2004. A comparison of geographical information systems-based algorithms for computing the TOPMODEL topographic index. *Water Resource Research, 40*.

Planchon, O., Darboux, F., 2002. A fast, simple and versatile algorithm to fill the depressions of digital elevation models. *Catena 46,* 159–176.

Pryde, J.K., Osorio, J., Wolfe, M.L., Heatwole, C., Benham, B., Cárdenas, A., 2007. Comparison of watershed boundaries derived from SRTM and ASTER digital elevation datasets and from a digitized topographic map. *ASABE Paper No. 072093*, St. Joseph, Michigan, USA.

Qin, C., Zhu, A.-X., Pei, T., Li, B., Zhou, C., and Yang, L., 2006. An adaptive approach to selecting flow-partition exponent for a multiple-flow-direction algorithm. *International Journal of Geographical Information Science*, 21(4), 443-458.

Ramesay E. and Rangoonwala A., 2015. Remote Sensing of Wetlands; Applications and Advances. CRC Press, Pp. 155-174.

Rebelo, L.-M., Finalyson, C.M., Nagabhatla, N. 2007. Remote sensing and GIS for wetland inventory, mapping and change analysis. *Journal of Environmental Management 90,* 2144-2153.

Remmel T.K., Todd K.W and Buttle J., 2008. A comparison of existing surficial hydrological data layers in a low-relief forested Ontario landscape with those derived from a LiDAR DEM. *The Forestry Chronicle, 84(6),* 850-865

Rodriguez, E., C.S. Morris, J.E. Belz, E.C. Chapin, J.M. Martin, W.Daffer, S. Hensley, 2005, An assessment of the SRTM topographic products, Technical Report JPL D-31639, Jet Propulsion Laboratory, Pasadena, California, 143 pp.

Rieger, W., 1993. Automated river line and catchment area extraction from DEM data. *Int. Arch. Photogramm. Remote Sens. 29*, 642–642.

Sahagian, D., Melack, H. (Eds.), 1996. Global Wetland Distribution and Functional Characterization: Trace Gases and the Hydrologic Cycle. IGBP Secretariat, Stockholm IGBP Report No. 46.

Schmidt F., and Persson A., 2003. Comparison of DEM data capture and topographic wetness indices. *Precision Agriculture 4(2),* 179-192.

Schumm, S. A., 1956. Evolution of drainage systems and slopes in badlands at Perth Amboy, New Jersey, *Geol. Soc. Am. Bull., 67*, 597–646.

Soille, P., 2004. Optimal removal of spurious pits in grid digital elevation models. *Water Resour. Res. 40*.

Sørensen R., Zinko, U., Seibert J., 2006. On the calculation of the topographic wetness index: evaluation of different methods based on field observations. *Hydrology and Earth System Sciences Discussions, European Geosciences Union, 10 (1),* 101-112.

Tarboton, D. G., 1997. A New Method for the Determination of Flow Directions and Contributing Areas in Grid Digital Elevation Models, *Water Resources Research, 33(2),* 309-319

Tarboton, D. G., Bras, R. L., and Rodriguez–Iturbe, I., 1991. On the Extraction of Channel Networks from Digital Elevation Data. *Hydrological Processes, 5*, 81–100.

Tiner, R.W., 1996. Wetlands. In: Manual of Photographic Interpretation, 2nd edition. Falls Church, Virginia: American Society for Photogrammetry and Remote Sensing, p2440.

Touzi, R., Deschamps, A., & Rother, G., 2009. Phase of Target Scattering for Wetland Characterization Using Polarimetric. *IEEE Transactions on Geoscience and Remote Sensing, 47(9),* 3241–3261.

Wang, L. & H. Liu. 2006. An efficient method for identifying and filling surface depressions in digital elevation models for hydrologic analysis and modelling. *International Journal of Geographical Information Science, 20(2),* 193-213.

Wdowinski, S., Kim, S., Amelung, F., Dixon, T. H., Miralles-wilhelm, F., & Sonenshein, R., 2008. Space-based detection of wetlands' surface water level changes from L-band SAR interferometry. *Remote Sensing of Environment, 112*, 681–696.

Whitcomb, J., Moghaddam, M., Mcdonald, K., Kellndorfer, J., & Podest, E., 2009. Mapping vegetated wetlands of Alaska using L-band radar satellite imagery. *Canadian Journal of Remote Sensing, 35(1),* 54–72.

White B., Ogilvie J., Campbell D.H.M, Hiltz D., Gauthier B., Chisholm H.K., Wen H.K., Murphy P.N.C., and Arp P.A., 2012. Using the Cartographic Depth-to-Water Index to Locate Small Streams and Associated Wet Areas across Landscapes. *Canadian Water Resources Journal 37(4),* 333-347.

Wood, E. F., M. Sivapalan, and K. Beven, 1990. Similarity and scale in catchment storm response, *Rev. Geophys., 28,* 1–18.

Wu Q., Lane C., Liu H., 2009. An effective method for detecting potential woodland vernal pools using high-resolution LiDAR data and aerial imagery. *Remote Sensing 61(11),* 1444-1467.

Yan W.Y., Shaker A., Habib A., Kersting A.P., 2012. Improving classification accuracy of airborne LiDAR intensity data by geometric calibration and radiometric correction. *ISPRS Journal of Photogrammetry and Remote Sensing. 67*, 35-44.

Yang J., Guangbo R., Yi M., Yanguo F., 2016. Coastal wetland classification based on high resolution SAR and optical image fusion. Geoscience and Remote Sensing Symposium (IGARSS), 2016 IEEE International. July 2016.

Yu, W., Su, C., Yu, C., X Wang, Feng, C., Zhang, X., 2014. An Efficient Algorithm for Depression Filling and Flat-Surface Processing in Raster DEMs. *Geosci. Remote Sens. Lett. IEEE 11,* 2198–22

Zoltai, S. C., & Vitt, D. H., 1995. Canadian wetlands : Environmental gradients and classification. Vegetation, 118, Pp131–137.

1

2

CURRICULUM VITAE

Name

Jae James Ogilvie

Universities Attended

University of New Brunswick, Saint John. 1999 - 2001

BSc. Computer Engineering

Completed 1st year of program prior to transfer into BSc. Forestry and Environmental Management.

University of New Brunswick, Fredericton. 2001 - 2006

BSc. Forestry & Environmental Management

Completed degree program with a minor in computer applications, focusing on Geographic Information Systems (GIS) and Remote Sensing analysis, as well as applied computer modelling and photogrammetry.

Publications

Articles in Refereed Journals

Furze S., Castonguay M., Jae Ogilvie J., Nasr M., Cormier P., Gagnon R. Adams G., Arp P.A. 2017. Assessing soil-related black spruce and white spruce plantation productivity. Open Journal of Forestry. 7, 209-227.

Keys K., Noseworthy, J., Ogilvie, J. Burton, D.L., Arp, P.A. 2016. A simple geospatial nutrient budget model for assessing forest harvest sustainability in Nova Scotia, Canada. Ecol. Modelling. Submitted.

Nijland W., Coops N., Macdonald E., Nielsen S., Bater C., White B., Ogilvie J., & Stadt J. 2015. Remote sensing proxies of productivity and moisture predict forest stand type and recovery rate following experimental harvest. Forest Ecology and Management. 357 (2015), 239-247.

Agren A. M., Lidberg W., Stromgren M., Ogilvie J. & Arp PA. 2014. Evaluating digital terrain indices for soil wetness mapping – a Swedish case study. Hydrology and Earth Systems Sciences, vol 18 (9), 3623-3634.

Jones M-F., Castonguay M., Nasr M., Ogilvie J., Arp PA., Bhatti J. 2014. Modeling hydrothermal regimes and potential impacts of climate change on permafrost within the south Mackenzie plain, Northwest Territories, Canada. Ecoscience vol 21 (1), 21-33.

White B., Ogilvie J., Campbell D., Hiltz D., Gauthier B., Chisholm K., Wen H., Murphy P., & Arp PA. 2012. Using the Cartographic Depth-to-Water Index to Locate Small Streams and Associated Wet Areas across Landscapes. Canadian Water Resources Journal, vol 37(4), 333-347.

Nasr M, Ogilvie J, Castonguay M, Rencz A & Arp PA 2011. Total Hg concentrations in stream and lake sediments: Discerning geospatial patterns and controls across Canada. Applied Geochemistry, vol 26, 11, 1818-1831.

Murphy PNC, Ogilvie J, Meng F, White B, Bhatti J & Arp PA. 2011. Modelling and mapping topographic variations in forest soils at high resolution: a case study. Ecological Modelling, 10.1016, 01. 003.

Nasr M, Ogilvie J, Raymond BA & Arp PA 2010. Modelling and mapping critical loads and exceedances for the Georgia Basin, British Columbia, using a zero base-cation depletion criterion. Journal of Limnology, vol 69, 181-192.

Murphy PNC, Castonguay M, Ogilvie J, Nasr, M, Hazlett P, Bhatti J & Arp PA 2009. A geospatial and temporal framework for modeling gaseous N and other N losses from forest soils and basins, with application to the Turkey Lakes Watershed Project, in Ontario, Canada. Forest Ecology and Management, 258 (2009) 2304-2317.

Vega-Nieva DJ, Murphy PNC, Castonguay M, Ogilvie J & Arp PA 2009. A modular terrain model for daily variations in machine-specific forest soil trafficability, year-round. Canadian Journal of Soil Science, vol 89, n1, 93-107.

Murphy PNC, Ogilvie J & Arp PA 2009. Topographic modelling of soil moisture conditions: a comparison and verification of two models. European Journal of Soil Science. European Journal of Soil Science, February 2009, 60, 94-109.

Murphy PNC, Ogilvie J, Castonguay M, Zhang C-F, Meng F & Arp PA 2008. Improving forest operations planning through high-resolution flow-channel and wet-areas mapping. The Forestry Chronicle, 84: 568-574.

Murphy PNC, Ogilvie J, Castonguay M, Meng F & Arp PA 2007. Verifying calculated flow accumulation patterns of mapped and unmapped forest streams by culvert location. The Forestry Chronicle, 83: 198-206.

Murphy PNC, Ogilvie J, Connor K & Arp PA 2007. Mapping wetlands: a comparison of two different approaches for New Brunswick, Canada. Wetlands 27 (4), 846-854.

Murphy PNC, Ogilvie J, Meng F & Arp PA 2007. Stream network modelling using lidar and photogrammetric digital elevation models: a comparison and field verification. Hydrological Processes. 10.1002/hyp.6770.

Refereed Conference Proceedings

Murphy PNC, Castonguay M, Ogilvie J, Connors T & Arp PA 2006. Forest operations planning based on high resolution wet areas mapping: verifications. Proceedings of the International Precision Forestry Symposium, Stellenbosch University, South Africa. 5-10 March 2006, 477-487.

Meng F, Castonguay M, Ogilvie J, Murphy PNC & Arp PA 2006. Developing a GIS-based flow-channel and wet-areas mapping framework for precision forestry planning. Proceedings of the International Precision Forestry Symposium, Stellenbosch University, South Africa, 5-10 March 2006, 43-55.

Conference Presentations

Papers presented at Professional and Technical Meetings

Ogilvie J & White B, 2011. Technical issues and solutions relating to Alberta's LiDAR-based Wet Areas Mapping initiative. Presented at the GeoAlberta 2011 Conference, Edmonton, Alberta. May 2011.

Ogilvie J, Campbell D, Arp PA & White B, 2010. Topographically-based ground reconnaissance with LiDAR: land-use management policy and planning implications. Presented at the Geomatics Atlantic 2010 Conference, Fredericton, NB. October 2010.

Ogilvie J, Arp PA, 2009. Mapping tools in riparian management: mapping wet (and dry) areas. Presented at the Riparian Research and Management (RIPNET) Workshop, Sault Ste. Marie, Ontario. March 2009.

Welch A, Ogilvie J & Arp PA, 2008. Mapping flow-channel, wet-areas, and depth-to-water over large areas, in combination with image-based soil moisture classifications: a new approach towards better land-surface characterization, with high geospatial resolution. Paper presented at Dendron-OMNR Information Session, OMNR, Sault Ste. Marie, Ontario. March 2008.

Ogilvie J, Castonguay M, Murphy PNC, Meng F-R & Arp PA 2007. SFMN wet areas mapping project update: towards better forest management planning and operations practices. Presented at the Knowledge Extension Workshop for Sustainable Forest Management Research and Practice. Paper presented at SFMN-KETE Workshop 2007, Fredericton, New Brunswick.

Ogilvie J, Arp PA 2007. High Resolution wet-areas mapping for large forest areas in Manitoba (Duck Mountain Provincial Park) and northern Alberta. Posters presented at the Sustainable Forest Management Network Knowledge Exchange Workshop: Management of Aquatic Systems in Forested Landscapes 2007, Winnipeg, Manitoba.

Murphy PNC, Ogilvie J & Arp PA. Soil physical and chemical properties along a boreal wetland-upland catena, coupled with LiDAR-based modelling of soil moisture conditions. Paper presented at the SSSA Annual Meeting 2007, New Orleans, U.S.A.

Murphy PNC, Ogilvie J, Meng FR & Arp PA 2007. LiDAR-based modeling of soil drainage and other physical and chemical properties. Presented at the Eastern Canada Soil and Water Conservation Centre, Quebec-New Brunswick Technical Exchange Workshop. August 14-15 2007. Grand-Sault, New Brunswick.

Murphy PNC, Ogilvie J, Meng F & Arp PA 2007. High resolution modeling of stream networks and soil moisture conditions using a LiDAR DEM. Poster presented at the SSSA Annual Meeting 2007, New Orleans, U.S.A. Paper presented at the SFMN-FN water/riparian research workshop. May 9-10, 2007. Edmonton, Alberta.

Castonguay M, Ogilvie J & Arp PA. 2007. Mapping flow-channels and wet areas for First Nations, with potential to focus on First Nations needs for hydrological risks assessments, with case studies. SFMN-FN Workshop, May 2007, Kamloops, BC

Zhang CF, Ogilvie J, Murphy PNC, Bhatti JS, Castonguay M, Meng FR, Brady M & Arp PA. Modeling and mapping hydrothermal regimes and potential impacts of climate change on permafrost within the South Mackenzie Plain, Northwest Territories, Canada. Paper presented at the First International Circumpolar Conference on Geospatial Sciences and Applications 2007, Yellowknife, N.W.T., Canada.

Arp PA, Ogilvie J, Castonguay M, Meng F-R, Bourque, C, Murphy PNC, Chi J, Zhang C-F, Moore J, Glode J, Nasr M 2007. Flow-channel, wet areas and depth-to-water mapping. Presented at Alberta Sustainable Resource Development Conference, October, 2007, Edmonton, Alberta.

Murphy PNC, Ogilvie J & Arp PA. Soil physical and chemical properties along a boreal wetland-upland catena, coupled with LiDAR-based soil wetness modeling: a case study for central Alberta. Paper presented at the AQSSS/CSSS Annual Meeting 2007, Quebec, Canada.

Murphy PNC, Ogilvie J & Arp PA. Towards high-resolution critical loads mapping for the Georgia Basin, British Columbia, Canada. Poster presented at the Georgia Basin-Puget Sound Research Conference, March 2007, Vancouver, Canada.

Murphy PNC, Meng F, Castonguay M, Ogilvie J & Arp PA. Towards a new soil disturbance mapping and prevention tools. Paper presented at the CSSS Annual Meeting 2006, Banff, Canada.

Murphy PNC, Vega Nieva DJ, Meng F, Castonguay M, Ogilvie J, & Arp PA. A GIS-based flow channel and wet soils mapping tool for soil and water protection in forest operations planning. Paper presented at the SSSA Annual Meeting 2006, Indianapolis, U.S.A.

Murphy PNC, Ogilvie J, Castonguay M, Connors T, Meng F & Arp PA. DEM-derived flow channel and wet area mapping: a new tool for forest operations planning. Paper presented at the Sustainable Forest Management Network Conference 2006, Edmonton, Alberta, Canada.

Murphy PNC, Castonguay M, Ogilvie J, Connors T & Arp PA 2006. Forest operations planning based on high resolution wet areas mapping: verifications. Paper presented at the International Precision Forestry Symposium 2006, Stellenbosch University, South Africa.

Meng F, Castonguay M, Ogilvie J, Murphy PNC & Arp PA 2006. Developing a GIS-based flow-channel and wet-areas mapping framework for precision forestry planning. Paper presented at the International Precision Forestry Symposium 2006, Stellenbosch University, South Africa.

Arp PA, Meng F-R, Castonguay M, Ogilvie J & Murphy PNC 2006. Depth to water mapping: developing a GIS-based flow-channel and wet-areas mapping framework for precision forestry planning. Paper presented at the Bowater-Mersey Woodlands Forestry Research Seminar 2006, Liverpool, Nova Scotia.

Castonguay M, Ogilvie J, Murphy PNC, Meng F-R & Arp PA 2005. Province-wide wet areas mapping: a new tool for high-resolution operations planning in Nova Scotia. Presented at NFA Partnership Meeting, 2005, Stewiacke, Nova Scotia.